Age-related Changes in Geometric Characteristics of the Pediatric Thoracic Cage and Comparison of Thorax Shape with a Pediatric CPR Manikin

A Thesis

Submitted to the Faculty

of

Drexel University

by

Amanda R. Comeau

In partial fulfillment of the

Requirements for the degree

of

Masters of Biomedical Engineering, Science & Health Systems

June 2010

Dedication

To my Mom:

Thank you for your faithful prayers. Thank you for your constant support. Thank you for your continuous and unceasing encouragement. Thank you for all the times you listened to me vent my frustrations and graciously helped me to keep moving forward. Thank you for teaching me by example how to work hard and to stay focused through every situation. Thank you for challenging me to do better than I thought that I ever could. And most of all, thank you for loving me unconditionally. I could not have finished this work, or made it to where I am today, without you. I thank God for such an amazing mom. I love you.

Acknowledgments

I would like to acknowledge the National Science Foundation (NSF) Center for Child Injury Prevention Studies (CChIPS) at the Children's Hospital of Philadelphia (CHOP) for sponsoring this study and its Industry Advisory Board (IAB) members for their support, valuable input and advice. The views presented are those of the authors and not necessarily the views of CChIPS, CHOP, the NSF, or the IAB members.

This project would not have been possible without the guidance of my advisor, Dr. Sriram Balasubramanian, whose direction and support allowed me to persevere through this project, despite our many challenges and setbacks.

I am grateful for the Biomedical Engineering faculty on my committee, Dr. Seliktar and Dr. Papazoglou, for their time commitment and insightful feedback.

I would like to thank Dr. Sorin Siegler from the Mechanical engineering department for being on my committee, as well as allowing me to use his computer lab for the entire duration of this project and for granting me access to Analyze software. Dr. Siegler has also given me invaluable guidance and support during this project.

I would like to sincerely thank all of my colleagues at The Children's Hospital of Philadelphia's Center for Injury Research and Prevention; Dr. Kristy B. Arbogast and Matthew R. Maltese continually offered their expertise and guidance and allowed me to gain understanding in the area of injury biomechanics. I am grateful for the help of Thomas Seacrist who spent many hours teaching and explaining MATLAB coding to me. I am also grateful for the help of Dr. Felipe García España for guiding me through the statistics of this project. And I am thankful for the other students on this project, Brynn Thallner, Sohaib K. Hashmi and Robin Stevenson, whose hard work in the lab made the completion of this project possible. It was an honor to work with all of you.

I would also like to thank Dr. Sabah Servaes for helping us with IRB, obtaining CT scans and being available to answer any questions we had.

I am grateful for the help of John Capone, who made himself available to help me navigate through ProEngineer.

Lastly, I would like to thank my family, friends, and anyone who supported me in any way during the completion of this project.

Table of Contents

List of Tables

List of Figures

Abstract

Age-related Changes in Geometric Characteristics of the Pediatric Thoracic Cage and Comparison of Thorax Shape with a Pediatric CPR Manikin

Amanda R. Comeau

Sriram Balasubramanian, Ph.D.

Pediatric cardiopulmonary resuscitation (CPR) manikins are currently used as training devices to simulate resuscitation methods for treating pediatric cardiac arrest or airway obstructions. In order for these manikins to meet clinically regulated CPR delivery guidelines and to function as effective surrogates, pediatric CPR manikins should have geometric and mechanical characteristics that are similar to pediatric human subjects. The objectives of this study were to (1) quantify the detailed geometric characteristics of the pediatric thoracic cage by using computed tomography (CT) scans obtained from pediatric human subjects, and (2) to compare the thorax shape of a pediatric CPR manikin (Little Junior CPR manikin, Laerdal, Stavanger, Norway) with a six year old pediatric human subject. Thorax CT scans were obtained from one, three, six, 10 and 18 year old male subjects (5 subjects per age group). Anatomical landmarks on the thoracic cage, such as costochondral junction, tubercle, external surface of the rib shaft etc., were digitized and a custom MATLAB code was created to compute the geometrical characteristics based on the Cartesian coordinates of these points. The key computed parameters include rib length, rib angle, longitudinal twist of the ribs, and radius of curvature of the ribs. Age-specific differences were observed in the pediatric thoracic structure in many of the computed parameters. The comparison of the outer thorax surface of the pediatric CPR manikin and a six year old child was performed in ProEngineer (Parametric Technology Corporation, Santa Clara, CA). Differences were observed in the overall thorax shape between the pediatric CPR manikin and the pediatric human subject. These shape comparisons indicate a need to modify the design of the pediatric CPR manikin thorax to be more representative of the pediatric human thorax.

Chapter 1: DETAILED PEDIATRIC THORACIC CAGE GEOMETRY

1.1 Background

1.1.1 Anatomy of the thoracic cage

The thorax is comprised of the thoracic cage (also called the rib cage), surrounding muscle, skin and subcutaneous fat, and the underlying soft tissue organs. The rib cage, an osseo-cartilaginous cage, consists of 12 pairs of ribs, 12 thoracic vertebrae and the sternum (Figure 1). The ribs attach to the sternum by means of 'costal cartilage', which extend from the anterior ends of ribs. The first seven ribs are called 'true ribs' as their costal cartilage connects directly to the sternum while ribs eight through ten are called 'false ribs' as their cartilage attaches to the costal cartilage immediately above. Eleventh and twelfth ribs are called 'floating ribs' as they are connected only to the thoracic vertebrae and not to the sternum or any rib cartilage. The costal cartilage of rib one curves downward and medially; cartilage of two is horizontal; cartilage of three and four, are straight and directed upward and medially; cartilage of ribs five through eleven curve upward and medially. Except for the first two ribs, the cartilage tapers medially, especially ribs eight through twelve, which are pointed. The costal cartilage attaches to the ribs and sternum at the costochondral and chondrosternal junctions, respectively.

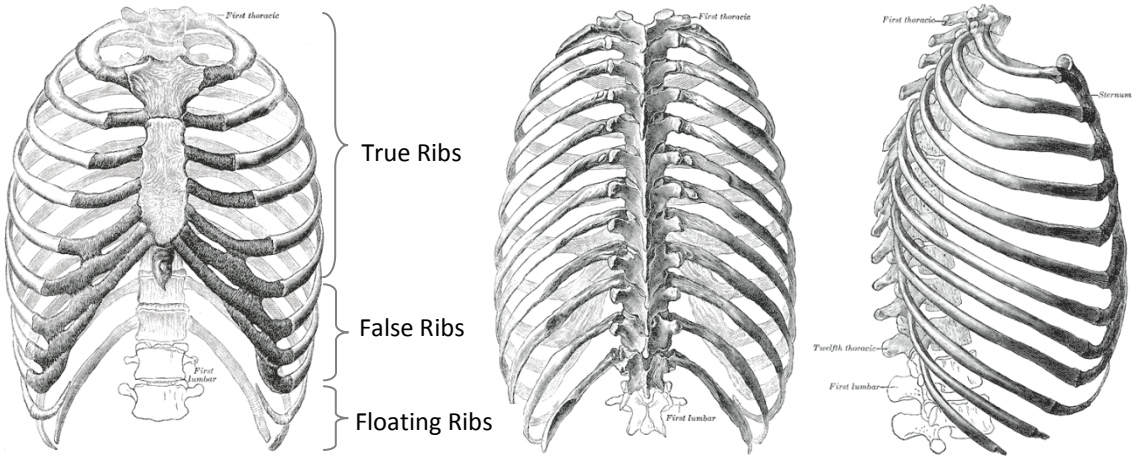

(a) (b) (c)

Figure 1: (a) Anterior, (b) Posterior, and (c) Lateral views of the Rib cage.

1.1.2 Anatomy of the thoracic musculature and soft tissue surrounding the rib cage

The anterolateral muscles of the thorax include internal and external intercostals, the diaphragm, internal and external obliques, pectoralis major and minor, serratus anterior, and the rectus abdominus. There are 11 pairs of internal intercostals muscles, whose function is to move adjacent ribs towards each other during exhalation to decrease the size of the thoracic cavity. These muscles are located in the intermediate layer of the intercostal spaces and have fibers that run at a right angle to the external intercostal muscles. The external intercostals (also 11 pairs) are found in the superficial layer of the intercostal spaces. They elevate ribs during inhalation and assist in expanding the chest during breathing. The fibers run anteriorly and interiorly from the top rib to the bottom rib (Tortora and Nielsen, 2009).

The diaphragm is an internal muscle that separates the thoracic and abdominal cavities. Its major role is to power breathing, however it also helps return venous blood to the heart and increase intra-abdominal pressure during urination and defecation. The internal and external obliques are the intermediate and superficial muscles respectively of the abdomen and lower thorax. They work together bilaterally to compress the abdomen and flex the vertebral column. The pectoralis major is the superficial muscle of the superior thorax. It is a thick, fan-shaped muscle that assists in movement and rotation of the arm and shoulder. The pectoralis minor lies just below the pectoralis major. The serratus anterior is found beneath the pectoralis muscles and covering the intercostals for the superior eight or nine ribs. These muscles are important in horizontal arm movement such as pushing and punching. The rectus abdominus starts at the pubic crest and extends to the cartilages of ribs 5-7, and assists in vertebral column flexion, especially in the lumbar region (Tortora and Nielsen, 2009).

The posterior muscles of the thorax include the trapezius, deltoids, infraspinatus, teres major and minor and the latissimus dorsi. All of these muscles assist with movement and rotation of the arms and shoulders. There are also complex muscles of the neck and back that move the vertebral column (Tortora and Nielsen, 2009). Extraneous to the rib cage is a layer of adipose tissue covered by skin. A transverse cross-section diagram of the thorax and muscles is shown in Figure 2.

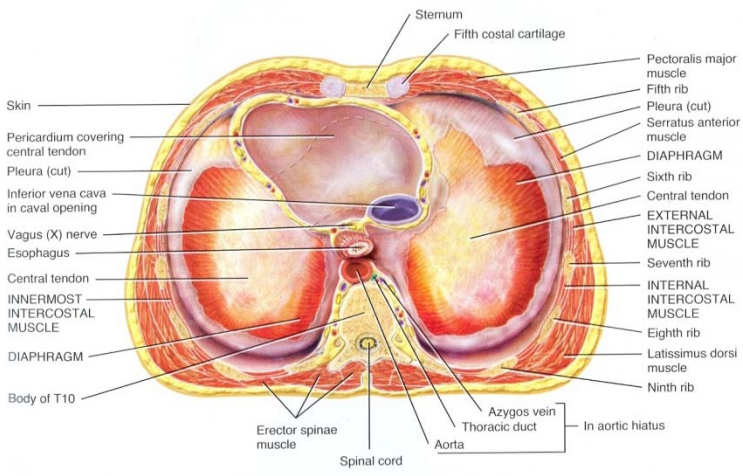

Figure 2: Superior view of the thorax. (Image from Tortora and Nielsen, 2009)

1.1.3 Thoracic cage evaluation through Imaging

Clinical evaluation of the thorax is performed using a variety of imaging techniques such as chest radiography (CXR), Computer tomography (CT), Magnetic Resonance Imaging (MRI). Three dimensional (3D) reconstructed CT images from the axial datasets may prove useful (Alkadhi et al., 2004) in examining the three dimensional geometry of the thoracic cage. Recent advances in CT imaging techniques offer much better resolution for delineating the 3D reconstructed thoracic cage for better image quality of the bony ribs and costal cartilage. While CT requires shorter scanning time per section and has less image degradation due to motion related artifacts, MRI is a modality with higher contrast resolution compared to CT, thus making it more suitable for soft tissue differentiation and characterization (Kangarloo, 1988).

1.1.4 Changes in the thoracic cage structure with age

The age-related changes in thoracic structure and function in the adult population have been extensively studied using imaging methods such as CXR, CT, MRI and Positron Emission Tomography (PET) (Gayzik et al., 2008; Givens et al., 2004; Kent et al., 2005; Wehrli et al., 2007; Well et al., 2007). Specifically, for the adult human, the rib cage dimensions (Fujimoto et al., 1984; Nussbaum et al., 1996), the shape and cross-sectional geometry of the ribs (Mohr et al., 2007; Takahashi et al., 1966; Yoganandan et al., 1998) and the chest wall thickness (Givens et al., 2004) have been comprehensively studied. Mohr et al. (2007)

reported detailed rib biometrics for adults such as the apparent rib curvature, longitudinal twist along the diaphysis, unrolled curvature of the outer cortical surface, cross-sectional geometry (height and width) of the ribs along their length, cortical thickness and area of the cortical and medullary canal.

However, there is very limited data in the literature on the age related changes in pediatric thorax geometry. Inspection of the torso maturation process reveals the substantial amount of time required for bones in the rib cage to appear and fuse. The sternum consists of six main bones – the manubrium superiorly, followed by sternebrae one through four and the xiphoid process (Figure 3). The 4th sternebra appears at age 12 months, while the xiphoid process appears at 3 to 6 years. Fusing between sternebrae begins at age 4 years and continues through age 20 years. The sternum as a whole descends with respect to spine from birth up until age 2 to 3 years, causing the ribs to angle downward when viewed laterally, and the shaft of the rib to show signs of axial twist deformation (Scheuer and Black, 2000).

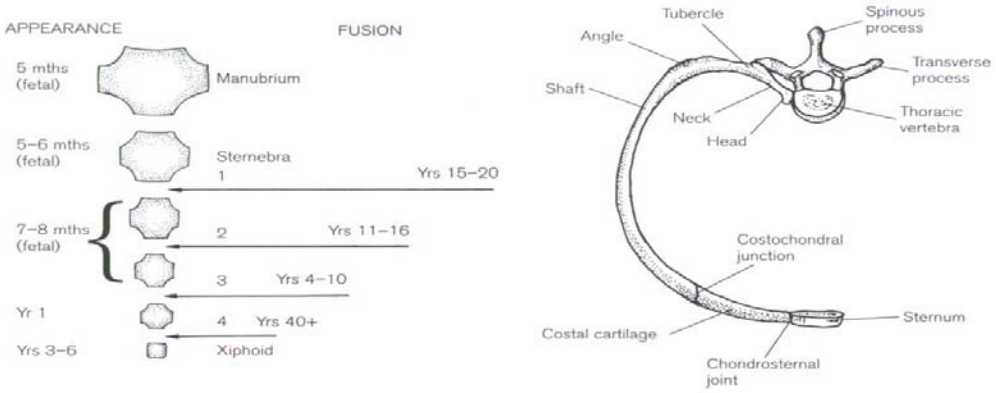

(a) (b)

Figure 3: (a) Development of the sternum and (b) the typical thoracic rib.(From Scheuer and Black, 2000)

Openshaw et al. (1984) analyzed chest radiographs (from 38 individuals aged 1 month to 31 years) and CT scans (from 28 individuals aged 3 months to 18 years) and reported that infants and very young children (<2 years) have a more horizontal rib angles and higher sternal clavicular heads and diaphragmatic domes than older children and adults. Also, the cross sectional chest shape was observed to change from the rounded infantile form to the more ovoid adult form by the age two. This age-related shape change was quantified by Doershuk et al. (1975) (Dean et al., 1987) using the Thoracic Index (TI), which was defined

as the ratio of the anteroposterior diameter of the chest to its lateral diameter (Table 1). If the value of TI is closer to one, it indicates a circular cross-section, while a value closer to zero indicates an oval cross-section.

Table 1: Thoracic dimension of human subjects – Adapted from Dean et al., 1987

	Lateral Diameter, cm	Anteroposterior Diameter, cm	Thoracic Index (TI)	Shape change
Newborn-1 mo	10	7.5	0.75	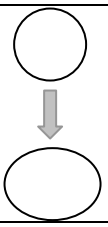
1-15 mo	14	9	0.64	
18 mo	15.5	10	0.64	
6-8 yr	19	11.5	0.60	
12-14 yr	25	14.5	0.58	
Adult	28	16.5-18	0.59-0.64	

Grivas et al. (1991) studied the posteroanterior chest radiographs obtained from 412 children in three age groups: infancy (0-2.999 years), childhood (3-10.999 years) and puberty (11-17.999 years). They reported the 'Thoracic ratios (TRs)', defined as the ratio of the 'distance between the middle of each thoracic vertebral body (T1-T12) and the lateral borders of the corresponding thoracic segment' to the 'total distance measured between the distal end plates of T1 and T12 (Figure 4). Between childhood and puberty, boys showed little to no change in TRs. However, girls displayed a relative narrowing of the lower chest (T7-T12) but little or no change in the upper chest (T1-T6). During infancy, no significant differences in TR were observed between genders. In childhood, girls were reported to have narrower chest at the left T6 to T10 levels, compared to boys. In puberty, however the narrower chest of girls was exhibited at most levels. The greater slenderness of the female thorax is consistent with the slenderness of the female vertebrae compared with the male (Glasbey, 1983; Schultz et al., 1984).

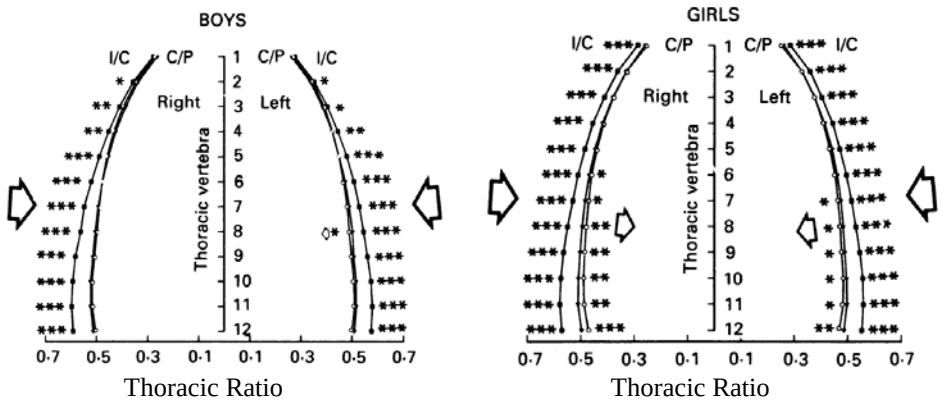

Figure 4: Thoracic ratios for boys and girls plotted by age group (infancy, childhood and puberty). I/C, infancy/childhood; C/P, childhood/puberty. ■, infancy; ▼, childhood; ○, puberty. * $0.01<p<0.05$; ** $0.001<p<0.01$; *** $p< 0.001$ (from Grivas et al., 1991)

The ribs are relatively soft and flexible in children; becoming progressively stiffer with increasing age. The costal cartilage also calcifies with age, likely influencing its flexibility. Also using frontal chest X-rays, the average ratio (L_C/L_R) of the breadth of the costal cartilage at a particular rib level (L_C) to the breadth of the rib (L_R) was found to be 0.55 for ribs two through five for subjects aged six and 18 years old (Hamilton et al., 1986). This provides evidence that the ossification of the ribs in the sternal region is complete before age six. More recently, Chang et al. (2007) performed 3D reconstructions of multislice CT images in pediatric subjects following Ravitch thoracoplasty, and quantified the volume of ossification in the costal cartilage by the removal of the bony thoracic cage at proper software window settings.

Total body fat content has been well characterized in the literature for the pediatric population (Brook, 1971; Durnin and Rahaman, 1967; Taylor et al., 1997); however measurements of chest wall thickness and thoracic subcutaneous fat and muscle layers throughout the thoracic structure in the pediatric population are limited. Skin and subcutaneous fat layer and thoracic muscle thickness have been studied in a limited population using chest radiographs and chest x-rays (Garn et al., 1959; Lagundoye, 1974). A study by Garn et al., 1959 measured fat thickness at the 10^{th} rib and compared it to body size for Ohio-born children age 1.5-17.5 years. While the correlations between fat thickness, size and skeletal age were reported, the data for fat thickness was not reported. Another study measured the thickness of the skin and subcutaneous fat layers, as well as muscle thickness for well-nourished and malnourished Nigerian children ages 1.5-8 years (Lagundoye, 1974). Thickness of the skin, fat and muscle was measured just below the 9^{th} and 10^{th}

ribs. In well nourished children, the mean total soft tissue thickness, subcutaneous fat thickness and muscle thickness were reported to be 5.74 ±1.58 mm, 2.93±1.67 mm and 2.69±0.83 mm respectively. To our knowledge, no other studies have been done in the pediatric population to characterize the soft tissue distribution surrounding the thoracic cage.

1.1.5 Limitations of current literature for pediatric thoracic geometry

There is paucity of detailed documentation of the age related anatomical changes in the pediatric thorax. Several studies on anatomical variations in the adult thorax have reported the geometric parameters of the ribs in great detail (Mohr et al., 2007; Gayzik et al., 2008). Detailed information on the intrinsic rib geometry does not exist in the pediatric literature. There is also very limited documentation of the quantitative relationship between age and the skeletal changes that occur during the maturation process of the torso, such as fusion of the various bones of the sternum and axial twist of the ribs (Scheuer and Black, 2000).While the current pediatric thorax literature provides a basic understanding of the global developmental changes in the rib cage, the lack of detailed pediatric thoracic geometry data might result in a poor understanding of the constitutive anatomy of the thoracic structures, and thereby lead to the inappropriate design and development of pediatric models. So, there is a need to obtain comprehensive data on the morphological changes in the bony geometry and material distribution of the pediatric thorax.

1.2 Objective

Since there is a paucity of data for age-related changes in the pediatric thoracic cage, the primary objective of this study was to quantify the three-dimensional structural characteristics (example: bony geometry) of the pediatric thoracic cage for male subjects ages 1, 3, 6, 10 and 18 years. To achieve this objective, CT scans of the thorax were used to measure rib cage parameters. Once these parameters are available, they can be used to advance clinical, medical device development and thorax injury response applications.

1.2.1 Design Criteria

1. Determine age related differences in the shape of the thoracic cage – the parameters used in the study should characterize the detailed geometry of the ribs, spine and sternum. The parameters used should also be practical to implement in a variety of applications.

1.2.2 Constraints

1. Use of medical imaging data – Due to the several ethical and logistic challenges associated with the use of pediatric cadavers, it is difficult to obtain data from pediatric cadaveric rib cage specimens. It would be more feasible to use data obtained from CT or MRI scans already obtained from normal pediatric human subjects.
2. Retrospective study – A prospective study that would allow us to pick specific subjects would be too costly and require a long time period to recruit and test subjects. It may also increase potential risk to human subjects. A retrospective study design would allow us to lower the cost, time and risk to subjects, however it limits the number of evaluable subjects.
3. Use of medical image analysis software – Developing a custom-code to analyze CT scan data would be very expensive and time-intensive. Due to limitations in the project duration and the amount of funding available for the project, a generic software (Analyze, Mayo Clinic's Biomedical Imaging Resource, Rochester, MN) which was available at Drexel University was used for CT scan analysis.

1.2.3 Study Design

After obtaining Institutional Review Board (IRB) approval at CHOP, CT scans with good image quality and multiple anatomical views were selected from normal subjects. Five male subjects were selected from each of the 1, 3, 6, 10 and 18 year old age groups, for a total of 25 subjects. Coronal, sagittal and transverse views of each scan were then merged in Analyze Software (Mayo Clinic's Biomedical Imaging Resource, Rochester, MN) to view and render high pixel count three-dimensional images of the rib cage. Several bony anatomical landmarks on the thoracic cage (such as the costochondral junction, tubercle, and outer surface of the rib shaft) were digitized and used in a custom MATLAB (The MathWorks Inc., Natick, MA) code to compute geometric parameters. Some of the key computed parameters include the lengths, angles and curvatures of each of the ribs, as well as lengths and angles of the spine and sternum. A detailed list of these parameters is provided in Table 2.

1.3 Methods

1.3.1 Subjects

The Normal Radiology database consists of patients presenting to The Children's Hospital of Philadelphia (CHOP) who received chest CT and MRI exams for indications of lymphoma, sarcoma, CCAM, sequestration, emphysema, cystic fibrosis, and pneumonia but were deemed normal. For this study, normal CT scans of pediatric subjects already obtained using standard clinical protocol (Appendix 1) were used. Five scans were selected for 1, 3, 6, 10 and 18 year old males for a total of 25 cases. The detailed subject anthropometry are provided in Table 3. Scans with motion artifacts, abnormal posture, skeletal and soft tissue pathologies such as scoliosis, bony tumors, osteochondral bone lesions etc. were excluded.

1.3.2 Data Collection and Analysis Summary

The CT images were obtained using Siemens Somatom Sensation scanners and Siemens Avanto / Sonata scanners (Siemens Medical Solutions USA, Inc, Malvern, PA). A sample chest CT scan obtained from a pediatric subject is shown in Figure 5.

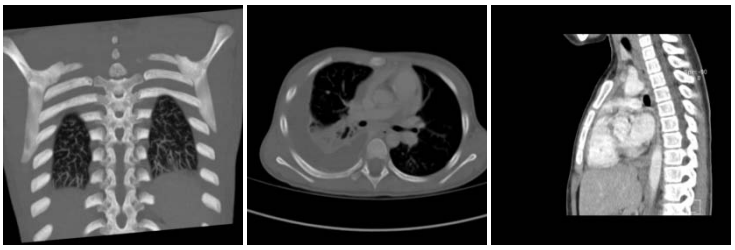

Figure 5: Sample chest CT images of a pediatric subject in the (a) coronal, (b) transverse and (c) sagittal views.

The images were saved as DICOM format in the Picture Archiving and Communication System (PACS) and were processed using specialized software (Analyze, Mayo Clinic's Biomedical Imaging Resource, Rochester, MN) to visualize and render 3D images of the thoracic cage. Previous studies have established the feasibility of this approach for the 3D reconstruction of the thoracic cage (Gayzik et al., 2008; Kent et al., 2005). Analyze software was provided by Dr. Sorin Siegler from the Mechanical Engineering department at Drexel University. Before usable scans were selected, they were viewed in Analyze to

confirm that the entire ribcage was scanned and that all anatomical features could be located. Also, the selection criteria for usable scans would require the subjects to have their age, height, weight, body mass index (BMI) and body surface area (BSA) recorded in the CHOP electronic health record system. Subjects in the 5^{th} – 95^{th} percentile ranges for height, weight and BMI were included in this study. Chest depth (anterior-posterior distance at the middle of the torso), and chest width (lateral distance of the torso at the nipple line) were also calculated and recorded for each subject using their CT scans.

Following the rendering of the rib cage, anatomical landmarks on the thoracic cage, such as the costochondral junction, tubercle and external surface of the rib shaft were digitized using Analyze software. A custom MATLAB (The MathWorks Inc., Natick, MA) code was created to compute the geometrical characteristics based on the Cartesian coordinates of the digitized points.

Statistical analysis for all measurements was performed using SPSS (SPSS Inc, Chicago, IL). Age group comparisons were performed using ANOVA and post-hoc tests. All tests were two-sided and the experiment wise error was held at the 0.05 level. There were no p-value corrections for multiple comparisons because of the small sample size and preliminary nature of the data. Means and standard deviations for all measured variables were also calculated.

1.3.3 Digitizing points from CT scans

After obtaining the CT scans from CHOP, the DICOM images from individual subjects were imported into Analyze software using the DICOM Tool. Coronal, transverse and sagittal views for each subject were uploaded into the Analyze workspace, and fused using the 3D Voxel Registration option, found in the Register option on the main toolbar. These files were then saved as Analyze AVW files for later use in Analyze.

As a first step in processing the chest CT scan data, a threshold (ranging from70 to100 Hounsfield units) was applied to each subject to obtain a 3D reconstructed image of the bony structures of the rib cage. The complete list of steps are provided in Appendix 2. Figure 6 shows a 3-D reconstructed view of the thoracic cage before and after clipping the scapulas and upper extremities.

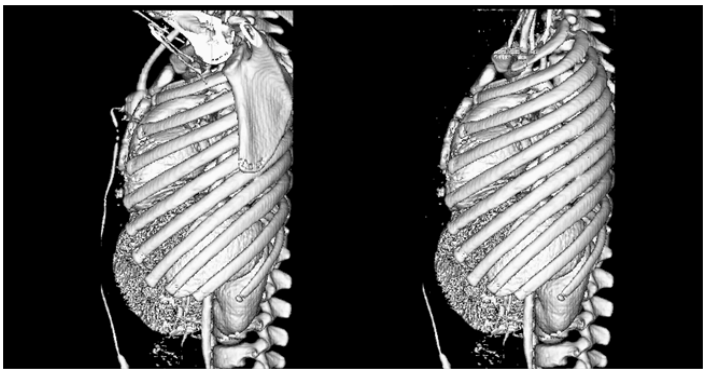

Figure 6: 3-D reconstructed view of a 6 year old thorax before and after the scapulas and upper extremities are clipped.

Each rib digitization consisted of three lines of points starting at the costochondral junction and ending at the tubercle. A linear sequence of points was placed evenly along the outer surface of each rib - one along the top margin of the rib shaft, one along the bottom margin of the rib shaft, and one along the middle. A lateral and posterior view of points placed along the rib shaft is shown in Figure 7. Points were also placed on the spine and sternum as described in Appendix 3.

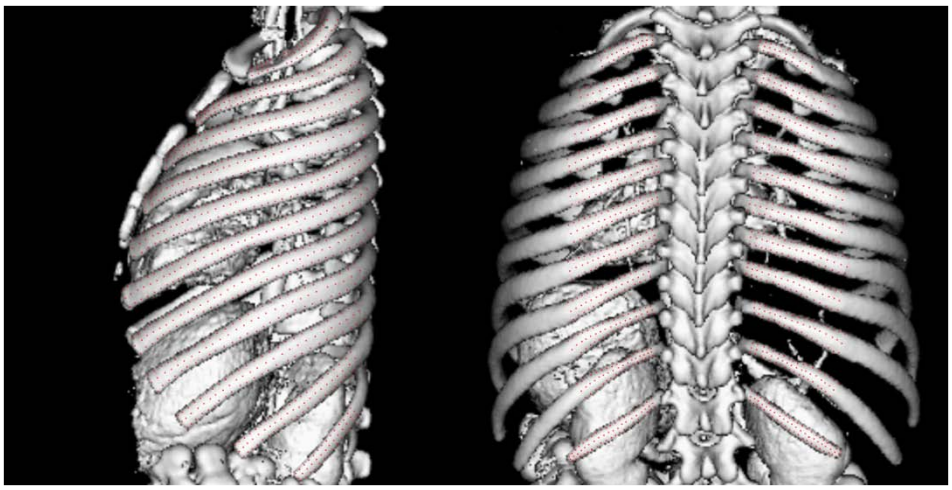

(a) (b)

Figure 7: (a) Lateral and (b) Posterior views of points (shown as red dots) placed along the rib shaft in Analyze.

1.3.4 Rib geometry calculations

A custom MATLAB code was used to process the Cartesian coordinates, scale the data set appropriately, calculate ribcage parameters, and output the calculated data. The MATLAB code is given in Appendix 4. The parameters calculated by the MATLAB code are listed in Table 2.

Table 2: List of measured parameters obtained from 3D reconstruction of the pediatric thoracic cage at all thoracic vertebrae levels

Imaging Modality	Measured Parameter
CT	- Rib Length - Segmental Thoracic Index - Radius of Curvature and Apparent Rib Curvature - Longitudinal Twist of the Ribs - Lateral Rib Angle - Curvature of the Sternum - Length and Width of the Manubrium and Sternum Body - Length and Curvature of the Thoracic Spine - Cobb Angle of the Thoracic Spine - Height, Width and Depth of Thoracic Vertebral Bodies - Polynomial Coefficients for each rib

The CT scans from PACS were received in the DICOM format with no scaling information. However during a CT scan, the volume is automatically scaled and a scale bar is generated on each slice of the volume. To address this issue, we used a 3D medical imaging software (Aquarius iNtuition, TeraRecon Inc., San Mateo, California) to measure the height and depth of the vertebral bodies. This location was chosen because it was the simplest measurement to take from each scaled CT scan that corresponded to a measurement that the MATLAB code already calculated. A scale factor was found for the height and depth of four vertebral bodies (thoracic levels 1, 4, 8 and 12) by dividing the actual length of the vertebral body by the calculated length. The average scale factor was then found and used as the overall scaling factor. Multiple lengths were found and the scale factor averaged to try to account for small errors in height and depth measurements. The entire data set for each subject was then multiplied by this overall scale factor to obtain data corresponding to the actual size of the subject.

The Cartesian coordinate points for each subject were moved to a coordinate system whose origin was the posterior tip of the spinous process of the first thoracic vertebrae. For the data analysis, a right-hand coordinate system was defined as the positive X-axis pointed forward, positive Y-axis pointed leftward and the positive Z-axis pointed upward (Figure 8).

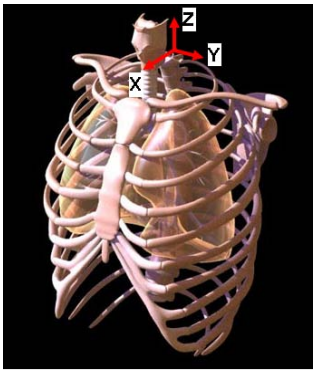

Figure 8: Right-hand coordinate system used for ribcage analysis with the origin at the posterior tip of the spinous process of the first thoracic vertebrae.

Regardless of the number of points originally selected along the rib surface, numerical interpolation was performed in MATLAB for generating 300 points for each rib. The points corresponding to the 10% to 90% of the rib length in 10% intervals were calculated. The tubercle was defined as being 0% of the rib length, and the costochondral junction was defined as 100% of the rib length. Parameters such as the radius of curvature, apparent curvature and longitudinal twist for each rib were calculated at 10% increments.

After the data for each subject were scaled appropriately and the 10-90% sites were determined, calculations were performed in MATLAB for each of the parameters listed in Table 2. These results from MATLAB were output to a Microsoft Excel document corresponding to the age of the subject. A detailed description of each computed parameter is provided below:

- Rib Length – Rib length was calculated using the interpolated middle line of points at each rib level, so the number of points per rib (n) was equal to 300. The formula for the three-dimensional distance between two points was applied and summed over the entire length of each rib.

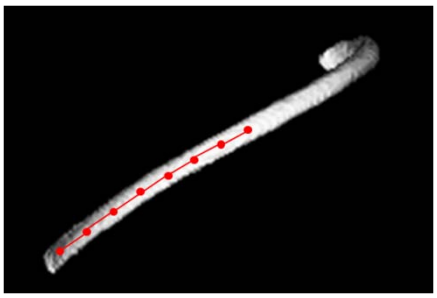

$$Rib\ Length = \sum_{i=2}^{n} \sqrt{(x_i - x_{i-1})^2 + (y_i - y_{i-1})^2 + (z_i - z_{i-1})^2}$$

Figure 9: Rib length calculation using the middle line of each rib.

- Segmental Thoracic Index– This parameter was defined as the anteroposterior distance of the chest divided by the lateral distance of the chest (Dean et al., 1987) measured at the level of the axilla. Thoracic index (as reported by Dean et al., 1987) was based on external chest measurements, however the parameter reported in the current study was calculated for each rib level using the middle line of points. It was calculated using the most anterior and posterior points to define the anteroposterior distance in the plane of the rib, and the most lateral points on the left and right to calculate the lateral distance. A value of thoracic index close to one indicates a more circular shape, while a value closer to zero indicates an oval shape. Figure 10 shows a diagram of how thoracic index was calculated at each rib level.

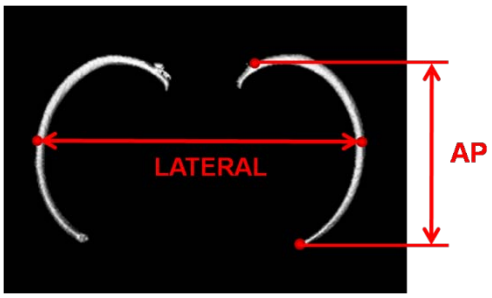

Figure 10: Thoracic index calculated by dividing the anteroposterior (AP) direction by the lateral distance.

- Radius of Curvature and Apparent Curvature – The radius of curvature (R) was computed at each percentage site for each rib level in the x-z plane by fitting a circle through three points (Mohr et al., 2007) and finding the radius using the Side-Side-Side (SSS) theorem of similar triangles. Point P2 (opposite of side c in Figure 11) defines the percentage site that is being measured. Points P1 and P3 are located plus and minus 5% of rib length from point P2. The apparent curvature (C_A) was defined as the reciprocal of the radius of curvature (Mohr et al., 2007). For example, a large circle would have a higher radius of curvature and therefore would be less-curved and subsequently have a lower apparent curvature.

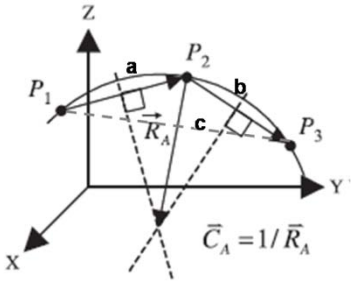

$$s = \frac{1}{2} \cdot (a+b+c)$$

$$K = \sqrt{s \cdot (s-a) \cdot (s-b) \cdot (s-c)}$$

$$R = \frac{(a \cdot b \cdot c)}{4K}$$

Figure 11: Diagram showing the radius of curvature and apparent curvature calculations. Formulas used are from the SSS theorem. a, b and c represent the lengths of each side of the triangle connecting the three points P1, P2 and P3.

- Longitudinal Twist of the Ribs– Longitudinal twist was defined as the angle the outer surface of the rib makes with the vertical (Mohr et al., 2007) and was computed at 10-90% intervals for each rib level. The line connecting the top and bottom points at each site is made in the y-z plane. The angle between this line and the z-axis is the longitudinal twist. A positive angle indicates an inward twist and a negative angle indicates an outward twist.

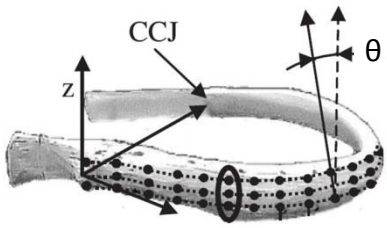

Figure 12: Longitudinal twist calculation shows the direction of twist of the rib surface.

- Lateral Rib Angle– Lateral rib angle was computed as the angle made by a line connecting the point at 0% (tubercle) and at 100% (costochondral junction) projected onto the sagittal plane and the z-axis (vertical) (adapted from Kent et al., 2005). A greater angle indicates a more horizontal rib.

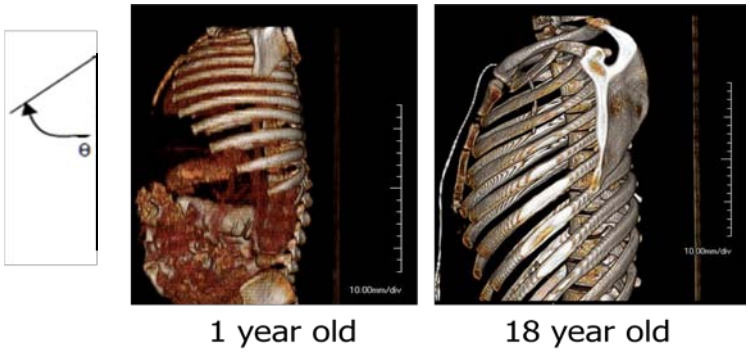

Figure 13: Example of the differences in rib angle between a 1 year old and an 18 year old.

- Length and Curvature of the Sternum and Thoracic Spine – The length of both spine and sternum were approximated using the formula for the length of a line. For the spine, line segments were made through the middle points of the sagittal measurements of the vertebral bodies and added together. For the sternum, the points placed along the anterior surface were connected with line segments, and the lengths of these segments were added together. The curvature was then found using the formula:

$$\theta = \frac{360L}{2\pi r}$$

- Cobb Angle of the Thoracic Spine – To calculate Cobb angle, based on a sagittal image of the thoracic spine, lines are extended from the superior surface of thoracic vertebral body three and the inferior surface of thoracic vertebral body nine until they intersect. Then, perpendicular lines are extended from these lines until they intersect. The Cobb angle is the smaller angle made between these lines (Goh, 2000). Cobb angle has been used to diagnose scoliosis in children (Goh et al., 2000).

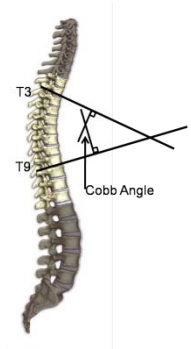

Figure 14: Diagram of the Cobb angle (Goh et al., 2000)

- Length and Width of the Manubrium and Sternum Body – From the antero-posterior view, a horizontal line was placed at the widest location of the sternum and manubrium. A vertical line was placed from the horizontal line to the bottom point of the sternum or manubrium.

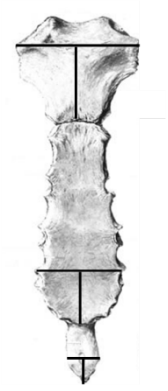

Figure 15: Diagram of sternum and manubrium measurements.

- Height, Width and Depth of the Thoracic Vertebral Bodies – The height and depth of each thoracic vertebral body were found using the vertical middle points taken from the sagittal view of the spine. The width was found using the horizontal middle points taken from the coronal view of the spine.
- Polynomial coefficients for each rib – The coefficients of a 2^{nd} order polynomial equation fitting each rib was found for every subject using the polyfit command in MATLAB. The polyfit command returns polynomial coefficients of a specified degree that fits data in one dimension using the method of least squares. Polynomial coefficients were found for each dimension X, Y and Z.

1.4 Results

1.4.1 Subject Anthropometry

Anthropometry data for all the 25 subjects evaluated is shown in Table 3. Height, weight and body surface area (BSA) were taken from hospital charting software on the date corresponding to the CT scan. Body mass index (BMI), and height and weight percentages were calculated using growth charts from the Centers for Disease Control (CDC) National Center for Health Statistics.

Table 3: Anthropometry measurements for all usable subjects (Percentages calculated from CDC Growth Charts (2000) Center for Disease Control and Prevention Growth Charts – Published May 30, 2000. http://www.cdc.gov/GrowthCharts/, 1 year old percentages calculated from http://www.cdc.gov/growthcharts/clinical_charts).

Subject #	Age (years)	Height (cm)	Height %	Weight (kg)	Weight %	BMI (kg/sq.m)	BMI %	BSA (sq.m)
1_1	1.17	84.0	99	11.28	75	-	-	0.51
1_2	1.10	72.0	7	9.4	16	-	-	0.43
1_3	1.27	78.5	78	10.8	61	-	-	0.49
1_4	1.21	72.0	7	11.1	70	-	-	0.47
1_5	1.25	72.0	7	8.8	6	-	-	0.42
3_1	3.14	93.3	22	13.9	34	16.1	54	0.60
3_2	3.04	92.6	24	15.4	72	18.0	93	0.63
3_3	3.34	93.3	16	15.3	60	17.6	90	0.63
3_4	3.47	97.8	44	16	68	16.7	77	0.66
3_5	3.52	97.2	33	14.6	34	15.5	38	0.63
6_1	6.45	114.1	18	21.5	44	16.5	76	0.83
6_2	6.76	125.5	83	28.5	92	18.1	91	1.00
6_3	6.57	112.5	11	20.4	29	16.1	68	0.80
6_4	6.78	123.4	71	29.3	95	19.2	96	1.00
6_5	6.60	115.8	31	18	7	13.4	3	0.76
10_1	10.31	148.3	90	38.3	79	17.4	62	1.26
10_2	10.44	143.5	74	39.5	84	19.2	83	1.25
10_3	10.86	139.6	32	32.6	33	16.7	43	1.12
10_4	10.73	131.6	6	27.5	8	15.9	27	1.00
10_5	10.95	142.8	47	43.4	82	21.3	90	1.31
18_1	18.17	182.5	81	72.9	68	21.9	50	1.94
18_2	18.27	165.2	6	60.5	23	22.2	52	1.67
18_3	18.01	172.2	29	69.6	58	23.5	69	1.82
18_4	18.42	170.8	21	55.1	6	18.9	7	1.64
18_5	18.62	179.2	65	80.7	83	25.1	79	2

Chest depth and width were measured from CT scans and the results are shown in Table 4. The subjects highlighted in yellow represent the subject from each age group closest to 50th percentile for chest depth and width (Snyder et al., 1977). Scaling factors for each subject are shown in Table 5.

Table 4: Chest depth and width for all subjects. All values are in mm. The subjects highlighted in yellow are closest to 50th percentile for chest depth and width.

Subject #	A-P Distance (depth)	Lateral Distance (Width)
1_1	115.6	160.0
1_2	112.1	154.1
1_3	114.5	155.9
1_4	128.0	159.3
1_5	115.8	141.8
3_1	139.5	180.1
3_2	140.0	180.6
3_3	136.1	200.8
3_4	139.1	180.1
3_5	131.7	189.6
6_1	150.8	213.5
6_2	160.8	216.4
6_3	146.5	202.0
6_4	153.0	215.0
6_5	147.0	194.5
10_1	186.5	163.9
10_2	179.2	256.0
10_3	169.8	223.0
10_4	156.5	219.6
10_5	194.7	248.0
18_1	208.7	302.0
18_2	228.9	309.4
18_3	207.6	317.8
18_4	207.0	289.2
18_5	241.0	317.5

Table 5: Scaling factors for each subject determined by height and depth of vertebral bodies at thoracic spine levels 1, 4, 8 and 12.

Subject #	**Depth**				**Height**				
	T1	**T4**	**T8**	**T12**	**T1**	**T4**	**T8**	**T12**	**Average**
1_1	0.668	0.642	0.594	0.661	0.511	0.532	0.546	0.717	0.609
1_2	0.889	0.689	0.723	0.648	0.718	0.761	0.860	0.673	0.745
1_3	0.534	0.445	0.540	0.485	0.472	0.484	0.499	0.505	0.495
1_4	0.564	0.496	0.583	0.500	0.631	0.481	0.521	0.447	0.528
1_5	0.719	0.734	0.707	0.694	0.682	0.565	0.699	0.565	0.671
3_1	0.593	0.606	0.585	0.643	0.633	0.607	0.533	0.563	0.595
3_2	0.817	0.709	0.737	0.786	0.901	0.696	0.896	0.793	0.792
3_3	0.718	0.617	0.758	0.702	0.582	0.585	0.596	0.540	0.637
3_4	1.237	0.974	0.849	0.743	1.155	0.877	0.883	0.950	0.959
3_5	0.600	0.630	0.611	0.596	0.606	0.578	0.572	0.516	0.589
6_1	1.024	0.949	0.872	0.977	0.845	0.965	1.015	1.037	0.961
6_2	-	0.783	0.689	0.705	-	0.700	0.664	0.679	0.703
6_3	0.676	0.657	0.636	0.632	0.691	0.526	0.643	0.633	0.637
6_4	1.033	1.098	0.919	1.035	0.996	0.784	0.977	0.994	0.979
6_5	0.741	0.675	0.703	0.640	0.634	0.610	0.652	0.629	0.660
10_1	1.125	1.019	0.927	0.849	1.269	1.052	1.117	1.251	1.076
10_2	0.903	0.842	0.877	0.832	0.852	0.877	0.875	0.925	0.873
10_3	1.493	1.192	1.005	0.959	1.063	1.196	1.219	1.133	1.158
10_4	0.810	0.810	0.789	0.752	-	0.621	0.800	0.791	0.767
10_5	0.876	0.937	0.857	0.768	0.914	0.873	0.888	0.755	0.858
18_1	1.621	1.583	1.675	-	1.596	1.592	1.582	-	1.608
18_2	1.201	1.469	1.164	1.227	1.250	1.534	1.300	1.295	1.305
18_3	1.737	1.376	1.424	1.289	1.562	1.390	1.400	1.429	1.451
18_4	1.187	1.096	0.876	0.794	0.942	1.026	0.974	0.984	0.985
18_5	1.068	1.044	1.134	1.135	1.179	1.081	1.174	1.149	1.120

1.4.2 Rib cage parameters

The following results are obtained from the custom MATLAB code created (Appendix 2). Graphs were created using Microsoft Excel. All data is from the right side of the rib cage because analysis of the right and left ribs showed very little differences in results. Numerical data for each subject in each age group, as well as average and standard deviation for each age group, are reported in the data CD attached to this manuscript.

Rib length

Figures 16-20 show graphs for rib length by age group. Each graph shows rib length for each subject for each rib, as well as the average rib length and standard deviation for the age group.

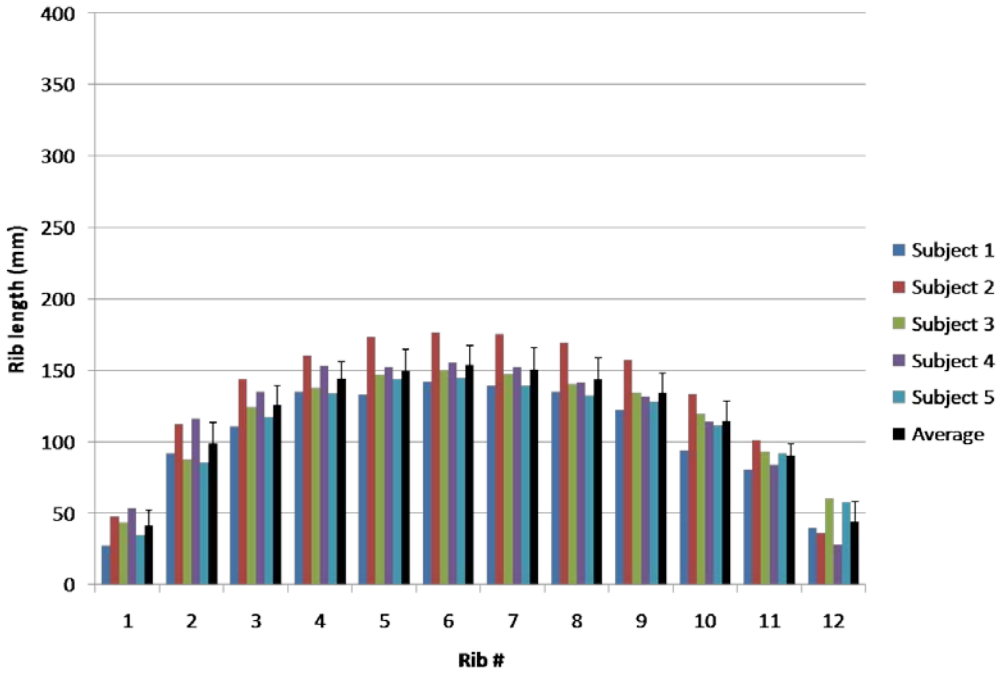

Figure 16: Rib length for 1 year olds for ribs 1-12.

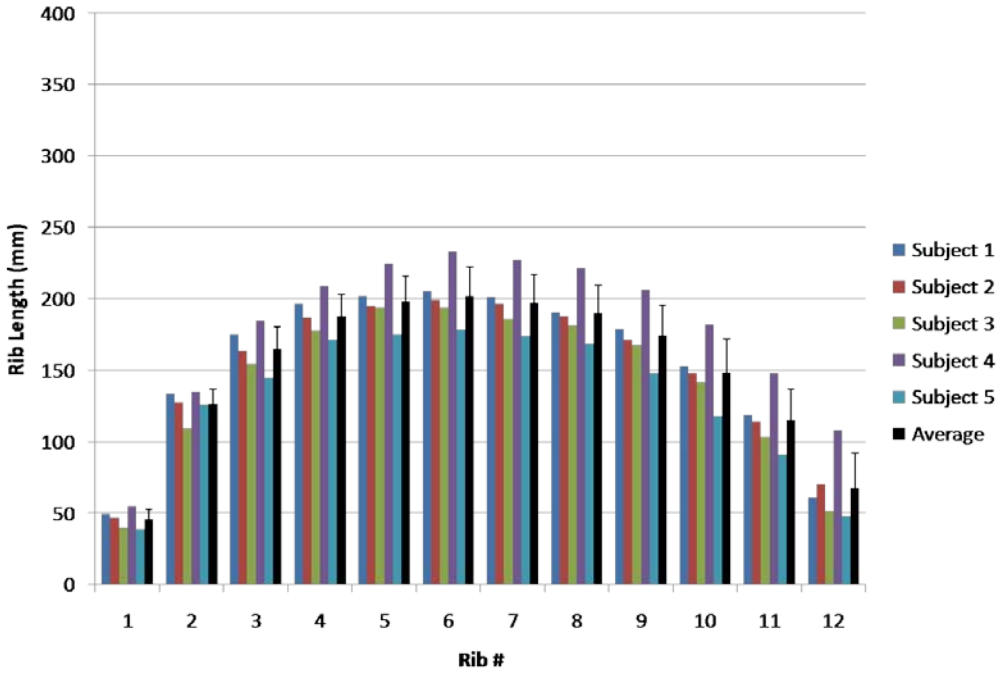

Figure 17: Rib length for 3 year olds for ribs 1-12.

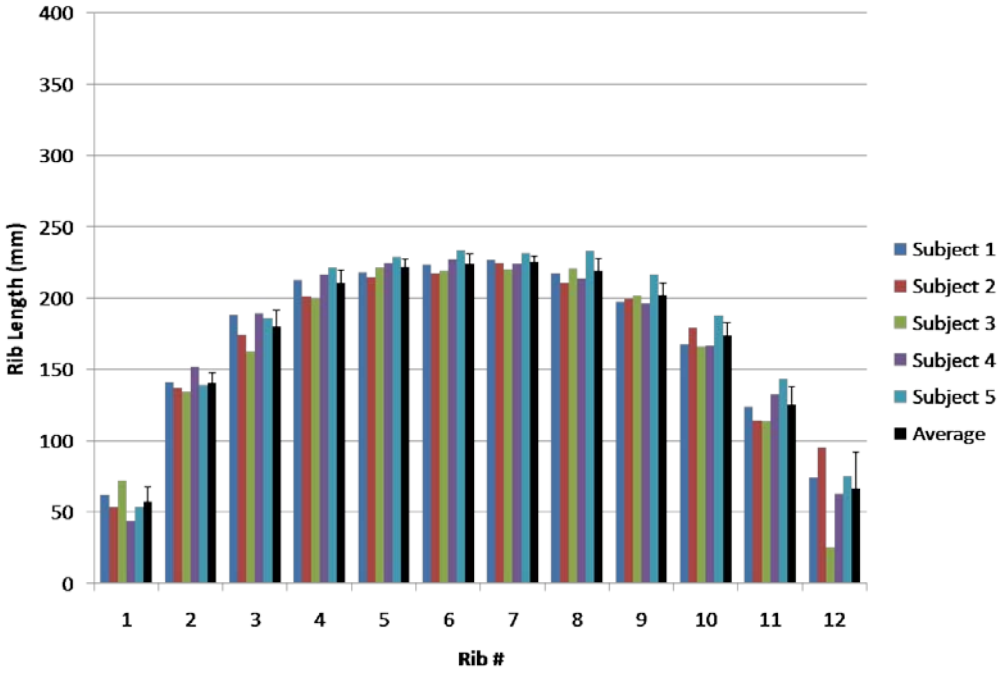

Figure 18: Rib length for 6 year olds for ribs 1-12.

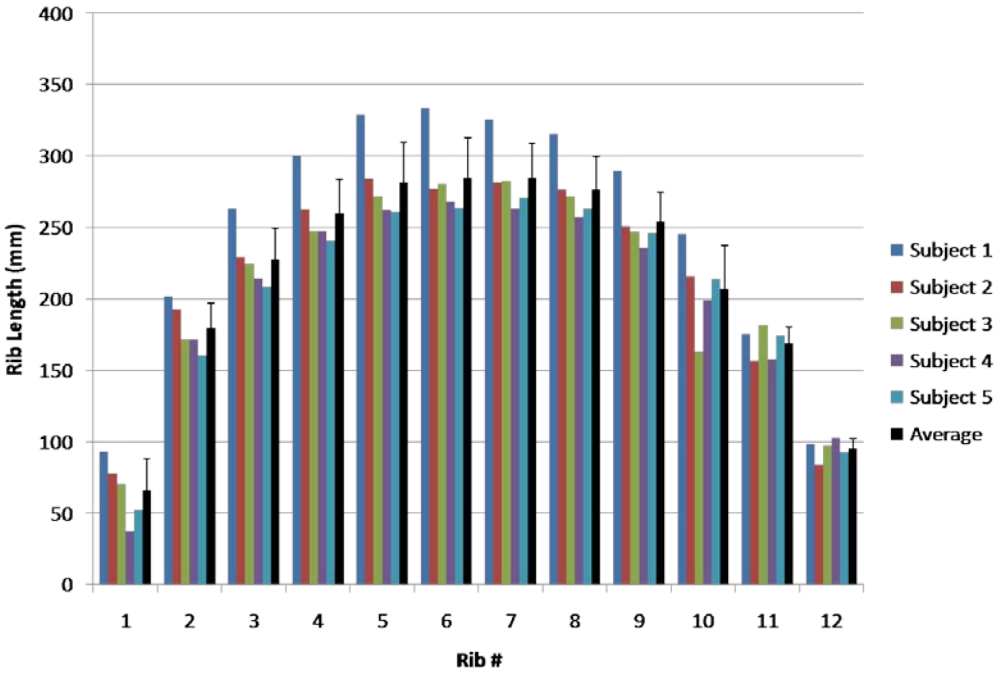

Figure 19: Rib length for 10 year olds for ribs 1-12.

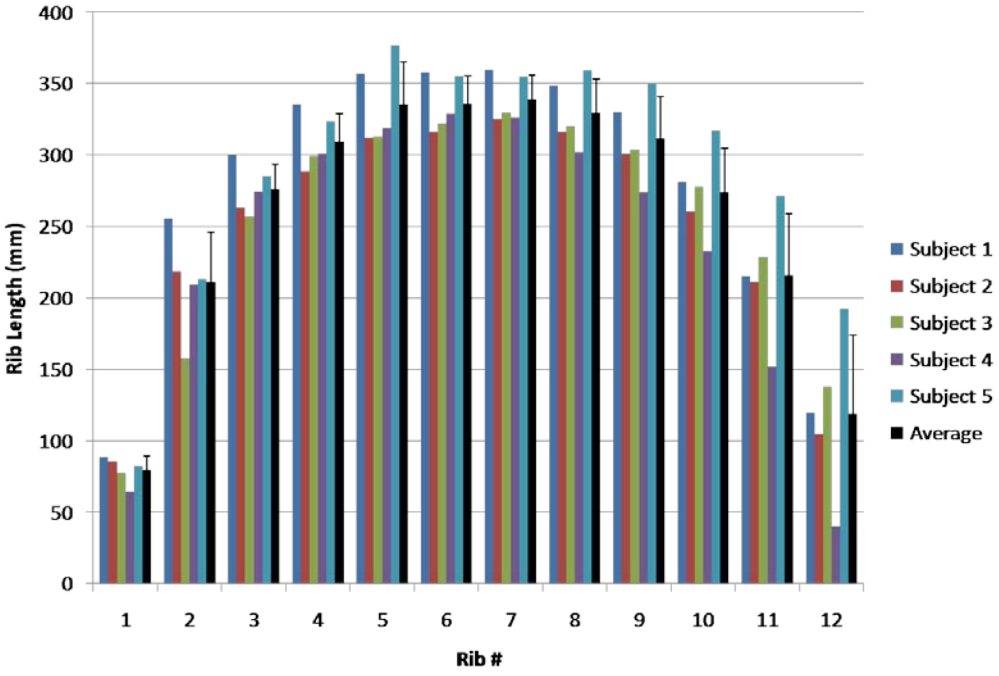

Figure 20: Rib length for 18 year olds for ribs 1-12.

The following graphs compare average rib length from each age group for each rib (Figure 21). Average rib length is significantly different across all age groups for ribs one through 12 ($p<0.01$), with one year olds having the shortest ribs and 18 year olds having the longest. When rib lengths were normalized by standing height (Figure 22), no significant differences were observed between any age group at any rib level.

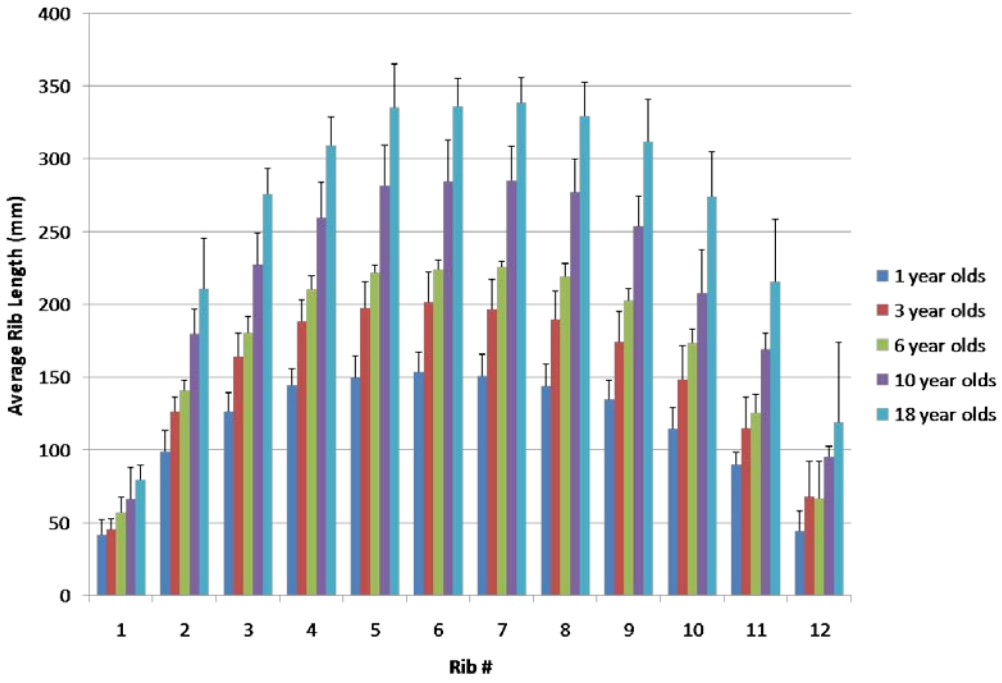

Figure 21: Average rib length (+SD) for all age groups for ribs 1-12. Average rib length is significantly different across all age groups for ribs 1-12 ($p<0.01$).

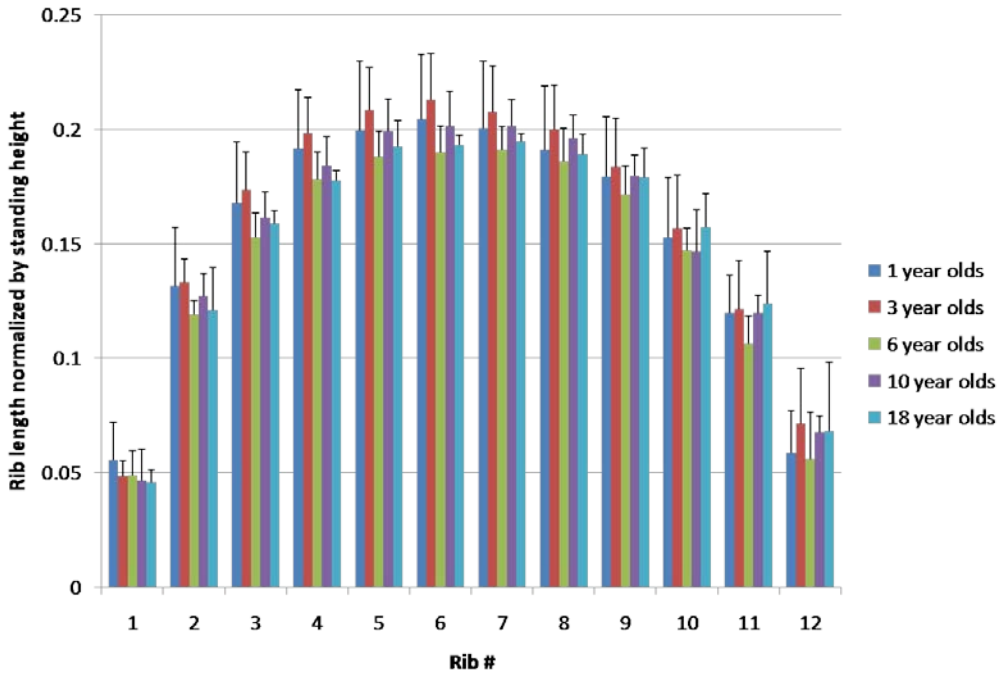

Figure 22: Average normalized rib length (+SD) for all age groups for ribs 1-12. No significant differences were found across any age group at any level.

Thoracic Index

Figures 23-27 show graphs for thoracic index by age group. Each graph shows thoracic index for each subject for each rib, as well as the average thoracic index and standard deviation for the age group. A value closer to one indicates a more rounded shape, while a value closer to zero indicates a more oval shape.

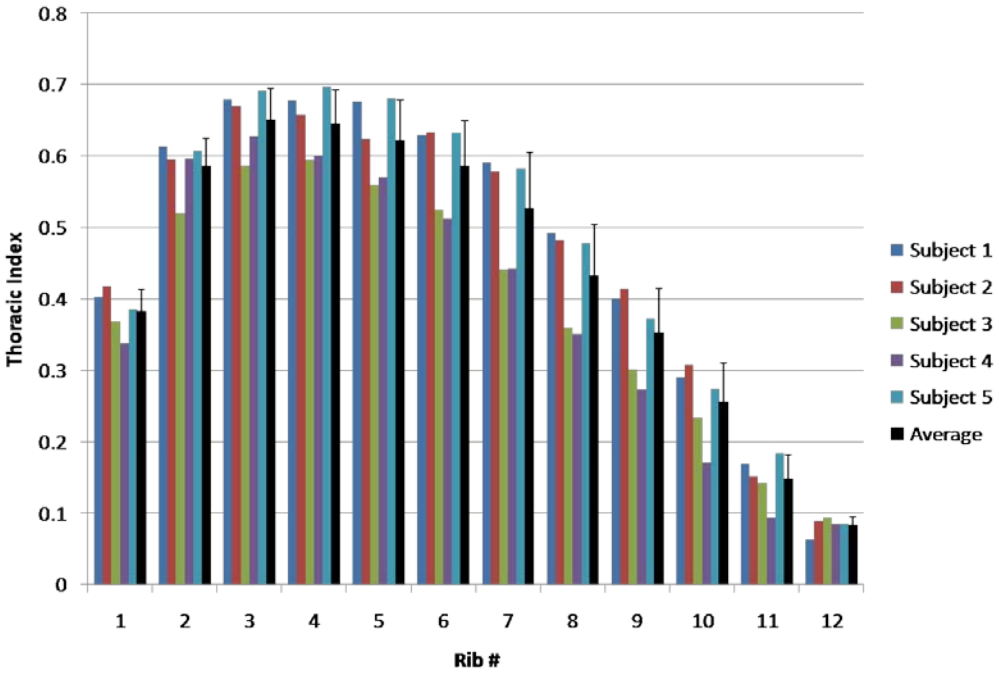

Figure 23: Thoracic index for 1 year olds for ribs 1-12.

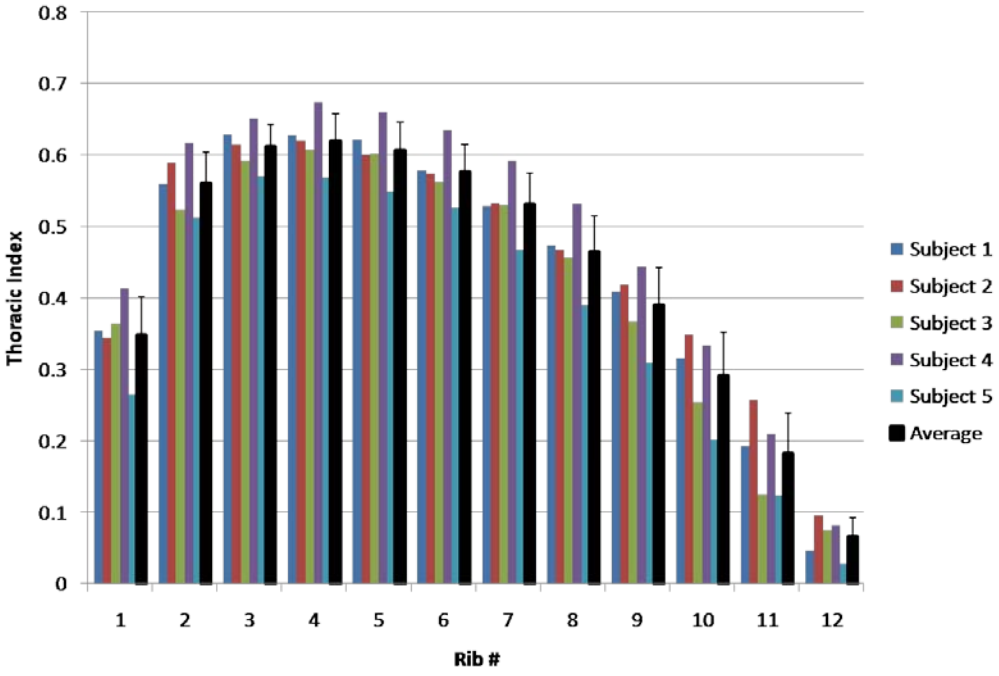

Figure 24: Thoracic index for 3 year olds for ribs 1-12.

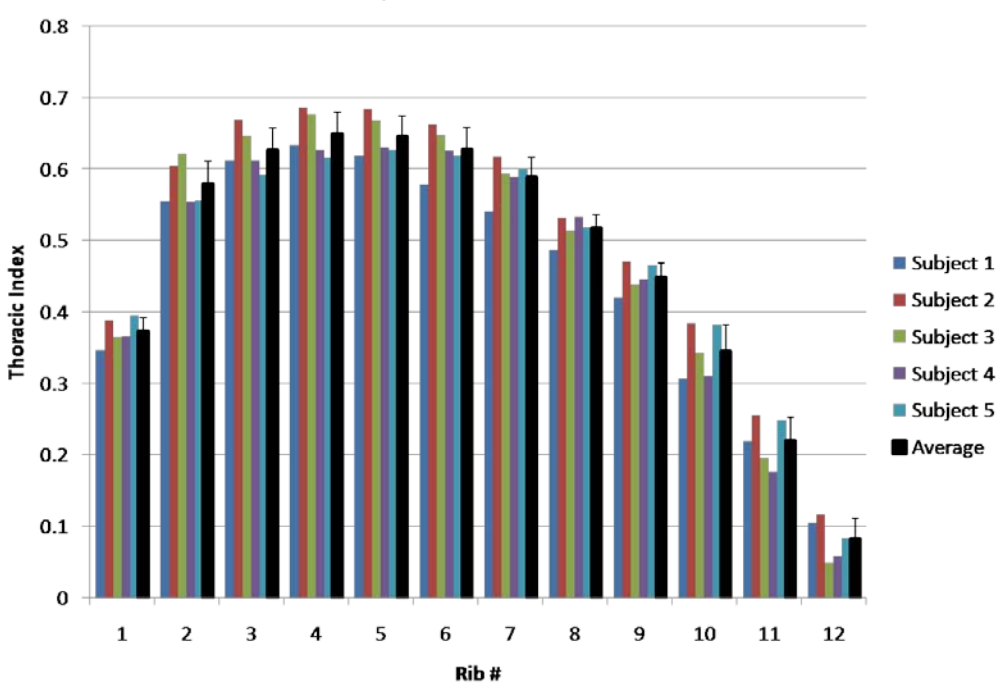

Figure 25: Thoracic index for 6 year olds for ribs 1-12.

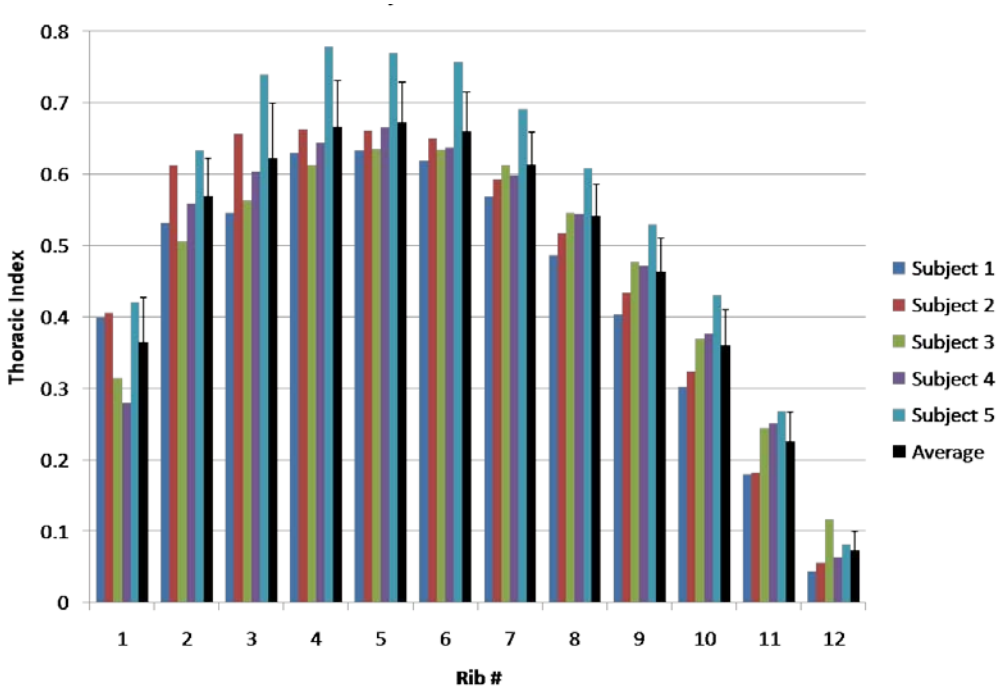

Figure 26: Thoracic index for 10 year olds for ribs 1-12.

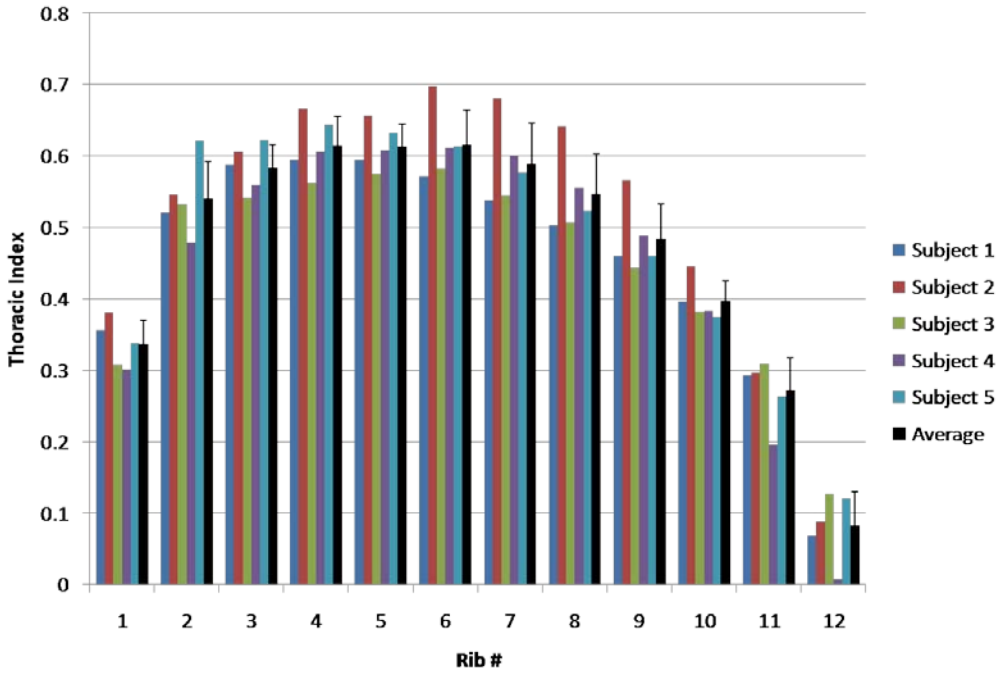

Figure 27: Thoracic index for 18 year olds for ribs 1-12.

The following graph compares average thoracic index from each age group for each rib (Figure 28). Observations show decreasing thoracic index with increasing age for ribs 1-3 and increasing thoracic index with increasing age for ribs 6-12. One year olds had significantly lower thoracic index than age groups 6, 10 and 18 for ribs 7-11 ($p<0.05$). The highest values for thoracic index were observed in ribs three through six, with a rage of 0.6 to 0.7.

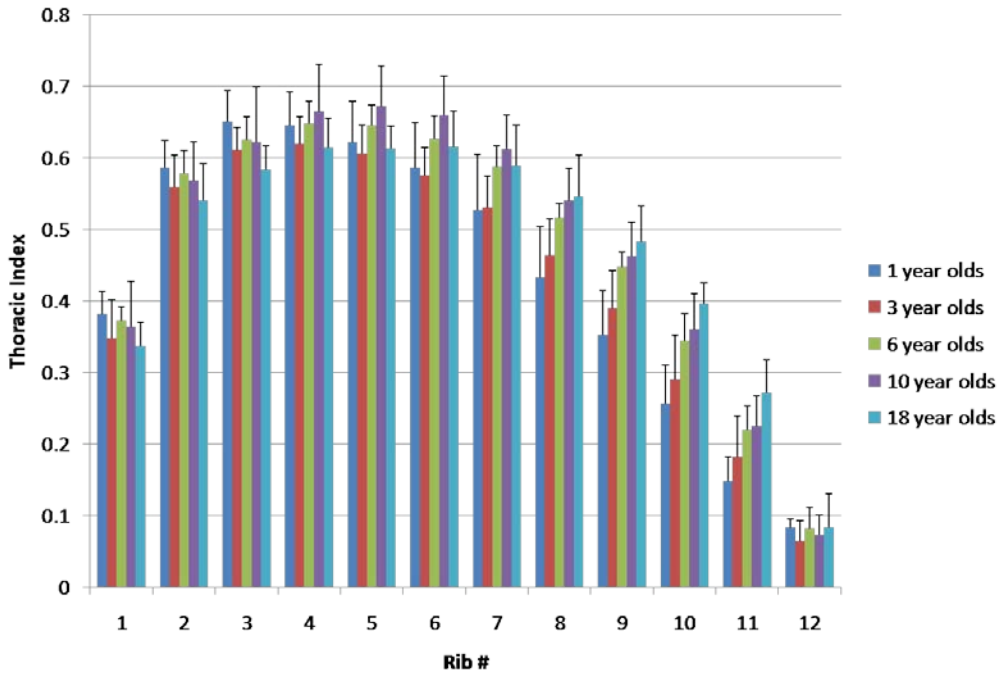

Figure 28: Average thoracic index (+SD) for all age groups for ribs 1-12.

Apparent curvature

Apparent curvature is the reciprocal of the radius of curvature and is indicative of how curved the ribs are. The following graphs show average apparent curvature for ribs three through nine for 10 through 90 percent of rib length. One plot is shown per age group. Apparent curvature for the overall ribcage shows a decreasing trend with increasing age. For many parameters reported, including apparent curvature, ribs 1-2 and 10-12 are not reported. These ribs are left out of the analysis because particular parameters do not make sense for all ribs. For example, for straighter ribs (ribs 11-12), the radius of curvature is very large. Therefore, the apparent curvature data were very small (since the reciprocal of a large number is small) and were very dissimilar to our results for ribs 3-9.

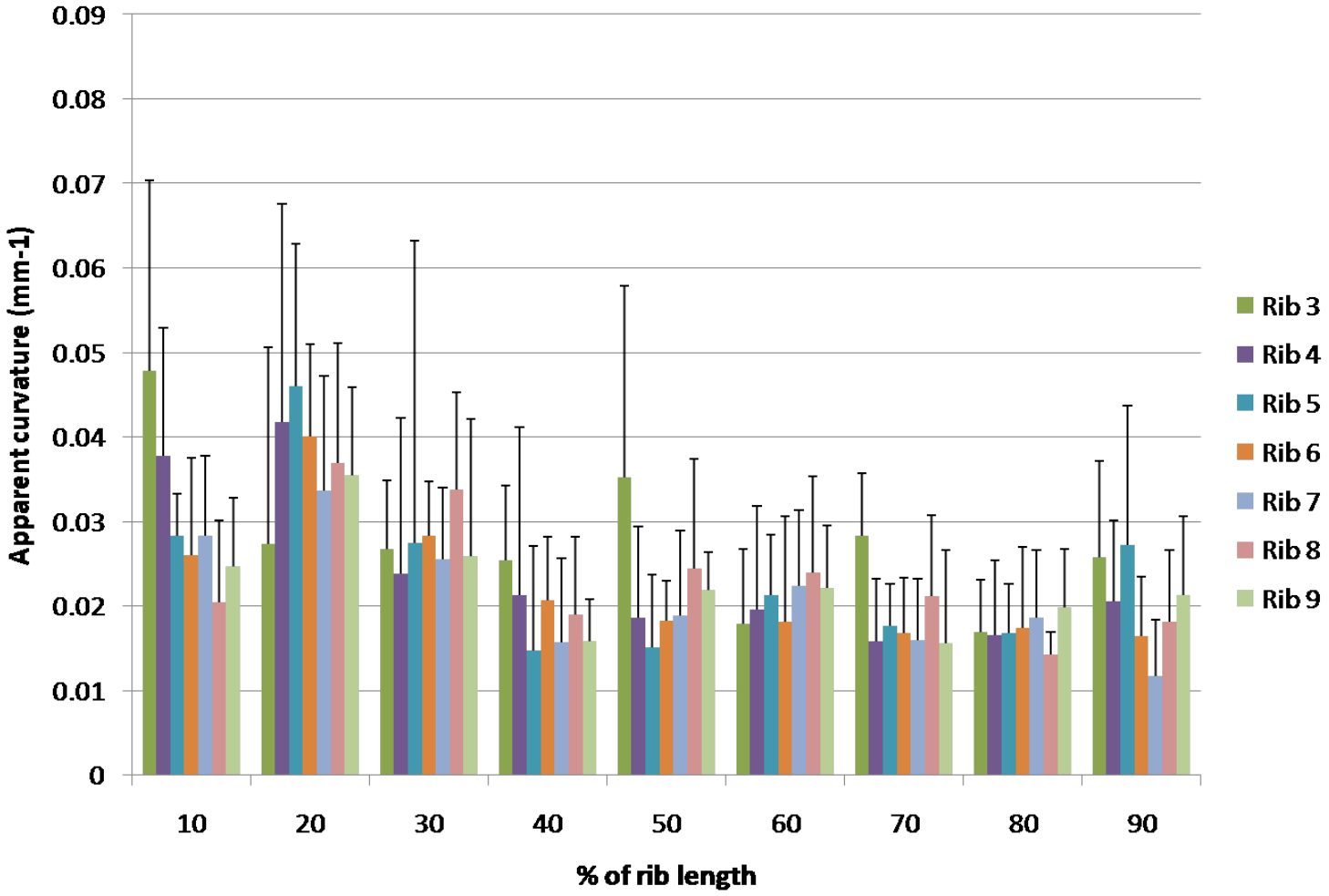

Figure 29: 1 year old average apparent curvature (+SD) for ribs 3-9.

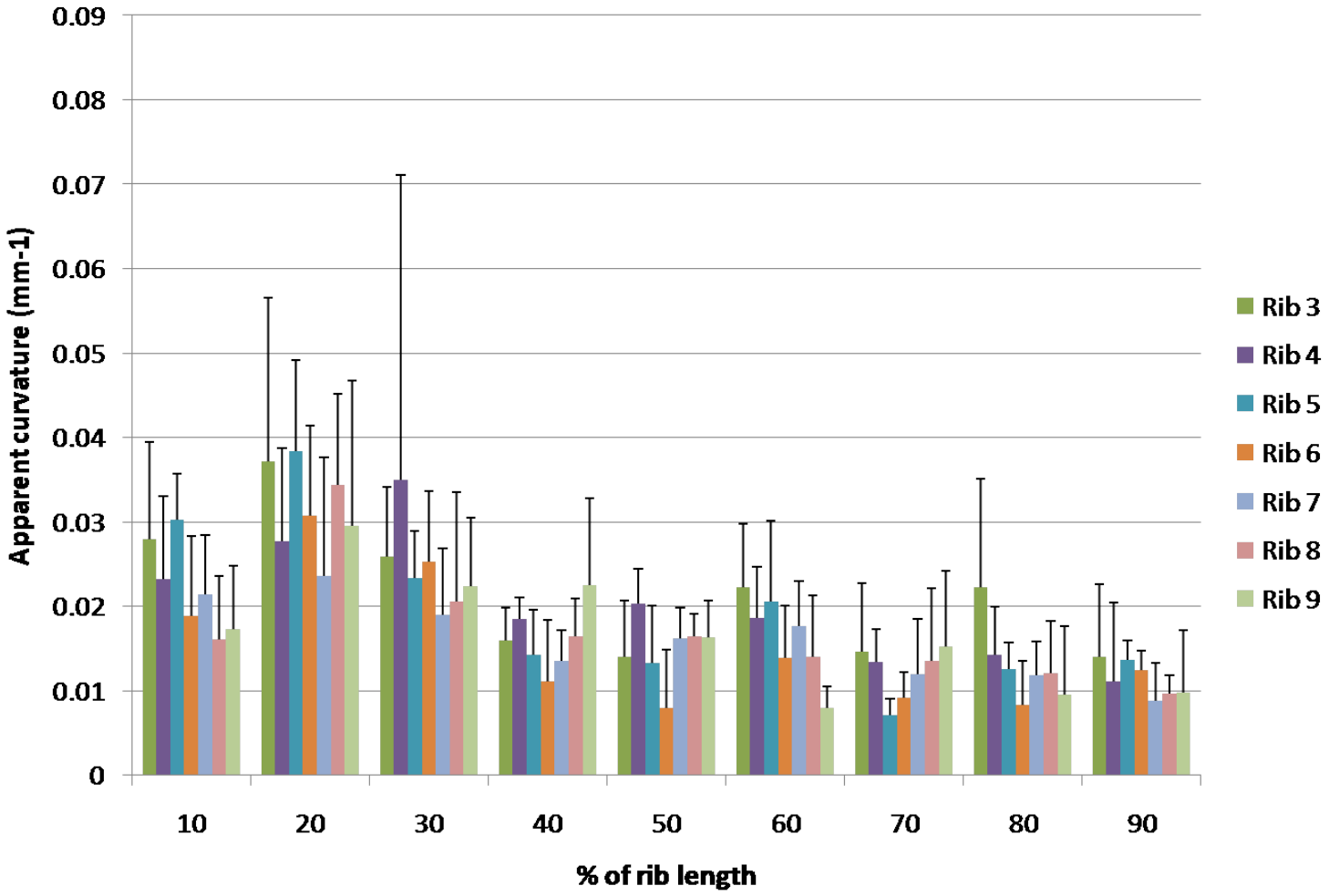

Figure 30: 3 year old average apparent curvature (+SD) for ribs 3-9.

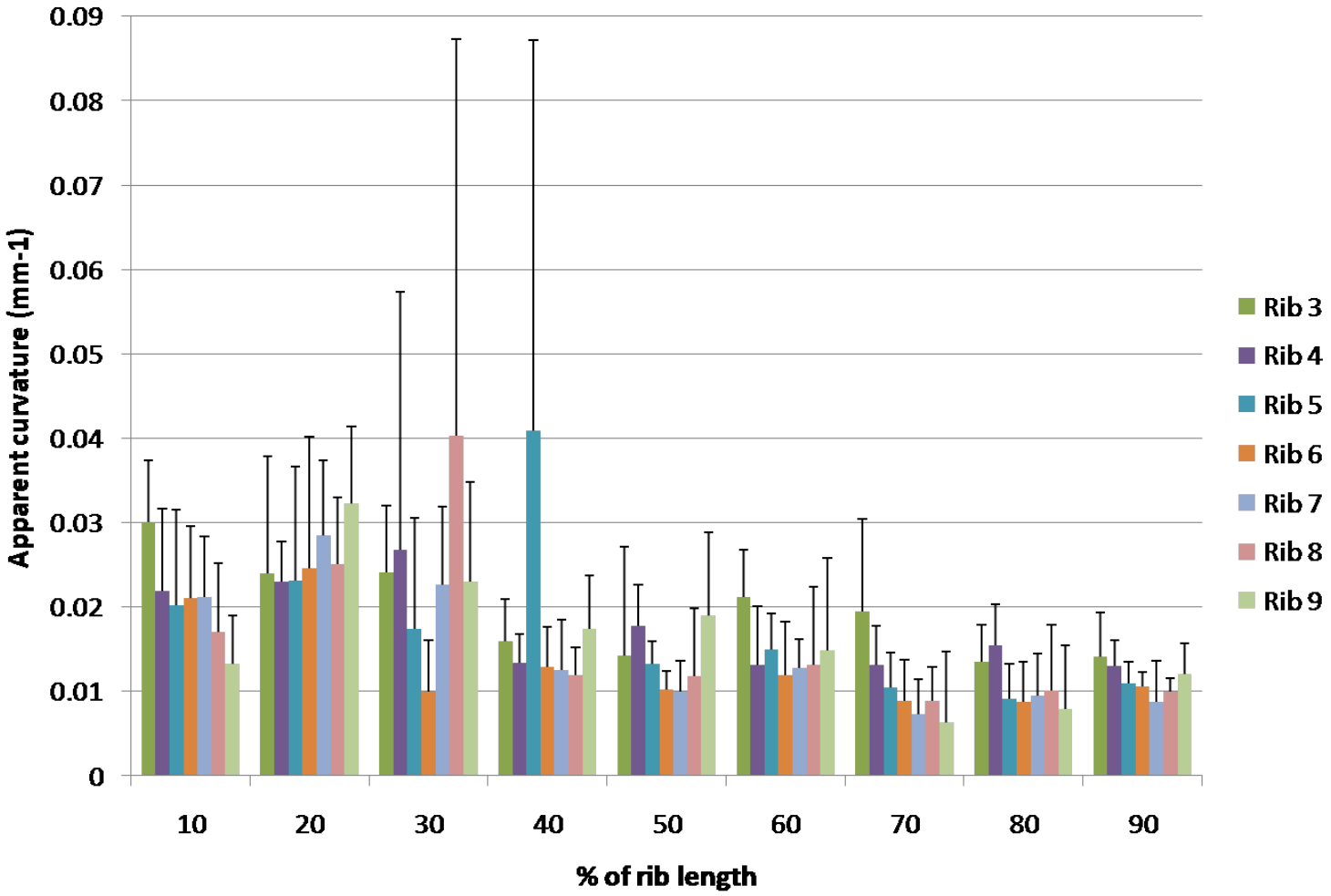

Figure 31: 6 year old average apparent curvature (+SD) for ribs 3-9.

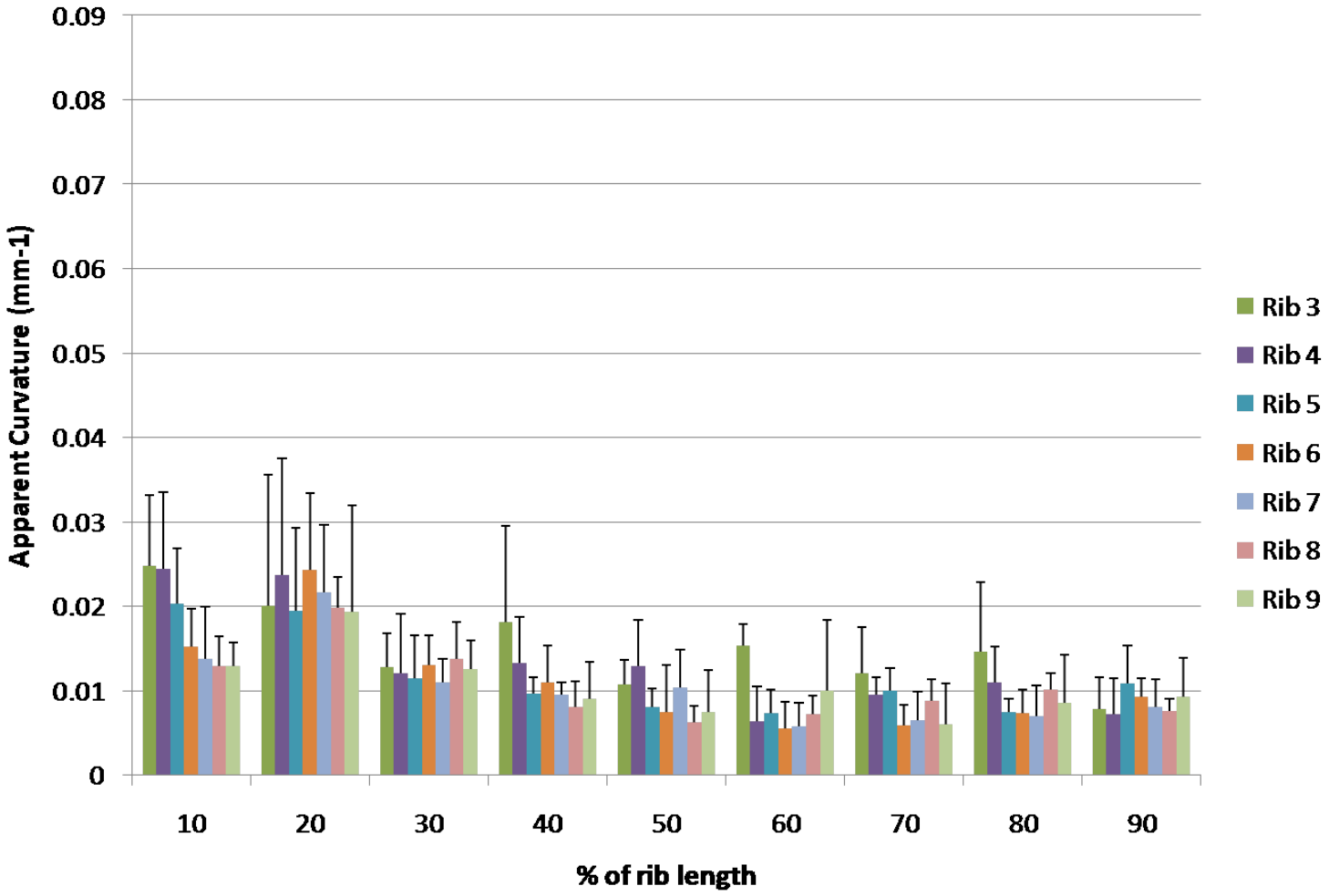

Figure 32: 10 year old average apparent curvature (+SD) for ribs 3-9.

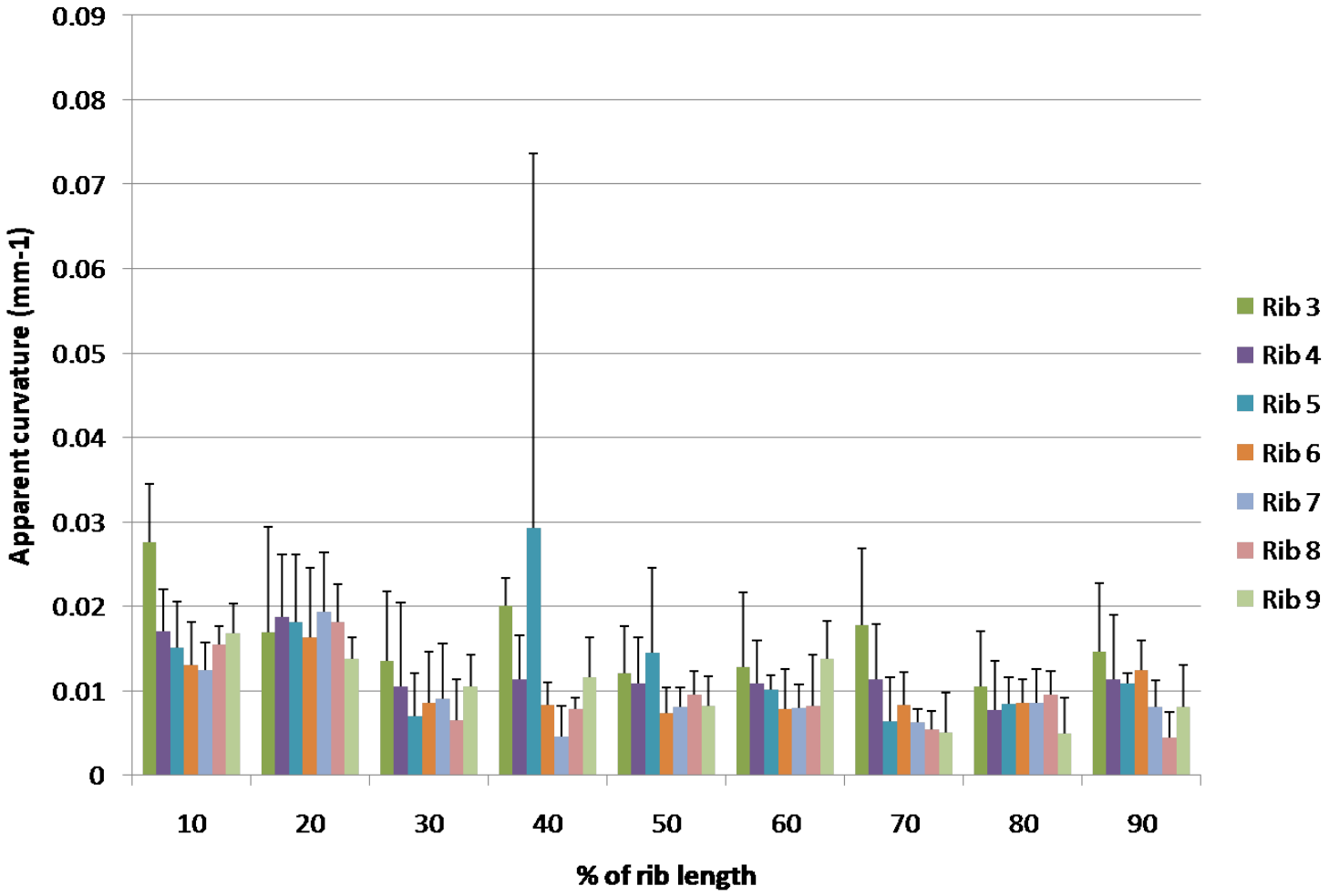

Figure 33: 18 year old average apparent curvature (+SD) for ribs 3-9.

Longitudinal twist of the ribs

Longitudinal twist was defined as the angle the outer surface of the rib makes with the vertical. A positive angle indicates an inward twist of the rib. Figures 34-38 show average longitudinal twist at 10 through 90 percent of rib length for each rib. One graph is shown per age group. Figure 39 shows the difference between the 90 percent site of the rib (near the costochondral junction) and the 10 percent site of the rib (near the tubercle) which indicates overall twist of the rib. For all age groups, ribs two through seven have an overall inward twist, and ribs 10 through 12 have an overall outward twist. Maximum twist was observed in rib two. There were no significant differences in longitudinal twist across any age group at any level.

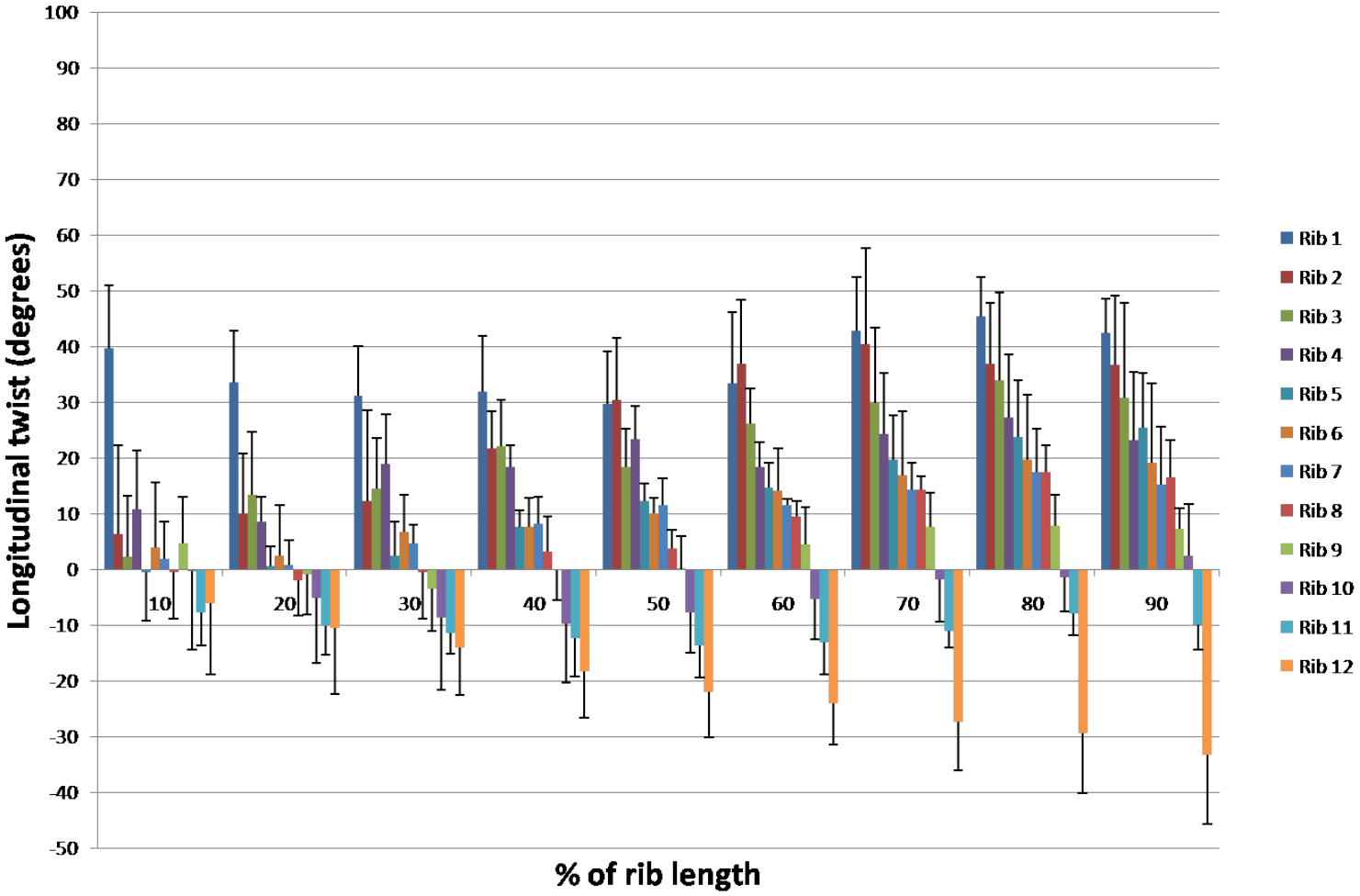

Figure 34: 1 year old average longitudinal twist (+SD) for ribs 1-12.

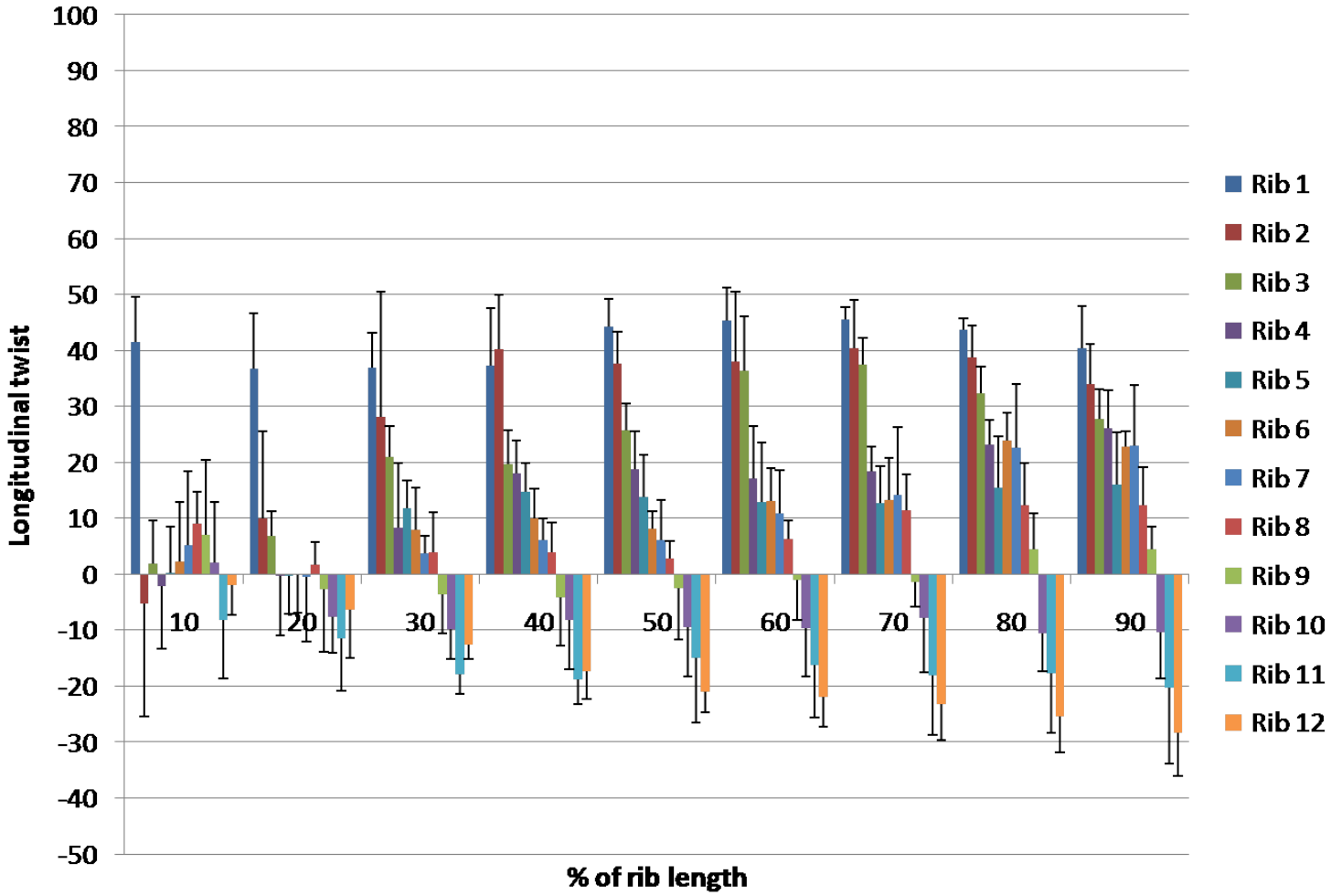

Figure 35: 3 year old average longitudinal twist (+SD) for ribs 1-12.

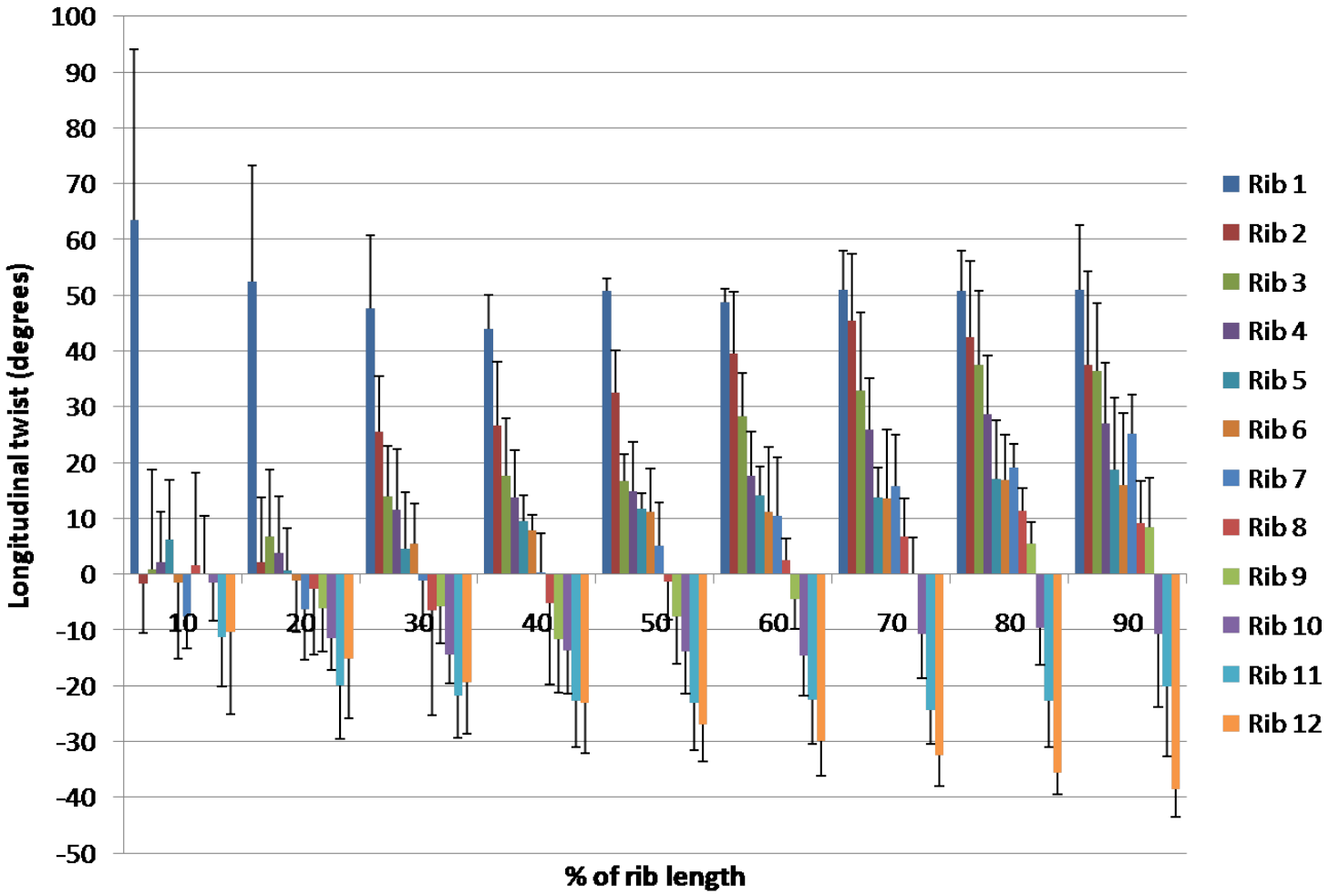

Figure 36: 6 year old average longitudinal twist (+SD) for ribs 1-12.

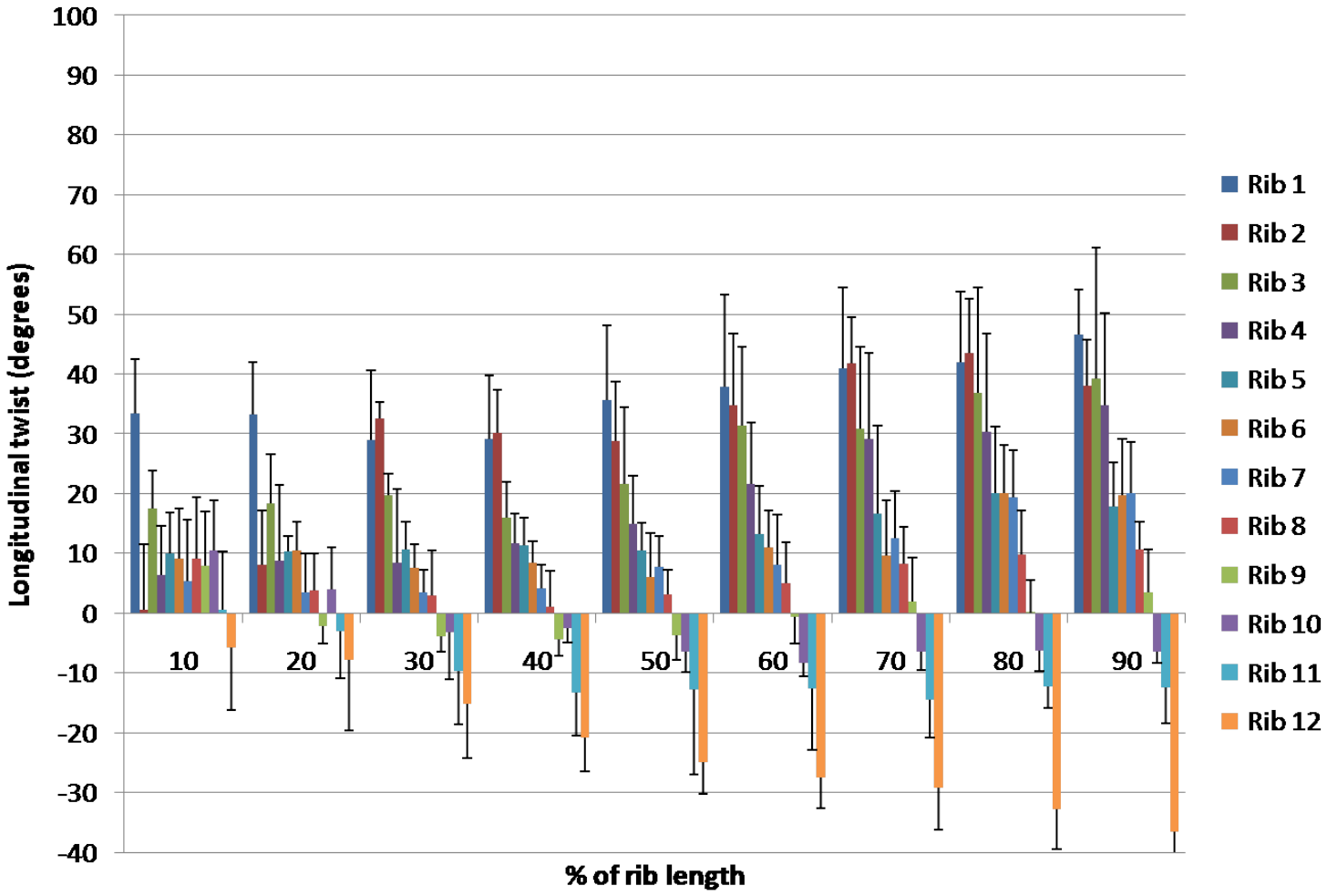

Figure 37: 10 year old average longitudinal twist (+SD) for ribs 1-12.

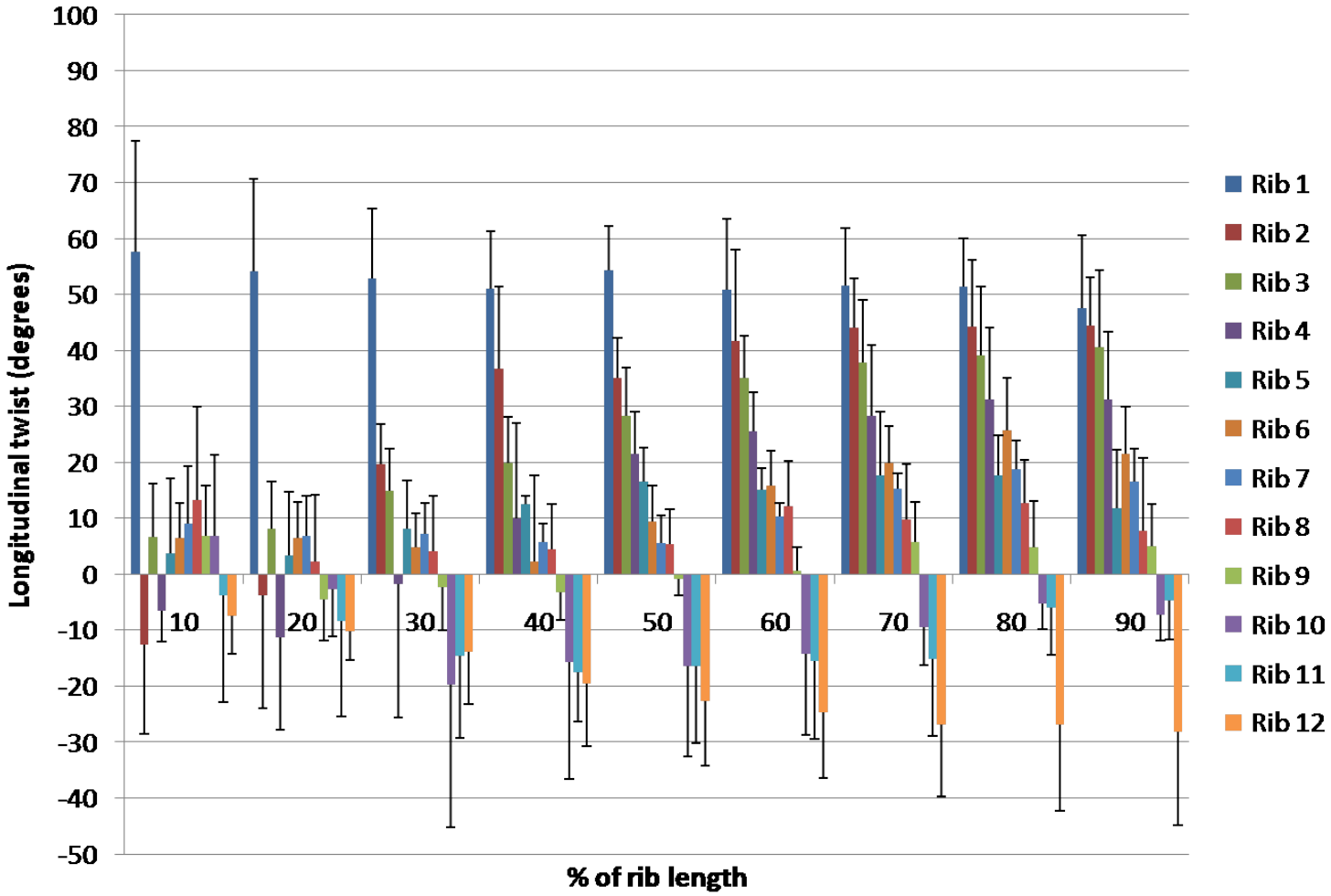

Figure 38: 18 year old average longitudinal twist (+SD) for ribs 1-12.

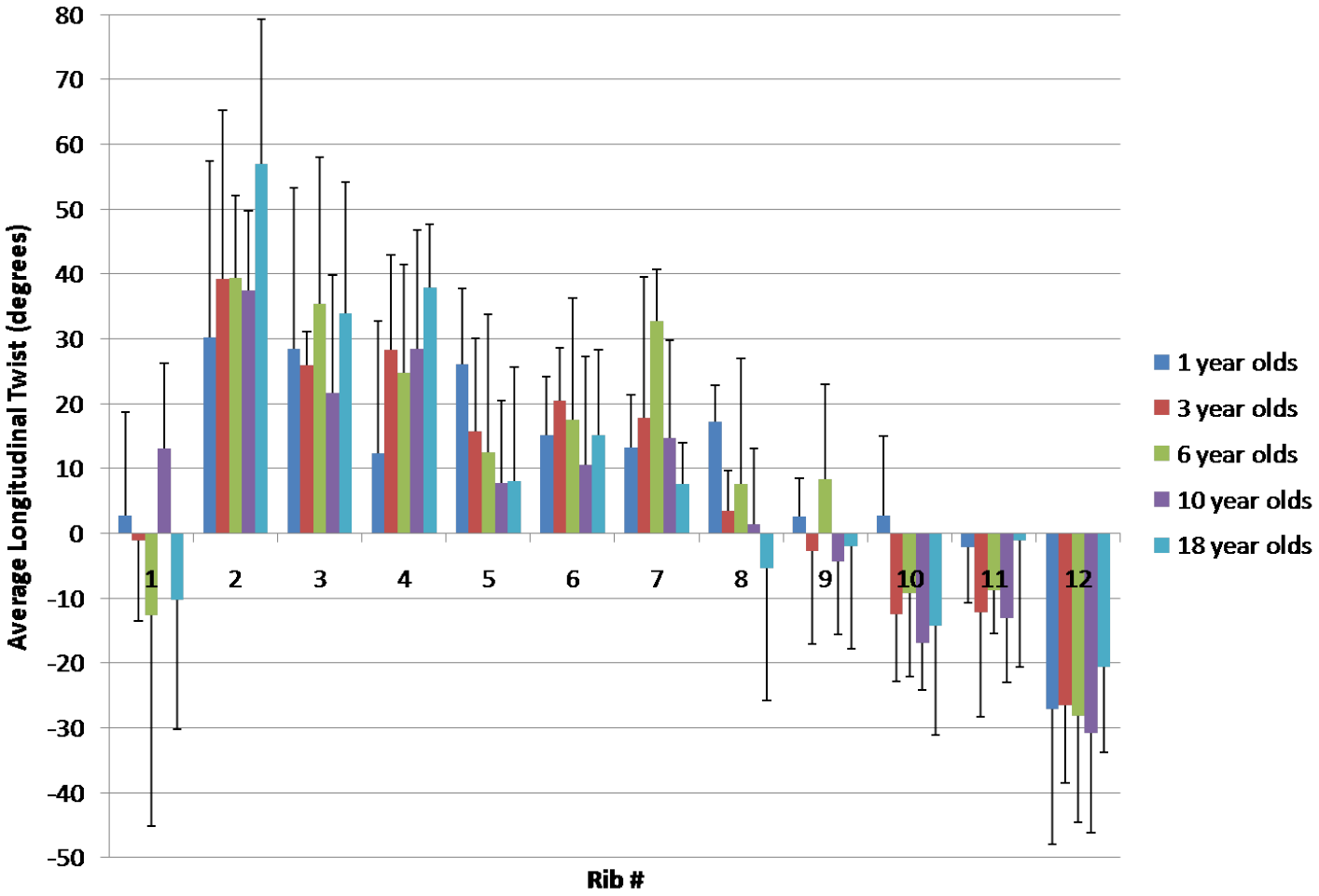

Figure 39: Average longitudinal twist difference (+SD) for ribs 1-12.

Lateral rib angle

Figures 40-44 show graphs for lateral rib angle by age group. Each graph shows the angle for each subject for each rib, as well as the average angle and standard deviation for the age group. A greater angle indicates a more horizontal rib.

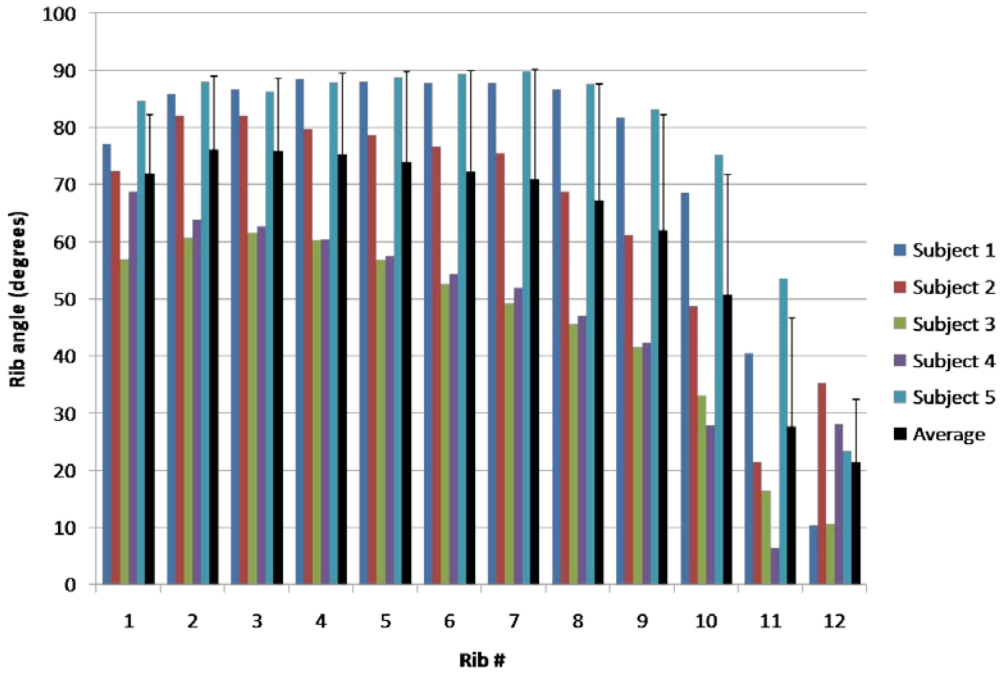

Figure 40: Lateral rib angle for 1 year olds for ribs 1-12.

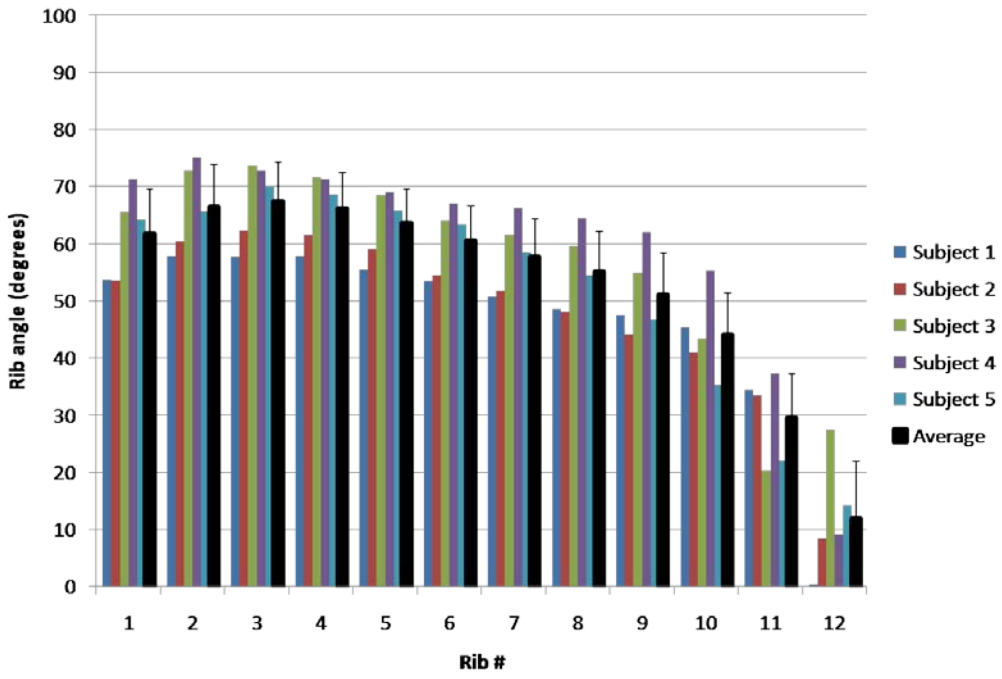

Figure 41: Lateral rib angle for 3 year olds for ribs 1-12.

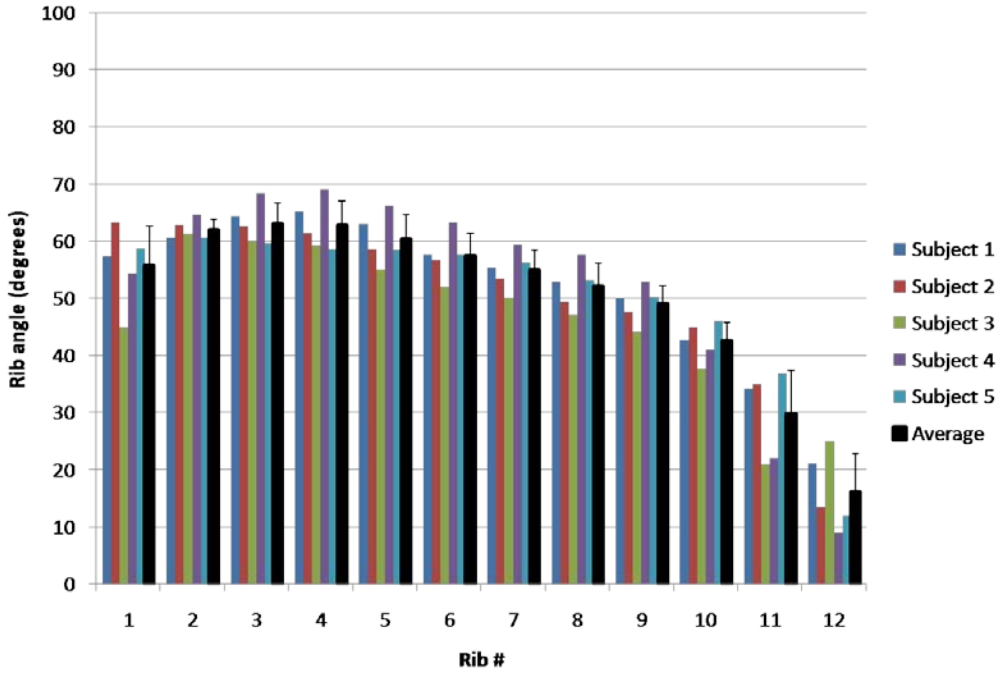

Figure 42: Lateral rib angle for 6 year olds for ribs 1-12.

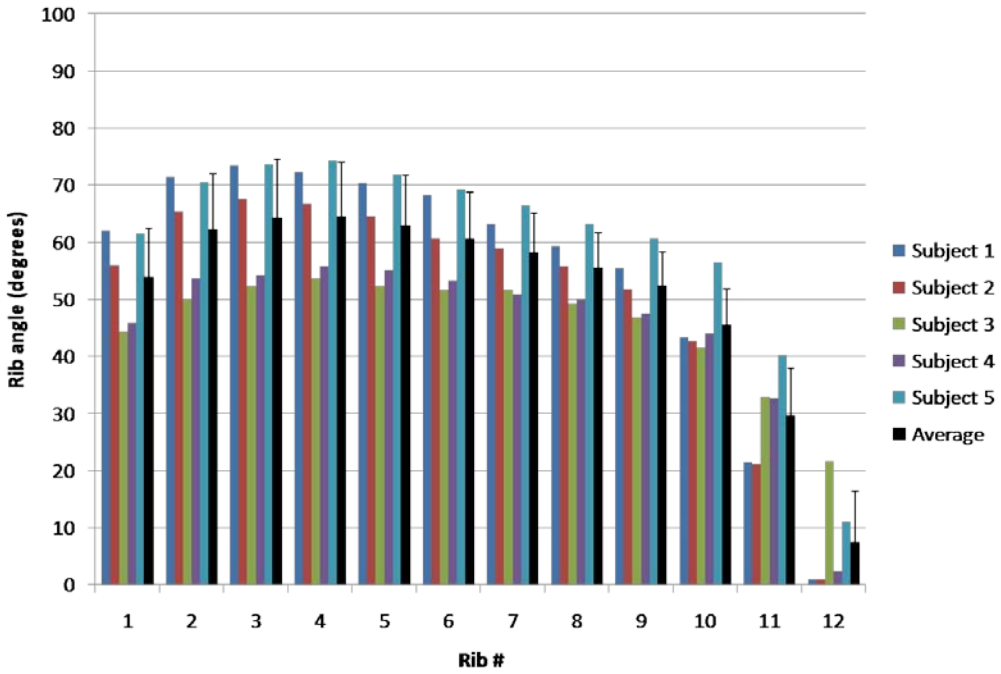

Figure 43: Lateral rib angle for 10 year olds for ribs 1-12.

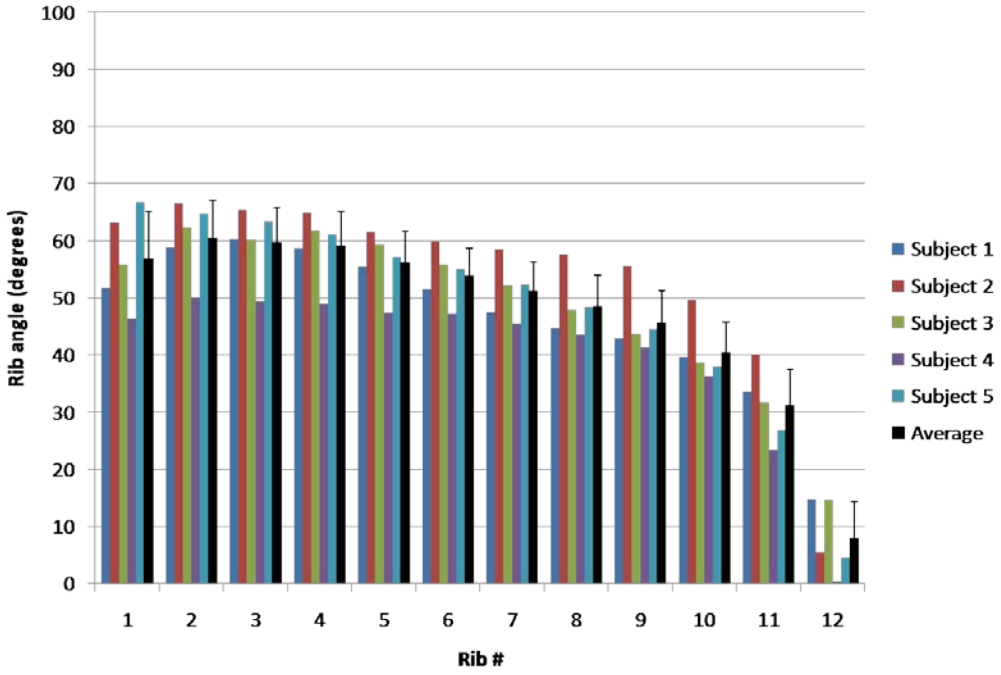

Figure 44: Lateral rib angle for 18 year olds for ribs 1-12.

The following graph compares average lateral rib angle from each age group for each rib (Figure 45). One year olds had significantly higher lateral rib angle than all other age groups for ribs one through eight ($p<0.05$). Average lateral rib angle shows a decreasing trend with increasing age except for the 10 year old age group. There is an increasing trend with increasing rib number for ribs one through four and a decreasing trend with increasing rib number for ribs four through 12 for all age groups.

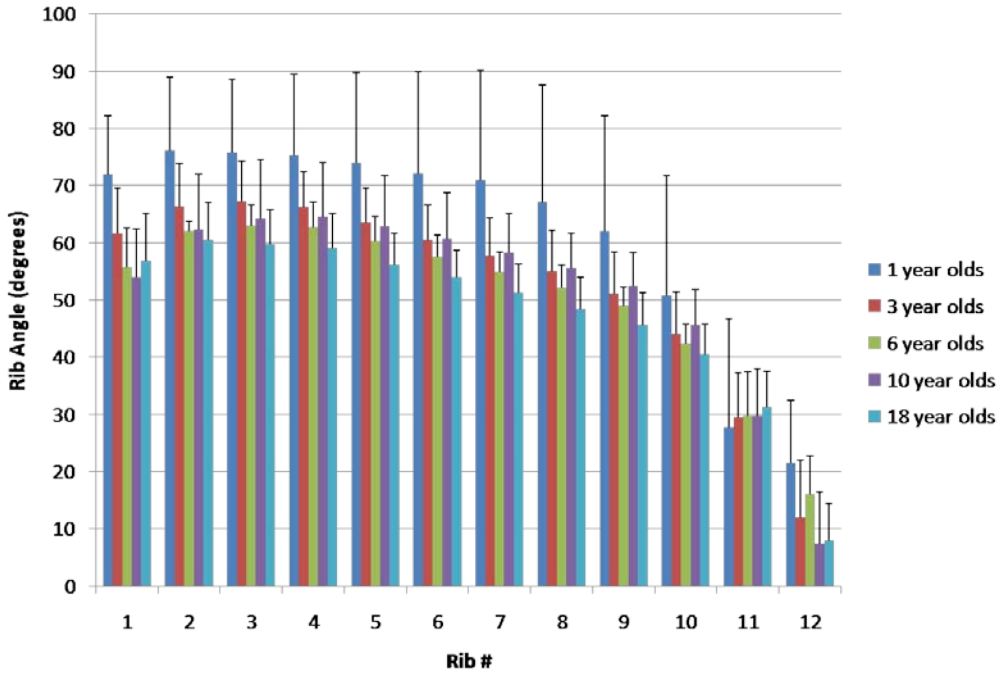

Figure 45: Average lateral rib angle (+SD) for all age groups for ribs 1-12.

Length and width of the spine, sternum and manubrium

Spine length (T1-T12), whole sternum length, sternum width and manubrium width plots are shown in Figures 46-47. These plots show an increasing trend of length and width with increasing age. One year olds have significantly lower length and width than the 6, 10 and 18 year old age groups ($p<0.01$) for each of these parameters. When spine length is normalized by height (Figure 48), significant differences were found between three and six year olds through 10 year olds ($p<0.05$). Length and width of the spine, sternum and manubrium are also reported for each subject in Table 6. The whole sternum length indicates

the length of every component of the sternum including manubrium, sternum body and the xyphoid (if present). All other sternum measurements include only the sternum body and do not include the manubrium or xyphoid.

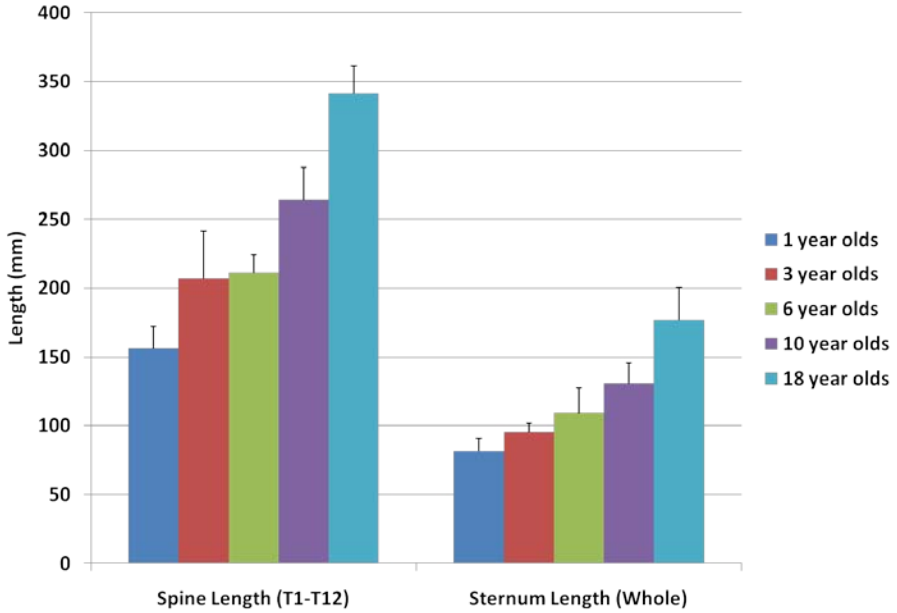

Figure 46: Average spine length (T1-T12) and whole sternum length (includes manubrium, sternum body and xyphoid) (+SD) for all age groups.

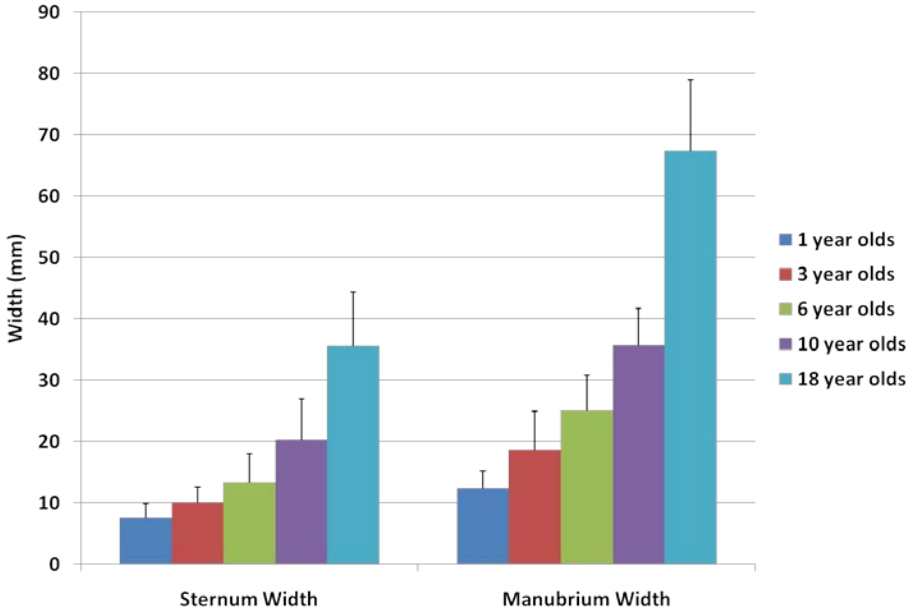

Figure 47: Average sternum and manubrium width (+SD) measured at the widest point for all age groups.

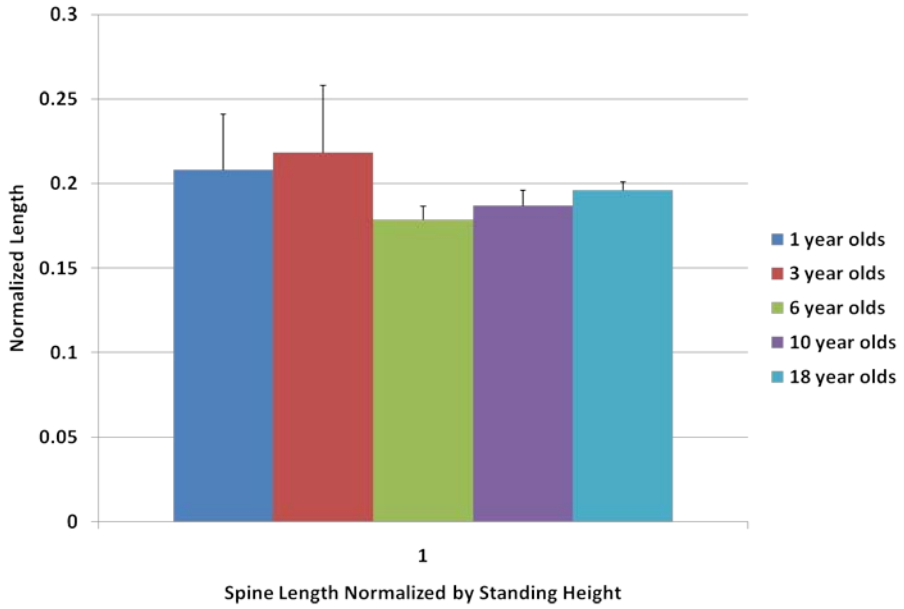

Figure 48: Average spine length (T1-T12) (+SD) normalized by standing height for all age groups.

Table 6: Length of the thoracic spine and length and width of the sternum and manubrium for all subjects.

Subject #	Spine Length, T1-T12	Spine Length, T3-T19	Sternum Length, Whole	Sternum Body Length	Sternum Body Width	Sternum Body Distance to Widest Pt.	Manubrium Length	Manubrium Width	Manubrium Distance to Widest Pt.
1_1	140.755	91.914	92.297	61.456	7.493	9.263	21.708	13.359	5.562
1_2	175.657	114.784	79.337	45.900	8.381	23.753	23.954	13.787	8.877
1_3	144.063	94.551	74.323	50.865	6.260	6.763	18.286	9.263	3.971
1_4	169.947	109.494	89.870	47.381	5.015	18.259	35.132	9.805	3.568
1_5	149.953	97.827	71.944	47.843	10.949	5.901	19.359	15.810	4.308
3_1	186.825	120.642	94.851	58.013	7.890	14.029	24.015	13.519	8.675
3_2	266.304	167.626	89.867	57.783	10.055	32.975	26.051	22.687	7.825
3_3	183.485	118.303	89.385	57.375	9.413	10.483	19.984	14.607	8.410
3_4	208.915	136.137	104.575	71.289	14.271	14.996	24.243	27.865	10.966
3_5	188.193	121.141	98.088	59.605	9.099	13.439	31.618	14.275	7.944
6_1	216.677	137.656	93.146	56.768	14.294	44.452	23.891	29.246	14.975
6_2	217.499	142.948	124.355	88.991	13.282	27.480	25.293	25.780	8.888
6_3	193.680	125.301	97.626	71.836	9.709	5.749	22.079	16.892	13.358
6_4	225.887	144.763	133.803	75.486	20.661	16.046	28.929	31.415	14.783
6_5	202.498	129.435	96.872	61.226	8.493	22.266	26.664	21.815	7.971
10_1	297.319	190.147	141.031	82.119	23.298	39.749	44.473	39.373	18.319
10_2	262.055	169.641	110.960	62.340	14.326	41.210	36.748	29.793	16.709
10_3	265.304	168.763	136.894	90.228	30.734	38.229	40.433	44.135	24.744
10_4	230.825	147.915	120.142	88.012	16.359	20.993	21.891	30.474	7.439
10_5	264.947	169.960	145.465	95.583	16.636	42.023	38.335	34.485	16.805
18_1	362.693	230.954	212.199	113.124	36.463	208.648	54.259	75.081	42.858
18_2	322.734	207.714	162.333	101.948	31.740	71.231	52.775	68.016	42.348
18_3	335.264	214.213	189.843	101.448	48.369	63.641	49.969	80.022	41.569
18_4	322.701	204.032	155.549	107.377	24.377	27.705	47.176	50.278	26.989
18_5	362.456	232.071	163.758	105.293	37.119	74.275	50.949	63.903	30.886

Curvature of the sternum and thoracic spine, and thoracic spine Cobb angle

Sternum angle, spine angle (T1-T12) and Cobb angle (T3-T9) are shown in Figure 49. Sternum and spine angles for each subject are shown in Table 7. Cobb angles for each subject are shown in Table 8. There were no clear trends observed in any of these angles and no significant differences were found across any age groups for any of these measurements.

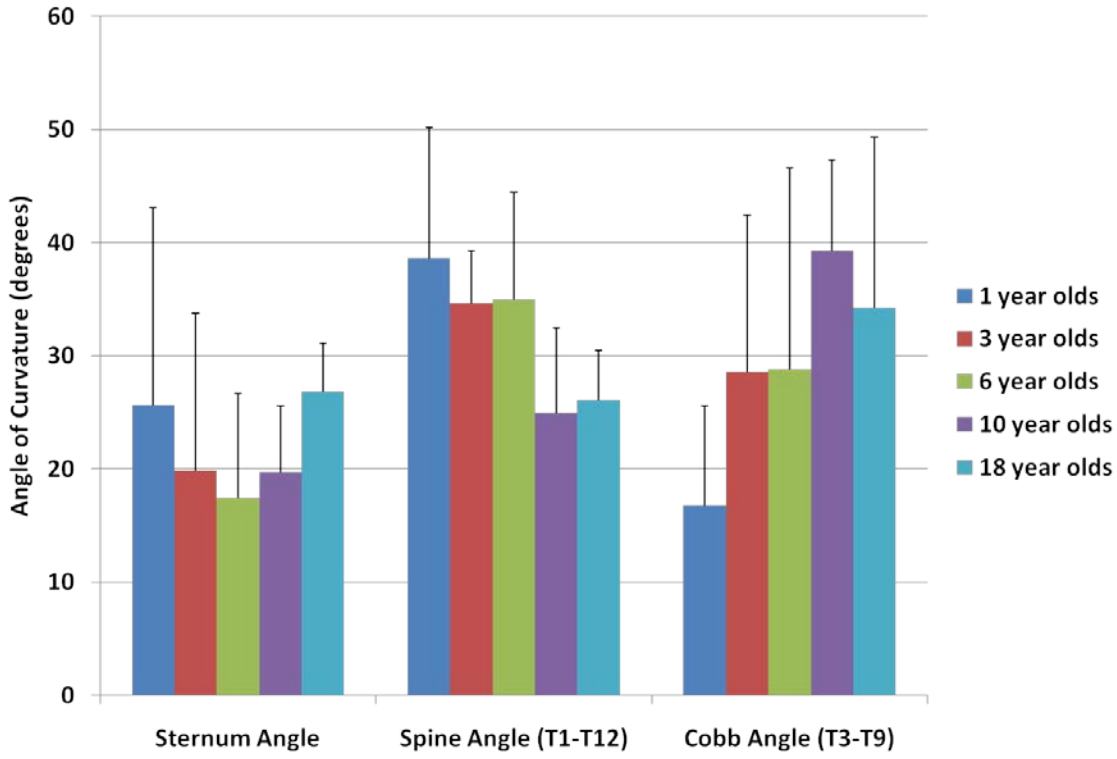

Figure 49: Average sternum angle, spine angle (T3-T9 and T1-T12) and Cobb angle of the spine (T3-T9 and T1-T12) (+SD) for each age group.

Table 7: Sternum and thoracic spine angles (degrees) for all subjects.

	Sternum Angle					Spine Angle, T3-T9					Spine Angle, T1-T12				
Age Group	**1**	**3**	**6**	**10**	**18**	**1**	**3**	**6**	**10**	**18**	**1**	**3**	**6**	**10**	**18**
Subject 1	35.191	30.237	20.782	25.660	31.782	4.688	28.023	39.754	25.631	11.049	10.923	34.369	49.131	38.910	19.574
Subject 2	20.959	30.896	37.057	15.753	25.948	4.894	40.226	12.716	18.980	46.623	6.031	48.382	18.506	27.805	55.435
Subject 3	47.171	40.669	41.460	32.317	19.486	21.561	10.114	22.201	36.426	17.257	29.100	17.998	24.375	47.403	20.994
Subject 4	50.485	33.134	44.523	18.766	26.403	14.614	18.920	8.690	26.884	31.724	18.893	28.745	7.020	46.347	41.964
Subject 5	39.183	38.275	31.211	32.138	26.679	14.102	5.673	36.834	23.673	32.130	18.884	13.332	44.841	35.892	33.425
Average	38.598	34.642	35.006	24.927	26.059	11.972	20.591	24.039	26.319	27.757	16.766	28.565	28.775	39.271	34.279
Standard Deviation	11.596	4.616	9.396	7.571	4.372	7.187	13.927	13.945	6.399	13.966	8.811	13.876	17.822	8.050	15.001

Table 8: Thoracic spine Cobb angle (degrees) for all subjects.

	Cobb Angle, T3-T9					Cobb Angle, T1-T12				
Age Group	**1**	**3**	**6**	**10**	**18**	**1**	**3**	**6**	**10**	**18**
Subject 1	9.723	39.034	23.159	20.788	25.364	22.620	39.774	48.180	28.330	22.586
Subject 2	10.138	28.756	10.784	11.079	33.983	5.194	33.783	30.256	31.176	39.273
Subject 3	31.339	17.103	14.818	23.199	23.112	30.466	23.009	25.647	36.769	28.301
Subject 4	51.870	7.125	8.130	26.340	24.624	31.860	29.567	7.001	38.817	48.598
Subject 5	25.168	7.240	30.343	17.292	27.070	15.857	19.373	30.396	38.089	28.526
Average	25.648	19.851	17.447	19.740	26.831	21.199	29.101	28.296	34.636	33.457
Standard Deviation	17.424	13.927	9.179	5.866	4.245	11.025	8.182	14.698	4.628	10.394

Height, width and depth of the thoracic vertebral bodies

Average thoracic spine vertebral body height, width and depth for each age group are shown in Figures 50, 51 and 52 respectively. Values for height, width and depth for each subject are shown in tables 9, 10 and 11 respectively. For vertebral body height, width and depth, all age groups are significantly different ($p<0.01$) at all thoracic levels. When normalized by standing height, significant differences were found in vertebral body height (Figure 53) for thoracic levels 1, 2, 6, 8, 10 and 11. For thoracic levels 1, 2, 8 and 10, 18 year olds were significantly different than all other age groups ($p<0.05$). For thoracic level 6, 18 year olds were significantly different from 10 year olds, and for thoracic level 11, 18 year olds were significantly different from 1 and 10 year olds. No differences were found in normalized vertebral body width for any age group at any level (Figure 54). Significant differences were found in normalized vertebral body depth (Figure 55) for thoracic levels 2 and 3. At the second thoracic level, 18 year olds were significantly different than one year olds ($p<0.01$). At the third thoracic level, 18 year olds were significantly different from one and three year olds ($p<0.01$).

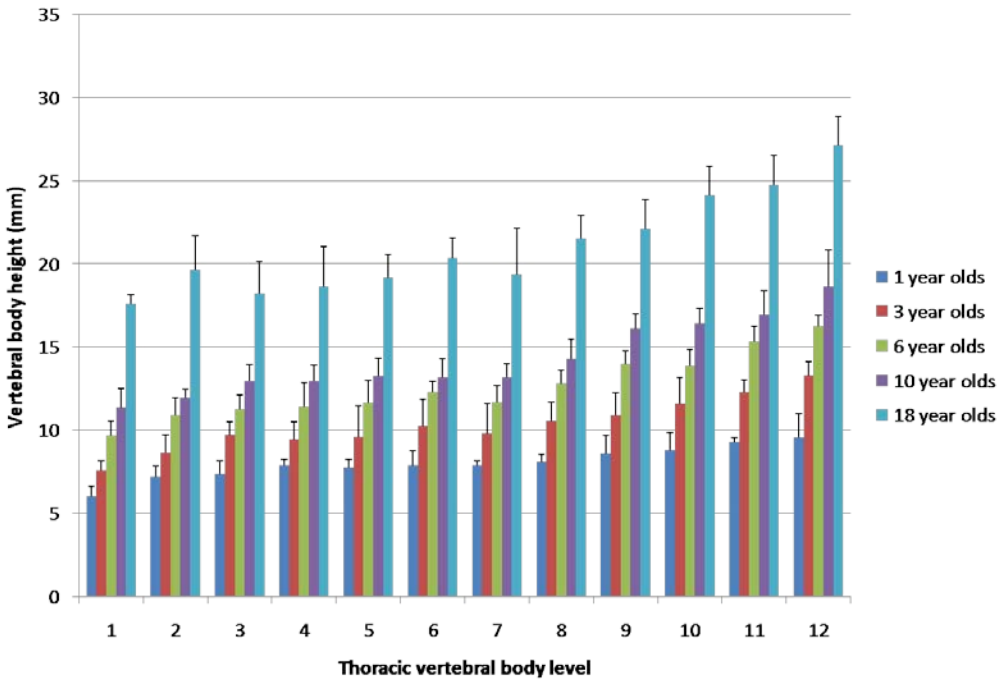

Figure 50: Average vertebral body height (+SD) for thoracic vertebral levels 1-12.

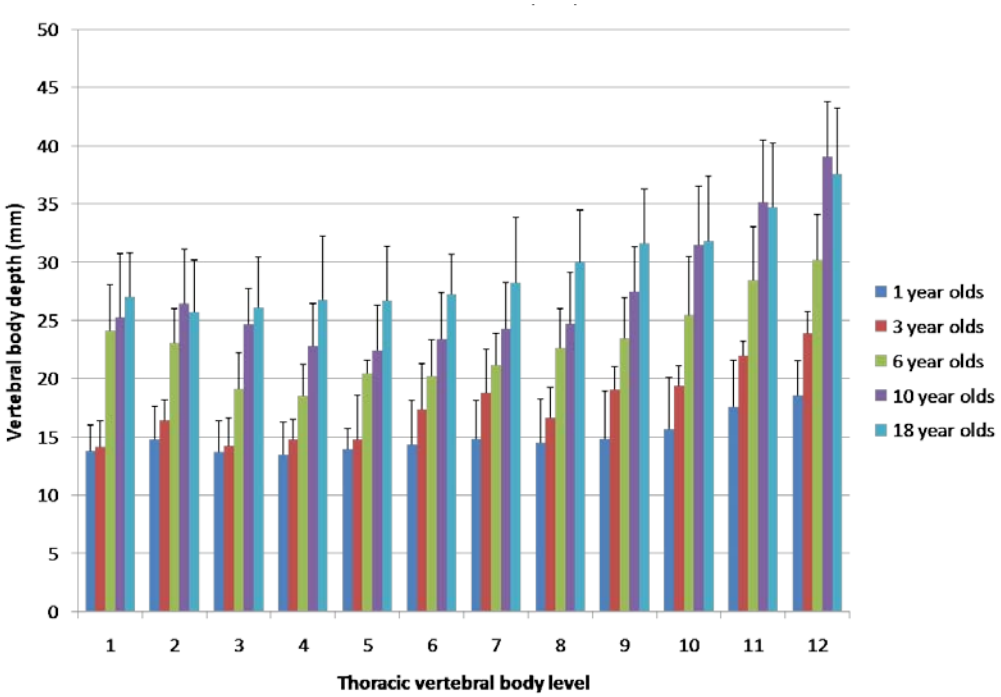

Figure 51: Average vertebral body width (+SD) for thoracic vertebral levels 1-12.

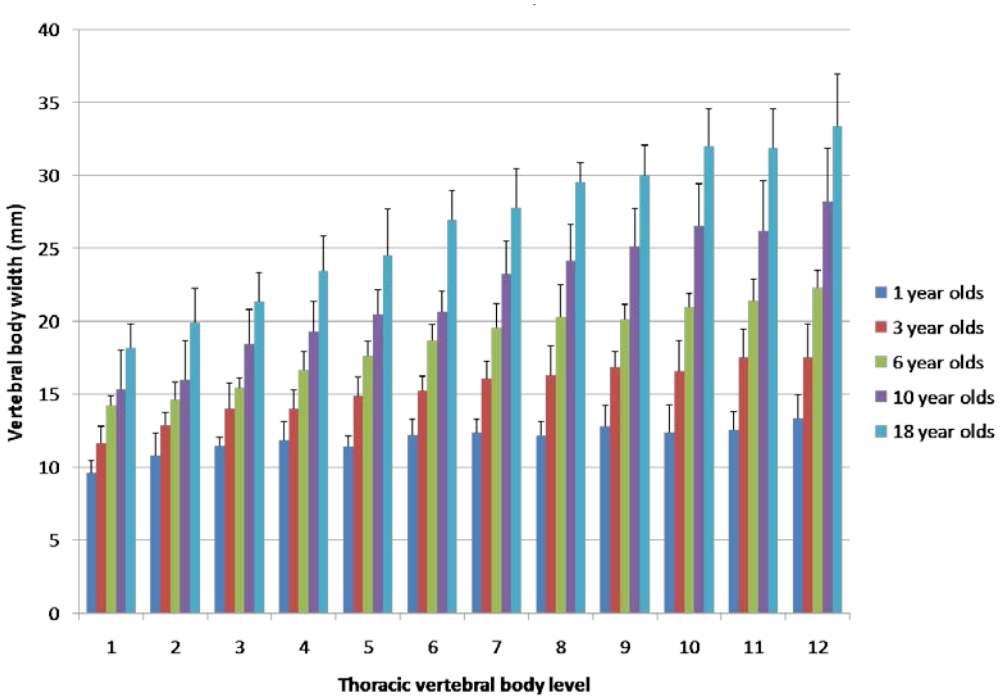

Figure 52: Average vertebral body depth (+SD) for thoracic vertebral levels 1-12.

Table 9: Vertebral body height (mm) for all subjects.

Subject #	VB 1	VB 2	VB 3	VB 4	VB 5	VB 6	VB 7	VB 8	VB 9	VB 10	VB 11	VB 12
1_1	6.56	6.94	6.94	8.01	7.33	8.55	7.91	7.91	7.94	8.01	9.15	7.31
1_2	6.75	8.20	7.45	8.23	8.23	9.06	8.23	8.23	8.97	9.71	8.97	11.18
1_3	5.78	6.46	6.74	7.36	7.50	7.50	7.99	7.45	7.93	9.42	9.42	8.93
1_4	5.69	7.36	7.09	7.80	8.35	7.05	7.85	8.71	10.38	9.52	9.56	10.16
1_5	5.41	7.00	8.72	8.08	7.41	7.41	7.50	8.16	7.65	7.41	9.39	10.08
3_1	8.27	9.76	9.41	9.32	9.32	9.62	10.94	10.40	11.12	12.04	12.14	13.22
3_2	6.77	7.80	8.86	8.53	6.77	8.08	8.75	8.75	8.75	8.86	11.12	11.88
3_3	7.88	7.27	9.28	8.50	9.28	10.38	7.27	11.54	11.00	12.81	12.76	13.45
3_4	7.30	8.84	10.93	10.93	11.86	12.50	11.54	11.50	12.46	12.46	12.50	13.72
3_5	7.68	9.49	10.08	10.08	10.66	10.61	10.60	10.60	11.19	11.77	12.96	14.14
6_1	10.35	10.35	10.74	11.24	11.88	12.82	10.57	12.49	14.41	13.48	15.40	16.58
6_2	9.38	10.46	11.60	11.45	12.68	12.74	12.66	14.08	14.08	15.49	14.08	16.90
6_3	8.94	10.67	12.11	10.90	11.46	11.46	10.90	12.87	14.02	12.75	15.28	15.29
6_4	10.82	12.73	11.79	13.75	12.77	12.77	12.77	12.73	14.72	13.75	16.65	16.65
6_5	8.86	10.34	10.08	9.75	9.46	11.70	11.53	11.96	12.70	13.87	15.20	15.85
10_1	10.60	12.27	12.27	12.27	12.96	11.89	11.89	12.91	15.11	17.22	15.11	16.18
10_2	12.71	12.71	14.40	11.65	11.65	14.07	13.99	14.86	15.71	15.74	16.58	17.54
10_3	12.52	11.40	13.55	13.55	14.64	12.94	13.89	15.09	17.40	17.36	18.52	20.84
10_4	10.44	11.71	12.13	13.60	13.25	12.37	13.05	13.05	16.12	15.35	16.12	17.67
10_5	10.62	11.67	12.29	13.76	13.76	14.59	12.90	15.47	16.33	16.51	18.35	21.04
18_1	18.33	19.89	16.79	17.98	17.98	19.56	21.15	21.45	20.97	25.78	25.78	28.99
18_2	17.75	19.40	18.68	16.51	17.75	21.52	19.58	20.88	20.88	24.06	25.34	24.38
18_3	17.65	19.36	17.95	20.77	20.52	20.52	20.77	23.21	23.21	23.40	26.12	27.72
18_4	16.83	16.83	16.30	16.51	19.02	18.69	20.89	19.72	20.77	21.75	21.69	27.73
18_5	17.39	22.69	21.26	21.55	20.66	21.41	14.61	22.44	24.67	25.77	24.75	26.91

Table 10: Vertebral body width (mm) for all subjects.

Subject #	VB 1	VB 2	VB 3	VB 4	VB 5	VB 6	VB 7	VB 8	VB 9	VB 10	VB 11	VB 12
1_1	10.96	10.35	9.15	9.91	11.03	9.15	9.76	9.74	9.13	9.82	12.19	14.02
1_2	17.15	17.90	16.39	17.20	14.92	19.43	17.94	18.76	19.43	21.62	22.36	21.62
1_3	12.92	14.37	13.88	11.90	14.37	13.88	14.40	14.40	15.88	15.39	18.88	18.88
1_4	13.82	16.41	14.80	14.82	15.40	15.84	17.43	17.50	17.46	17.96	19.60	20.70
1_5	14.08	14.77	14.23	13.48	14.15	13.43	14.65	12.07	12.15	13.48	14.77	17.45
3_1	13.70	16.68	14.30	13.11	12.63	13.70	14.88	14.34	16.08	18.49	21.50	20.87
3_2	10.42	13.56	11.09	14.28	12.70	20.61	19.80	19.16	19.16	19.95	21.40	23.78
3_3	15.93	16.62	16.58	15.99	12.11	14.25	16.05	13.38	20.49	16.68	20.44	24.30
3_4	14.51	18.21	12.46	13.42	21.11	22.46	24.40	17.25	18.21	20.22	23.00	25.90
3_5	15.99	17.16	16.49	17.16	15.35	15.89	18.87	18.87	21.23	21.32	23.55	24.75
6_1	22.09	23.07	18.25	18.35	21.15	21.13	21.13	22.11	21.15	24.03	25.94	26.90
6_2	21.11	20.59	16.90	17.64	19.69	18.34	19.00	19.74	20.45	20.51	26.02	28.84
6_3	29.31	25.50	21.01	20.38	21.02	22.29	24.20	26.74	28.01	31.19	35.01	34.38
6_4	27.44	26.45	23.51	21.55	21.55	23.51	23.59	25.48	26.46	30.38	31.36	34.30
6_5	20.48	19.86	15.85	14.53	18.68	15.86	17.83	19.25	21.22	21.13	23.86	26.49
10_1	33.38	33.43	29.06	28.00	25.83	26.19	26.99	29.06	30.13	35.53	40.91	43.10
10_2	20.97	23.63	25.37	25.33	27.12	28.80	28.86	29.73	30.55	33.27	35.79	41.98
10_3	27.80	28.96	25.47	19.71	18.56	22.27	21.12	20.84	23.18	24.34	30.29	34.90
10_4	19.97	22.27	20.95	20.19	19.20	20.01	19.19	20.74	23.23	28.41	29.25	33.01
10_5	24.09	24.03	22.33	20.60	21.46	19.76	25.13	23.19	30.15	36.06	39.68	42.41
18_1	24.17	22.74	24.17	22.51	22.57	24.33	24.12	28.99	30.59	32.16	35.38	41.84
18_2	26.23	23.81	23.53	32.42	34.25	32.31	36.96	36.91	38.80	27.68	30.27	31.32
18_3	26.16	23.62	23.21	22.19	24.71	25.05	24.71	26.75	26.12	26.28	30.61	33.40
18_4	24.80	24.70	25.77	23.82	23.82	25.62	24.70	25.77	29.81	32.56	33.61	36.44
18_5	33.63	33.63	33.69	32.97	28.10	29.15	30.77	31.55	32.80	40.47	43.75	44.82

Table 11: Vertebral body depth (mm) for all subjects.

Subject #	VB 1	VB 2	VB 3	VB 4	VB 5	VB 6	VB 7	VB 8	VB 9	VB 10	VB 11	VB 12
1_1	8.48	9.91	10.42	9.76	11.03	10.35	11.58	10.98	11.58	9.82	11.58	10.96
1_2	8.97	11.28	12.01	12.86	11.20	12.75	13.43	13.49	14.18	14.92	14.23	15.65
1_3	10.21	10.86	11.77	12.70	10.59	12.14	11.49	11.56	12.54	11.90	12.92	13.37
1_4	10.20	13.04	11.59	12.55	12.28	13.36	12.36	11.87	11.38	11.91	11.14	13.30
1_5	10.26	8.95	11.42	11.42	12.07	12.37	13.18	12.81	14.45	13.41	12.90	13.43
3_1	11.45	13.38	13.85	13.06	13.59	14.31	14.59	15.88	17.76	17.05	16.76	16.12
3_2	12.80	13.06	16.04	15.30	16.04	16.04	17.30	16.33	16.02	14.28	16.65	15.92
3_3	10.30	11.29	11.75	12.70	13.76	14.25	15.42	13.45	15.99	14.67	15.35	15.99
3_4	10.93	13.56	15.46	15.46	16.41	16.41	17.28	19.19	18.21	19.17	20.15	21.28
3_5	12.86	12.86	13.00	13.55	14.73	15.32	15.91	16.48	16.49	17.75	18.85	18.26
6_1	14.63	15.90	16.41	17.71	18.65	19.43	21.15	23.13	21.15	22.11	22.28	24.49
6_2	14.50	14.50	15.04	16.88	16.94	18.29	18.30	19.71	19.69	20.41	21.10	21.85
6_3	14.98	15.61	15.49	17.93	18.47	19.74	19.99	19.83	20.46	20.62	20.38	21.65
6_4	13.75	12.88	15.67	15.79	17.66	18.84	20.94	21.64	20.78	21.75	23.51	21.57
6_5	13.37	14.22	14.48	14.77	16.31	16.98	17.48	17.37	18.60	19.81	19.82	21.88
10_1	14.44	17.02	19.07	20.70	21.55	22.63	25.92	26.93	28.06	30.21	30.44	32.45
10_2	18.66	19.69	21.98	21.98	22.10	19.52	22.71	22.69	23.63	27.07	26.19	28.42
10_3	11.40	12.94	17.63	17.97	20.21	21.34	24.42	25.47	25.47	25.49	24.42	27.88
10_4	15.54	13.84	15.54	16.76	17.72	19.25	19.97	20.72	21.61	22.37	21.49	22.47
10_5	16.67	16.51	18.21	19.06	20.67	20.62	23.32	25.02	26.95	27.48	28.31	29.86
18_1	20.34	23.90	23.90	26.52	28.08	28.08	30.72	30.72	32.32	35.41	35.41	35.41
18_2	18.68	18.68	19.88	20.26	20.26	24.06	26.13	30.04	27.90	30.13	30.55	27.65
18_3	16.54	19.08	19.73	23.93	22.52	26.28	25.05	27.61	27.72	29.02	29.02	33.87
18_4	16.51	18.08	20.30	22.02	25.24	26.88	30.59	30.59	31.53	33.03	34.00	37.07
18_5	18.78	19.85	23.10	24.47	26.63	29.47	26.37	28.57	30.33	32.51	30.33	32.67

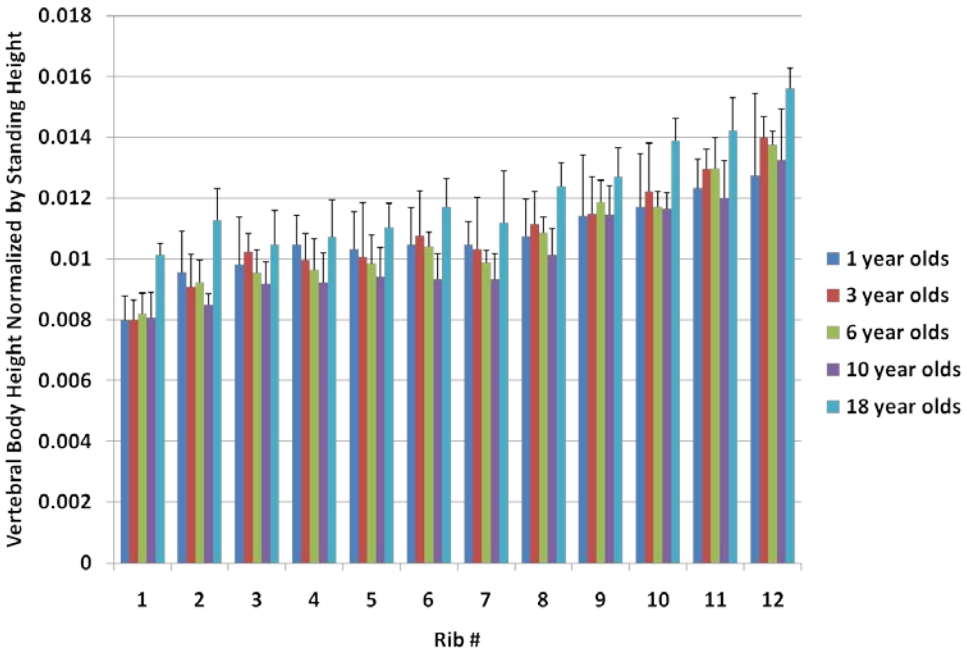

Figure 53: Vertebral body height normalized by standing height for all age groups.

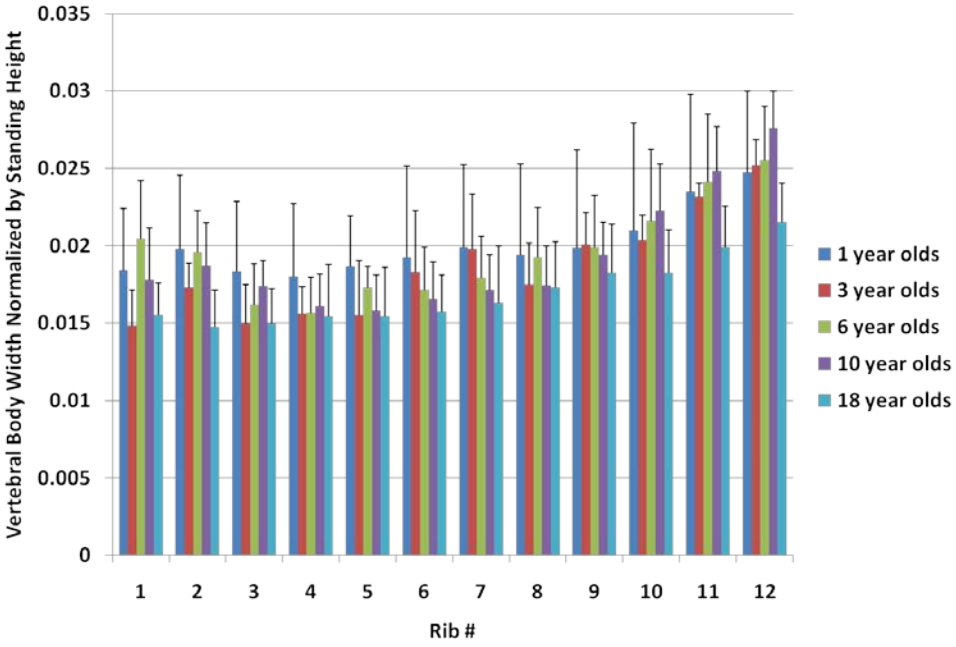

Figure 54: Vertebral body width normalized by standing height for all age groups.

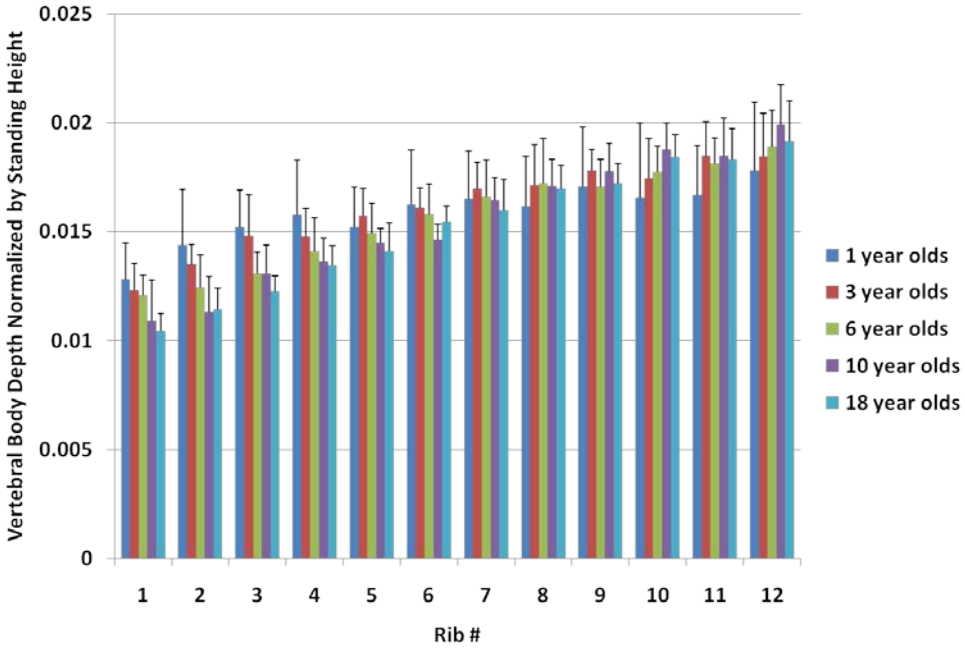

Figure 55: Vertebral body depth normalized by standing height for all age groups.

Polynomial coefficients for each rib

Coefficients for a second and third order polynomial equation were calculated using the polyfit command in MATLAB. No difference was found between the second and third order equations, therefore only the second order coefficients are reported. Tables for right and left coefficients for each rib for each subject are reported in Microsoft Excel format on the attached data CD attached to this manuscript (filename: Second Order Polynomial Coefficients for all subjects).

1.5 Discussion

1.5.1 Subjects

Subjects were selected who had good quality CT scans with all ribs visible, as well as anthropometric information recorded on the date of the CT scan. An attempt was made to choose subjects as close to the 50th percentile for height, weight and BMI as possible, however due to the difficulty of obtaining a large number of good quality scans, this was not always possible. All three to 18 year old subjects were between six and 90 percent for weight, six and 95 percent for height, and three and 96 percent for BMI in their

respective age groups. Choosing appropriately sized subjects is important in this study because we are making a comparison to an object that is designed to represent all children. All efforts were made to do this, but since this is a retrospective study design, we were unable to recruit subjects within a narrower height, weight and BMI range.

A comparison of each of the subjects' height, weight, chest width and chest depth compared to the 5^{th}, 50^{th}, and 95^{th} percentile values of the child population for each age group was performed using data from Snyder et al. (1975) and Snyder et al. (1977). In each of these anthropometry data sets, only combined gender data was available for all age groups, and chest depth data was only available for ages 1-13. Plots for each of these comparisons are shown in Figures 56-59. Deviation from 50% for height and weight increases as subject age increases. Chest width and depth are higher than 50% for ages 3, 6, 10 and 18 with the exception of one 10 year old subject. This may be explained by the chest shape difference between supine and standing positions. Anthropometric data were measured in the standing position, while the CT scans were taken in a supine position. In the case of CPR manikins, the supine position is a more accurate position, since a child is lying on their back during the administration of CPR. However in most other applications, a difference between standing and supine positions would not be beneficial. In studies based on adult volunteers, no significant differences were observed in rib cage structure or geometry between supine and seated positions. Beillas et al. (2007) performed a positional MRI scan study on 9 adult subjects. They studied effects of posture in the position, shape and volume of abdominal and thoracic organs in the seated, standing, forward-flexed and supine positions. No significant differences were observed in distance between T7 and sternum, but there is large subject to subject variation. Agostoni et al. (1965) tested 13 adult subjects to measure the relationship between rib cage circumference and lung volume in standing, seated and supine positions. They observed no significant changes in circumference between seated and supine positions.

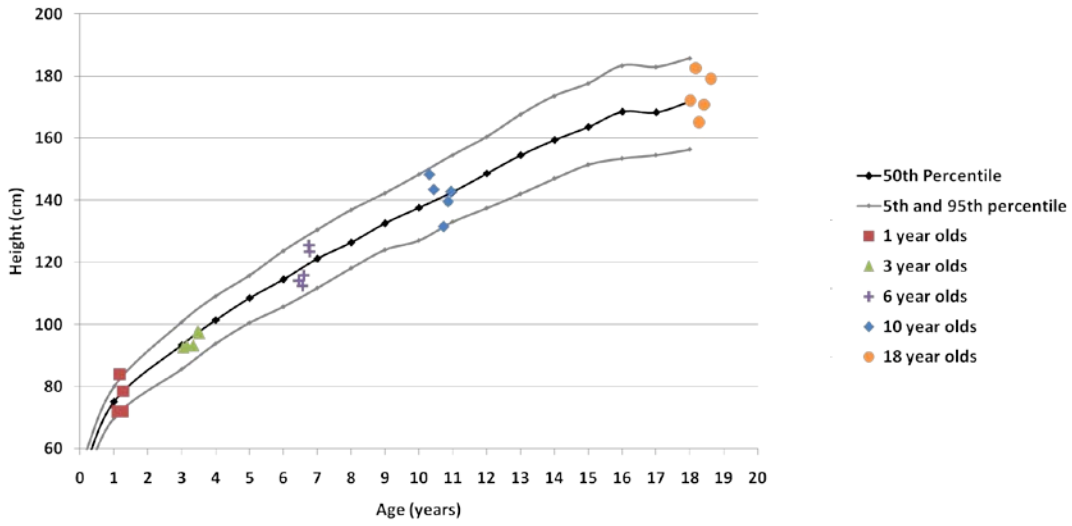

Figure 56: Comparison of study subjects and 50th percentile of the child population for height (0-2 year olds: CDC Growth Charts http://www.cdc.gov/growthcharts/clinical_charts.htm; 2-18 year olds: Snyder et al., 1977). Anthropometry data is for males and females.

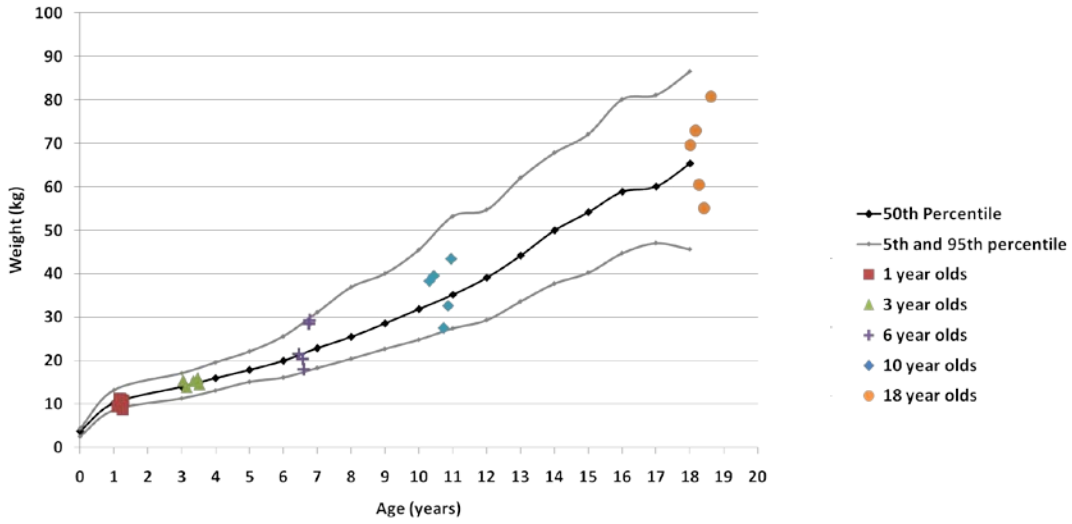

Figure 57: Comparison of study subjects and 50th percentile of the child population for weight (0-2 year olds: CDC Growth Charts http://www.cdc.gov/growthcharts/clinical_charts.htm; 2-18 year olds: Snyder et al., 1977). Anthropometry data is for males and females.

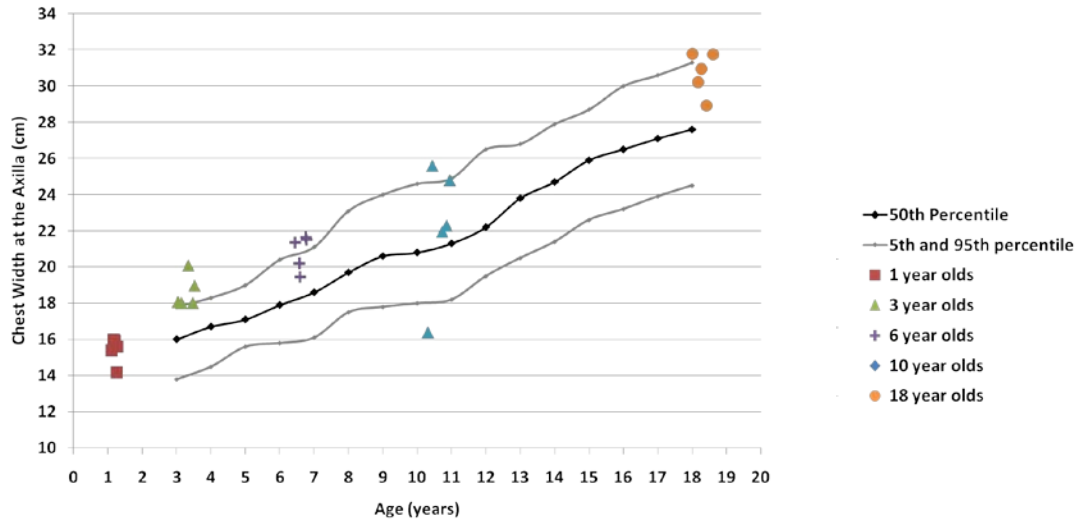

Figure 58: Comparison of study subjects and 50th percentile of the child population for chest width at the axilla (Snyder et al., 1977). Anthropometry data is for males and females.

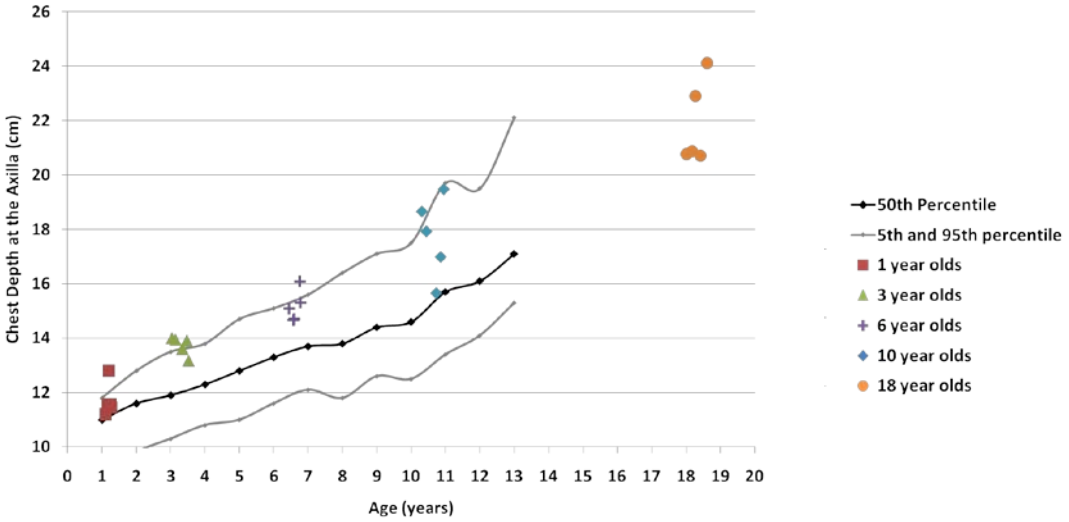

Figure 59: Comparison of study subjects and 50th percentile of the child population for chest depth at the axilla (Snyder et al., 1975). Data was not available for children over 13 years. Anthropometry data is for males and females.

Limitations of our subject group include small sample size and the evaluation of only male subjects. The amount of usable scans, as well as the time required to evaluate one subject (about 10-12 hours per subject) contributed to the small sample size. To increase the statistical significance of these findings, more subjects should be evaluated. Since the time required to analyze the data for the subjects was high, we chose not to evaluate females to eliminate the gender variability within an age group. For future studies,

similar analysis could be performed on female subjects. We also chose to group our subject by age, as opposed to an anatomical variable such as height or weight. We chose to do this because most child modeling, including FE analysis, CPR manikins and ATDs are grouped by age. It would be difficult to use this data in these areas if subjects were grouped by another variable.

1.5.2 Ribcage Parameters

Even though it is difficult to compare our data to an actual child or animal, comparison of our data to other published studies is possible. Since all studies that have previously measured rib cage parameters in adults, and to our knowledge, no similar studies have been performed on healthy children, exact comparisons were not possible. Therefore, our results from the 18 year old age group were compared to adult data. The following comparisons include thoracic index, apparent curvature of the ribs, longitudinal twist of the ribs and lateral rib angle.

Thoracic index has been calculated for humans at the widest part of the chest (Dean et al., 1987; Doershuk et al., 1975). Thoracic index of the overall chest decreases as age increases, from a value of around 0.75 for infants to around 0.60 for adults. This indicates a shift from a more circular shaped chest to a more oval shape. This measurement also includes the soft tissue surrounding the rib cage. Our thoracic index values indicate roundness of the ribs at each level, not overall chest shape. Our thoracic index measurements are also taken in the plane of the ribs; whereas external thoracic index is measured in the axial plane. Even though our study calculated internal thoracic index, we found similar values at some rib levels. In ribs three through six we calculated values of approximately 0.60-0.70 for all age groups. Even though exact comparisons were not valid, we can see that our calculations are in the same range as external measurements.

We also found that thoracic index decreased with increasing age for ribs one through three and increased with increasing age for ribs six through 12. This trend does not agree with the trend found in Dean et al. (1987) and Doershuk et al. (1975), as well as our initial assumption that the infant thorax tends to be more round. There are two points to consider in understanding thoracic index. The first is that our calculation does not take into account external soft tissue, which may cause the chest shape to be more rounded. The second point is that in infancy, ribs are not fully developed and have a shorter length. The anteroposterior

distance is calculated to be the distance in the X-Z plane from the front to the back of the rib. Because infants have less developed ribs (that is, they have not grown long enough at many rib levels to curve around to the front of the thorax as much as older subjects), the anteroposterior distance is not necessarily a calculation of the overall thorax shape. Therefore, the shape of the infant thorax may be more rounded, but because of the definition of our calculation, the ribs seem to have a more oval shape. For this same reason, thoracic index of the twelfth rib may not accurately represent the shape of the ribcage at that level. Since it tends to be a long, straight rib, the anteroposterior distance is very small.

Analysis of the curvature of the ribs may be a better way to characterize how round or flat a rib is at a certain point. In our study, we found that curvature decreases as age increases, which indicates more curved ribs in younger children. Even though the thoracic index does not indicate that infant ribs are more circular, apparent curvature does indicate that they are more rounded at each percentage point.

When we compare our 18 year old apparent curvature with apparent curvature found in the literature from adults, we calculate similar values. Mohr et al. studied apparent curvature in 8 human cadavers age 59 ± 13 years. Results from his study were converted into mm^{-1} for comparison purposes (Figure 60, compare to our calculated apparent curvature in Figure 33). Mohr et al. performed calculations at 15 through 85 percent of rib length at 10 percent intervals. These results are the same order of magnitude as our results, and they are most similar to our 18 year old subjects. The highest curvature in Mohr's data was at the 15% site of rib length, and the highest curvature in all age groups in our study was observed at 20%. Our data does show a higher variation in apparent curvature values, which is most likely due to the fact that our subjects are still growing (male subjects continue to grow until their early twenties). A growing adolescent population tends to have higher variation for anatomical measurements.

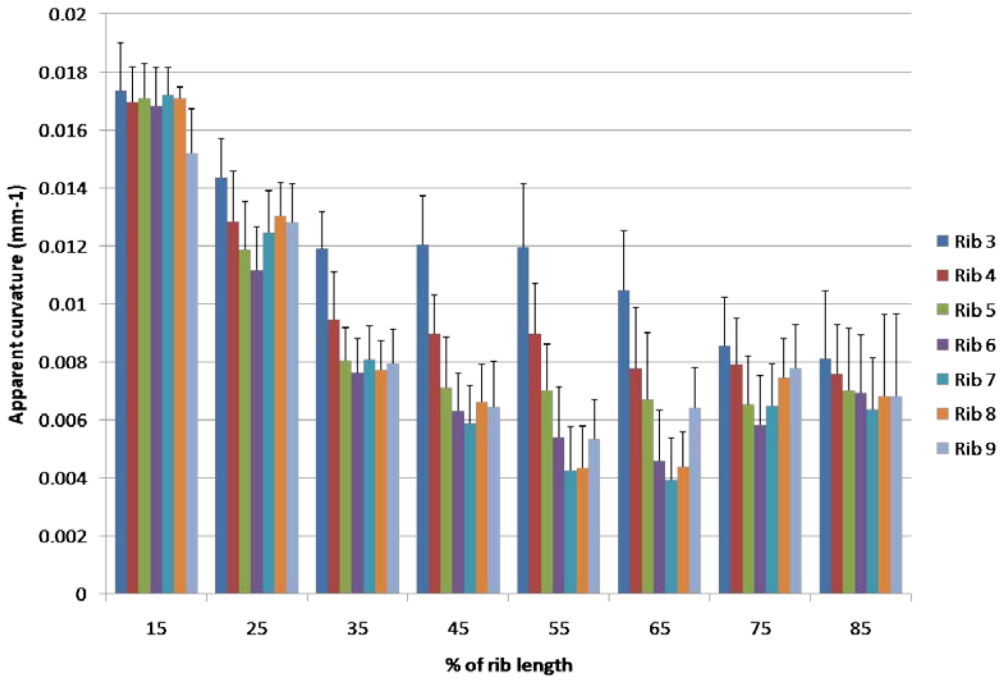

Figure 60: Apparent curvature reported in Mohr et al., 2007. Units were converted from m^{-1} to mm^{-1} for comparison.

Longitudinal twist was also calculated by Mohr et al. (2007) using the same cadaveric specimen. Results from that study are shown in Figure 61. In Mohr et al., results are presented as overall twist of the rib, where the 15 percent site is subtracted from the 85 percent site (compare to our longitudinal twist difference plot in Figure 39). Our results were different than those presented by Mohr et al. (2007). In their analysis, longitudinal twist increases with increasing rib number for ribs three through nine, our data shows decreasing longitudinal twist with increasing rib number. One possible explanation is that in Mohr et al. (2007), each cadaver rib was detached from the rib cage, eliminating any internal stresses on the ribs.

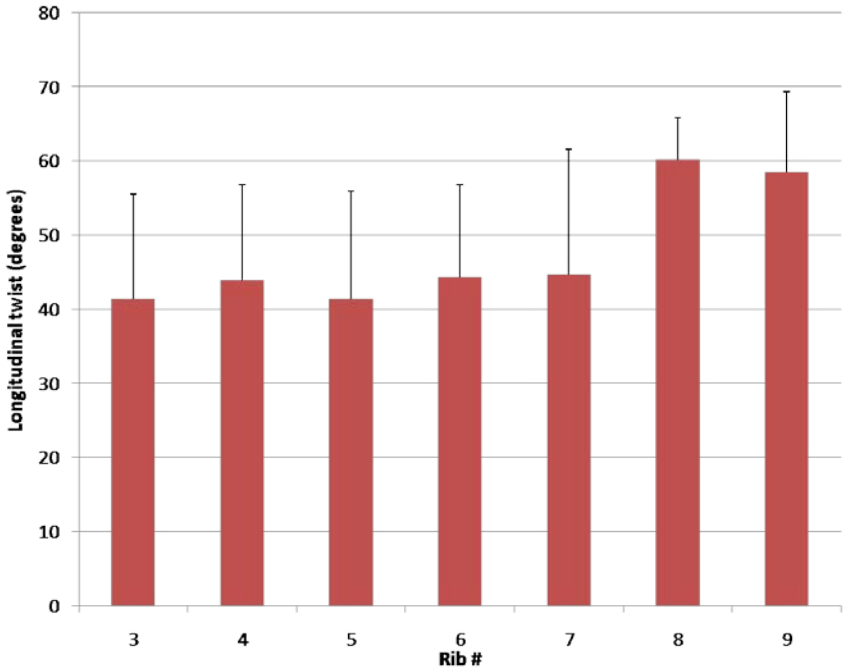

Figure 61: Longitudinal twist results from Mohr et al., 2007.

The final comparison of our data is lateral rib angle which was studied by Kent et al. (2005) based on retrospective CT scans. They studied 18 through 89 year old adult subjects, and reported an increase in lateral rib angle with increasing age. Our study showed a trend of decreasing rib angle with increasing age. These data may not be conflicting since the populations studied are in different age groups. The angle of the ribs may change throughout the life span, decreasing in adolescence and increasing in older age. There may be two reasons that the ribs change from horizontal to more vertical in adolescence. The first is that the sternum descends with respect to the spine from infancy until ages two through three. The descending sternum would cause the ribs to angle downward. This has been reported in human subjects (Scheuer and Black, 1996). The second reason is that muscle tone increases from infancy to childhood, causing the ribs to shift downward. The effects of muscle tone on rib angle have not been studied. The increase in rib angle with old age may also be explained by muscle tone, which begins to decreases again after the young adult stage of life.

1.5.3. Significance of the study of the pediatric rib cage

The study of the pediatric thoracic cage presents many opportunities for the improvement of health care and injury prevention applications related to the pediatric thorax. In the area of health care, applications include, but are not limited to, medical simulation tools, medical implant design and development, rib reconstruction and scoliosis treatment. The vertical expandable prosthetic titanium rib (VEPTR) is a device used to treat thoracic insufficiency syndrome of the pediatric rib cage, which is usually caused by scoliosis (Campbell et al., 2007; Smith et al., 2006). This device has been designed with limited knowledge of the detailed structural characteristics of the pediatric rib cage. Data for age-related changes in the pediatric rib cage structure will allow physicians to more accurately correct scoliosis, as well as design age-specific VEPTR devices.

In some medical applications, specific treatments for children have not been designed, so methods used for adult treatment are used for the pediatric population. An example of this problem is chest wall reconstruction (Tuggle et al., 2004; Smith et al., 2006). Indications for chest wall reconstruction are usually tumor-related, however, congenital defects or injuries occasionally require this type of surgery. Materials are widely available for adult reconstruction, and pediatric surgery generally uses these adult materials. Recent investigations of pediatric chest wall reconstruction have used bioabsorbable materials for reconstruction to eliminate the need for removal when the child grows (Tuggle et al., 2004). These materials are superior to non-resorbable materials in children (Smith et al., 2004). Further improvements of these types of devices include age-specific sizes and geometry to eliminate the need to fit a device to a child during surgery, and therefore decrease surgical time. Medical devices should be designed and developed specifically for growing children; however, lack of pediatric thoracic structure data has made this a challenge. Age-specific thoracic data will be useful for any type of thoracic cage medical device, but uses of the data are not limited to patient-specific applications.

Medical simulation tools are designed to represent a larger pediatric population and are an aspect of health care training that can benefit from a shape analysis of the pediatric rib cage. A variety of medical simulation tools are available to medical professionals to practice medical guidelines before having any patient contact. These include basic life support manikins (CPR manikins), advanced life support trauma

manikins, needle stick arms, maternity simulations, and many more. It is important that these medical simulation tools be as accurate as possible to give the trainee a more realistic experience. In the case of CPR manikins, chest shape can influence how CPR is administered. In children, the correct administration of CPR affects compression of the heart and blood flow to the brain and body (Dean et al., 1987). Chest shape for pediatric CPR manikins should therefore accurately represent the human child population. The second part of this study focuses on using pediatric data to analyze the outer shape of the pediatric thorax, and identify how a commercially available pediatric CPR manikin could be improved. Currently, the 5-6 year old CPR manikin is used to represent a wide range of pediatric ages. In the future, this data could be used to design and develop age-specific CPR manikins with internal and external anatomical features to give trainees age-specific CPR experience on a variety of pediatric age groups.

In the field of injury prevention, potential applications for structural characteristics of the pediatric rib cage include finite element (FE) modeling, design of anthropometric test devices (ATDs, also known as crash test dummies), motor vehicle crash responses and any other type of impact response of the pediatric thorax. ATDs and computational models are currently used to evaluate automotive restraint systems for child occupants. The geometric and structural biofidelity of the thorax of the pediatric ATD governs how the restraint system interacts with the subject. Differences in thoracic shape influence seatbelt fit, which may affect the injury risk for children. Improper belt fit causes the seatbelt to move away from the skeletal structures that can bear high loads without injury, creating excessive loads on the abdomen and spine (Reed et al., 2009). Pediatric ATDs are scaled geometrically based on adult data, and therefore may not accurately reflect the mechanical response of a child in an automobile accident due to the shape differences of the thorax. Once the structural characteristics of the pediatric thoracic cage are established, this information can be used to improve ATD design for the pediatric population. Better ATD designs can then more appropriately guide restraint system designs and injury assessment values.

There is a clear need to collect detailed pediatric rib cage geometry data. Information about global developmental changes of the rib cage has limited use in cutting edge research, but intrinsic rib geometry data will allow researchers the ability to design more accurate pediatric rib cage models. There is a wide

range of technology applications for this data that can improve child safety and quality of life, as well as medical training.

1.5.4 Future work and opportunities for improvement

Future work for this data includes an average shape analysis of the rib cage, as well as the inclusion of more subjects. Average shape analysis can be performed using a principal component analysis approach. Principal component analysis is a way to statistically compare two data sets by reducing the number of variables. Two types of principal component analysis are the Generalized Procrustes Analysis (GPA) and Linear Regression Analysis. Each of these numerical approaches will output an average shape of the rib cage for each age group. Once an average shape is found for an age group, our data can be shown as a single model that represents an entire age group.

There are a few aspects of this study that could be improved for future studies of the pediatric thoracic cage. The inclusion of more subjects in future studies is important. In order to represent the entire pediatric population, a broader range of subjects is necessary. This includes analysis of more male subjects, as well as the inclusion of female subjects. Another aspect is the collection of data from the CT scans. In our study design, Cartesian points were collected manually and subjectively along the surface of the rib shaft. Future studies could design or identify an algorithm that systematically places points along the rib, or directly analyzes the shape from the CT scan. This would increase the accuracy of each measurement and calculation made in this study.

Chapter 2: COMPARISON OF THORAX SHAPE WITH A CPR MANIKIN

2.1 Background

2.1.1 Cardiopulmonary resuscitation

In the 1960's, Asmund S. Laerdal, along with Dr. Bjorn Lind and Dr. Peter Safar developed the first CPR manikin, Resusci-Anne. They recognized the need for mouth-to-mouth resuscitation as well as life-like simulation to train people to perform ventilation in emergency situations. In 1974, the American Heart Association (AHA) and the American Medical Association (AMA) recommended that CPR training be available to lay people. Since then, CPR manikins have been improved to increase the quality of training. Growing concerns about patient safety and cost efficiency have led to the increased use of patient simulation for CPR, with manikins capable of measurement and feedback to improve CPR performance (50 years of evolving needs and solutions, www.laerdal.com).

CPR is the "method of providing oxygen and blood circulation through the delivery of rescue breathing and chest compressions to victims of sudden cardiac arrest (Quality CPR, www.laerdal.com)." This is done to ensure a flow of oxygenated blood to the brain and other organs. Most victims of cardiac arrest also need defibrillation (also known as shock delivery), which is most successful if performed within five minutes of sudden cardiac arrest. CPR should be performed both before and after defibrillation (Circulation Part 3: Overview of CPR).

The American Heart Association published guidelines for adult and child CPR. CPR involves checking breathing, rescue breaths and chest compressions. Differences in the AHA recommended guidelines for infants (0-1 years), children (1-8 years) and adults (>8 years) are outlined. Checking the patient's breathing requires determining the absence or presence of breathing. In children, abnormal breathing patterns are adequate to qualify the patient as breathing. In adults, abnormal breathing indicates cardiac arrest and the need for CPR. A rescue breath requires blowing into the patient's mouth for one second. Effective breaths produce noticeable movement in the patient's chest. It is especially important to give effective breaths to infants and children since asphyxia arrest is more common in these age groups. The airway may need to be re-opened before an effective breath can be delivered. Infants and children should receive 12-20 breaths

per minute and adults should receive 10-12 breaths per minute. Rescue breaths should be given without chest compressions (Circulation Part 3: Overview of CPR).

Chest compressions for children should be administered hard and fast (100 compressions per minute). The chest should be compressed to one third or one half the depth of the chest. One or two hands can be used, whichever is required to compress the chest an appropriate amount. A 30:2 compression-ventilation ratio should be used. Infants should be given compressions just below the nipple line (the lower half of the sternum). Compressions for adults and children should be between the nipples (Circulation Part 3: Overview of CPR).

2.1.2 Background: Little Junior CPR manikin

The Little Junior CPR manikin is the most basic child CPR manikin. It is made up of a hard plastic back section, a plastic rib plate, overlaying skin, a head with a mouth that can be opened for breathing, and a compression spring to give the manikin thorax appropriate stiffness. An optional 'clicker' is available to produce audible feedback each time a compression is given. Product features include an oral and nasal passage, head tilt and chin lift. This manikin is light-weight and easy to carry and store. It has anatomical landmarks on the surface of the manikin, including nipples, manubrial and sternal notches, clavicle and outline of the bottom of the rib cage. Each part of the Little Junior is shown in Figure 62. These parts were taken from the Laerdal parts catalog. Other pediatric CPR manikins include the Resusci Junior and the Resusci Baby Basic manikins. The Resusci Junior is a full-body child manikin and the Resusci Baby is a full-body infant manikin. Specifications for each of these dummy are shown in Table 12.

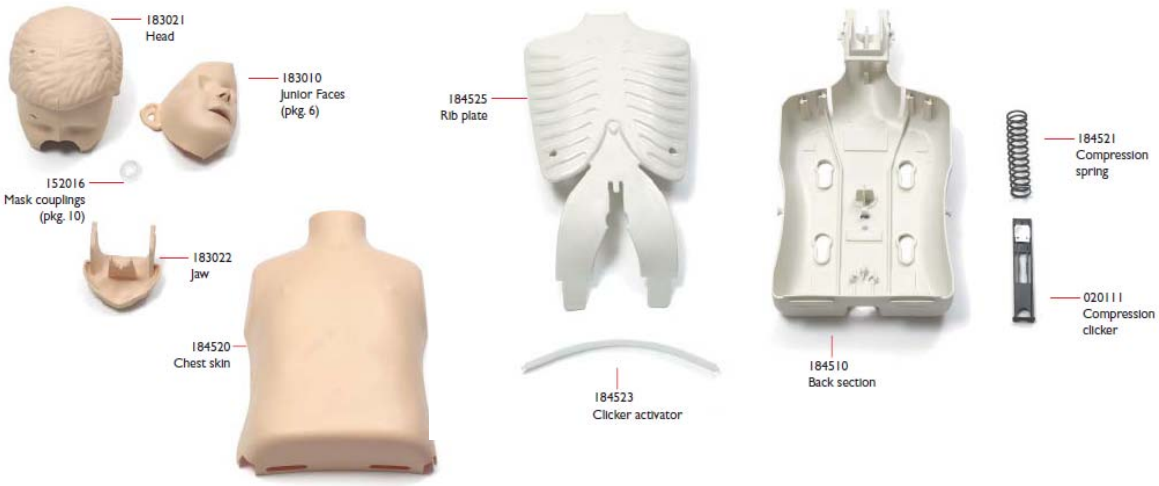

Figure 62: Parts of the Little Junior CPR manikin (from the Laerdal Parts Catalog, http://www.laerdal.com)

Table 12: Little Junior CPR manikin specifications. Adapted from the Laerdal website, http://www.laerdal.com.

Specification	Little Junior	Resusci Junior	Resusci Baby Basic
Where marketed	Worldwide	Worldwide	Worldwide
Type	Male torso child	Male full-body child	Female full-body infant
Airway	Non-breathing, disposable	Non-breathing, disposable	Non-breathing, disposalble
Cartoid Pulse	No	Yes	Yes (brachial)
Ribs, Xyphoid	Yes	Yes	Yes
Gastric distension simulation	No	No	No (Yes with skill guide)
Navel	Yes	Yes	Yes
Tongue/teeth	No	No	No
Adam's apple	Yes	Yes	No
Chart recorder	No	No	No
Metronome	No	No	No
Length (cm)	55	112	51
Weight (kg)	2.7	6	2.3
Other Specifications	Lightweight with realistic features. Supplement to Resusci Junior: Softpack, 4-pack version, choking kit available. Removable face mask made of polyvinylchloride (PVC). Soft nose which can be occluded.	Water update kit available.	Optional skillguide provides interactive feedback on ventilations, compressions, wrong hand position and stomach distension.

2.2 Objective

In order for pediatric CPR manikins to meet the American Heart Association CPR delivery guidelines and function as effective surrogates, they should have geometrical characteristics that are similar to pediatric human subjects. So, the secondary objective of this study is to quantify the external thoracic geometry and shape of the Little Junior cardiopulmonary resuscitation (CPR) manikin and compare with a six year old pediatric human subject.

2.2.1 Design Criteria

1. To directly compare the outer shape of the Little Junior CPR manikin thorax with one pediatric human subject – The experimental design must incorporate a direct comparison of the CPR manikin surface (physical object) with a human subject (CT scan in electronic format).
2. To quantify the shape difference between the CPR manikin and one pediatric human subject – the comparison of these outer surfaces should incorporate quantitative data to show how much shape difference exists and in which locations these differences exist.

2.2.2 Constraints

1. Analysis of Little Junior CPR manikin must be performed from an actual manikin - No electronic files of the CPR manikin were available, therefore an actual CPR manikin must be analyzed.
2. Analysis of the human subject must be performed using CT scans – Child cadavers and real human subjects were not available for us to use, therefore retrospective CT scans must be analyzed.
3. Analysis of Little Junior CPR manikin must be inexpensive – High quality surface analysis of the CPR manikin may have been possible (example: laser scanning), however this is a more costly option. An inexpensive alternative is necessary to keep the project within budget.
4. Use free or low-cost software – Software for image analysis and mathematical calculations must be available through The Children's Hospital of Philadelphia or Drexel University due to the limited amount of funding received.

2.2.3 Study Design

An outer surface analysis of the Little Junior CPR manikin and a six year old human subject was performed using a software-based approach. First, the surface of one six year old human subject was characterized by segmenting the skin, fat and muscle from the internal organs and bone in using a CT scan. Next, the surface of the Little Junior CPR manikin was characterized using a three-dimensional desktop digitizer (Microscribe G2, Immersion Corporation, San Jose, CA). Each of these surface characterizations was then imported into a solid modeling program in STL format. Quantitative analysis was performed by measuring the distance between corresponding points of each surface, as well as by calculating chest depth and angles of the sternum and shoulders.

2.3. Methods for human and manikin comparison

2.3.1 Outer surface characterization

An outer surface comparison of the 6 year old human and CPR manikin was performed in order to determine differences in the two shapes. In order to accomplish this, it was necessary to characterize the outer surface of each. Human surface characterization was performed using Analyze software to extract bone and internal organs from the outer skin, fat and muscle layers. Manikin surface characterization was performed using a desktop digitizer.

The 6 year old with the chest depth and width closest to 50^{th} percent (subject 6_3) was selected for chest surface characterization. The subjects CT scan was loaded into Analyze and the surface was analyzed using the methods listed in Appendix 5.

The CPR manikin surface was digitized using a MicroScribe G2 Desktop Digitizing System (Immersion Corporation, San Jose, CA, Figure 63). In order to digitize points in a systematic way, lines were drawn on the manikin surface as a guide. First, a mid-sagittal line was drawn along the manikin thorax, starting at the manubrial notch and ending at the bottom of the manikin. Next, horizontal lines were drawn perpendicular to the mid-sagittal line, spaced every one centimeter. A total of 30 horizontal lines were drawn. A photo of the CPR manikin with lines is shown in Figure 64. The MicroScribeUtility software was set to auto scan every 5 mm along the curves. The MicroScribe stylus was moved along each line and collected Cartesian point coordinates every 5 mm. These points were recorded in Notepad and were

transferred into Microsoft Excel. The points were then mirrored across the mid-sagittal plane to create points for the other side of the manikin.

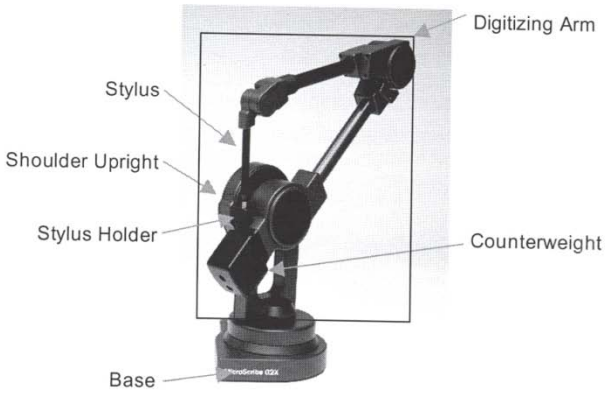

Figure 63: MicroScribe G2 Desktop Digitizing System (Immersion Corporation, San Jose, CA)

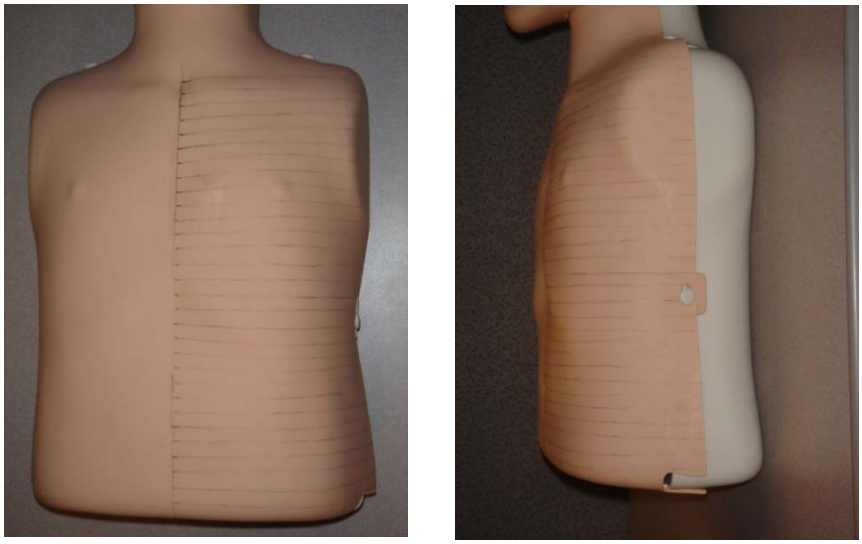

Figure 64: Little Junior CPR manikin with a line drawn on the vertical axis from the manubrial notch to the bottom of the manikin, and horizontal lines drawn perpendicular to the vertical line every 10 mm.

These points were then opened in Rhinoceros 4.0 (McNeel North America, Seattle, WA). The Mesh from Points command was used to create a mesh through the digitized points using the parameters sampling

density plus noise =12.2, auto adjust grid = yes and number of contouring grid cells = 50. The mesh was then exported as an STL file.

After each STL file was obtained, they were opened in ProEngineer (Parametric Technology Corporation, Needham, MA) and saved as part files. The human surface needed to be scaled by the scaling factor found for subject 6_3, which was performed in ProEngineer using the Scale Model command found in the Edit menu. An assembly was then created and each surface was imported and aligned. The first constraint used was aligning the back surfaces of each model. Since the manikin doesn't have points digitized for the plastic back component, the height of the component was measured and the digitized skin surface was offset from the back of the human model by that distance (53mm). Mid-sagittal datum planes were also created for each model and aligned in the assembly. To fully constrain the assembly, datum planes through the manubrial notch in the transverse plane were created and aligned.

In order to have a quantitative measurement of the difference between the two surfaces, corresponding points were placed on each model in a grid, so that the distance between them could be measured. Starting at the manubrial notch, curves were placed along the surface of each model every 2cm. A total of 15 lines were placed. In order to create a curve on each model, first datum planes need to be created in intervals of 2cm. Then cross sections can be created using the X-section tool in the View Manager. A curve can then be inserted at each 2cm interval using the curve tool and selecting the cross sections. Next, points were placed along the curves starting at the mid-sagittal plane of the model and every 2cm in each lateral direction. In ProEngineer, points are not placed along the distance of the curve. They are placed by moving the sagittal plane to the left or right by 2cm. Because points are placed in this manner, t is guaranteed that corresponding points on each model will match up. Five or six points were placed on each curve on the right and left side, depending on the lateral distance of each model at each curve. Figure 65 shows each model with curves placed along the surface, and Figure 66 shows each model with points placed along the curves.

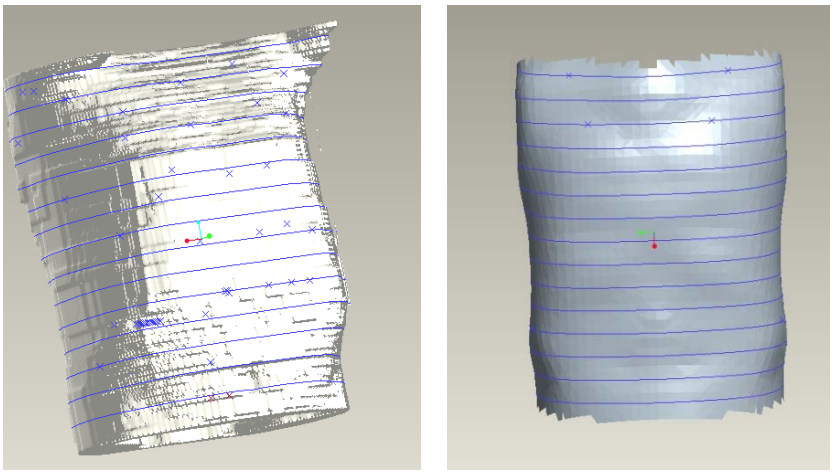

(a) (b)

Figure 65: (a) Human and (b) CPR manikin models in ProEngineer with curves spaced 2 cm apart starting at the manubrial notch.

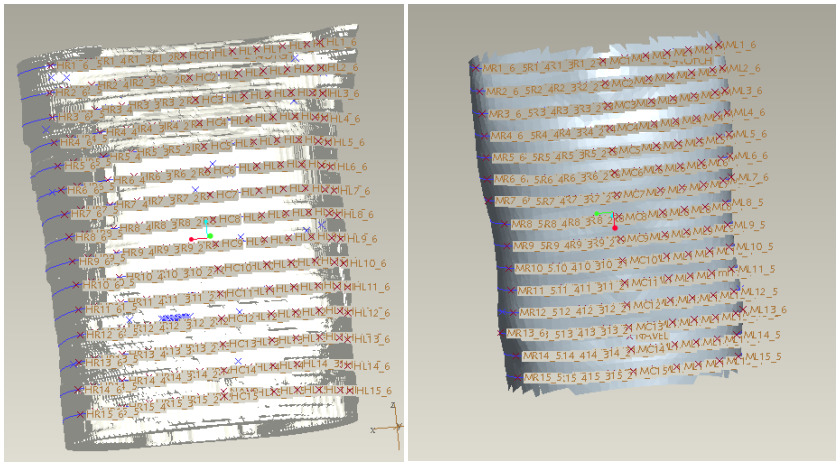

(a) (b)

Figure 66: (a) Human and (b) CPR manikin models in ProEngineer with curves and points spaced 2 cm apart.

After points were placed, the chest depth along the mid-sagittal plane was calculated for both the human and manikin using the Distance tool found in the Analysis menu in ProEngineer. The distances between corresponding points on the human and CPR manikin models were also calculated using the Distance tool. Distance measurements were copied to an excel spreadsheet for analysis.

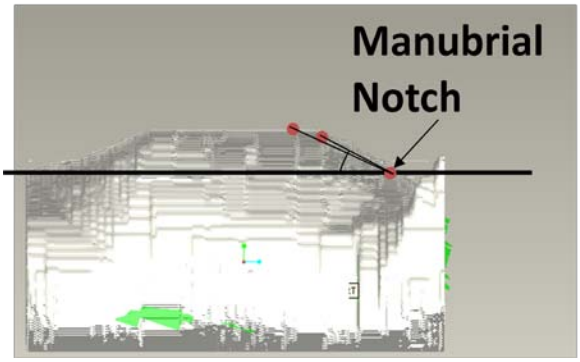

Figure 67: Diagram of how sternum angle was calculated for the human and manikin surfaces.

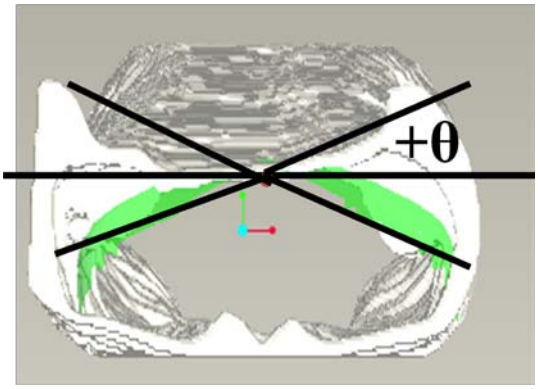

Figure 68: Diagram of how lateral chest angles were calculated for the human and manikin surfaces.

2.4 Results

The results of the direct surface comparison of the pediatric CPR manikin and 6 year old human subject show substantial differences in the shapes of each model. Isometric, top, front and right side views of the assembly in ProEngineer are shown in Figure 69. Each of these views shows the divergence of the manikin surface from the human surface at the manubrial notch. Even though most of the manikin surface is below the human surface, the manubrial notch is well above the human surface at this point. The isometric, front and right side views indicate a divergence of the manikin surface from the human surface at the lower end of the thorax near the navel. In the right side view, the manikin clearly shows a flat surface from manubrial notch to navel, while the human surface has an angled chest, a flat stomach, and an angled lower thorax.

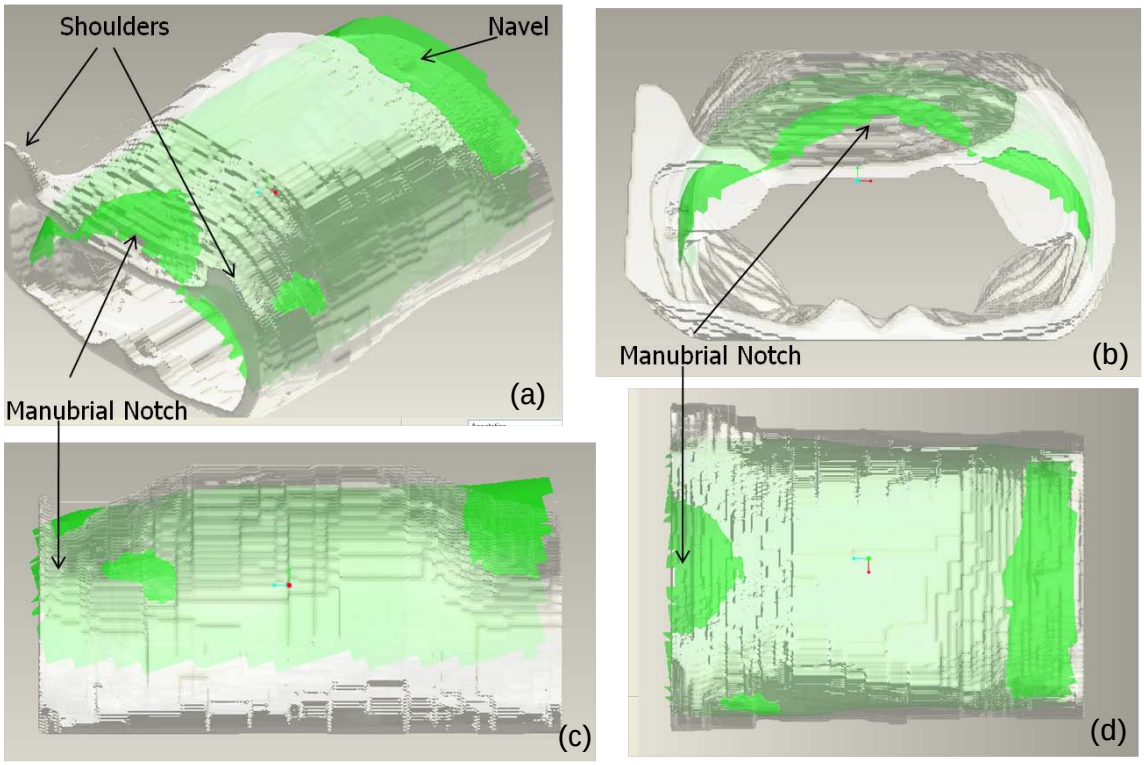

Figure 69: Direct surface comparison in ProEngineer. (a) Isometric view, (b) top view, (c) right side view, and (d) front view.

From these models, the chest depth at the mid-sagittal plane was calculated. Results show that at the mid-sagittal plane, the manikin chest depth is higher than the human for the first 60 mm from the manubrial notch, lower than the human for the next 200 mm, and then higher for the remaining 40 mm. The maximum chest depth is approximately 160 mm for the human and 145 mm for the manikin. A plot of the mid-sagittal chest depth is shown in Figure 70, and a table with exact values as well as the difference between the two chest depths is shown in Table 13.

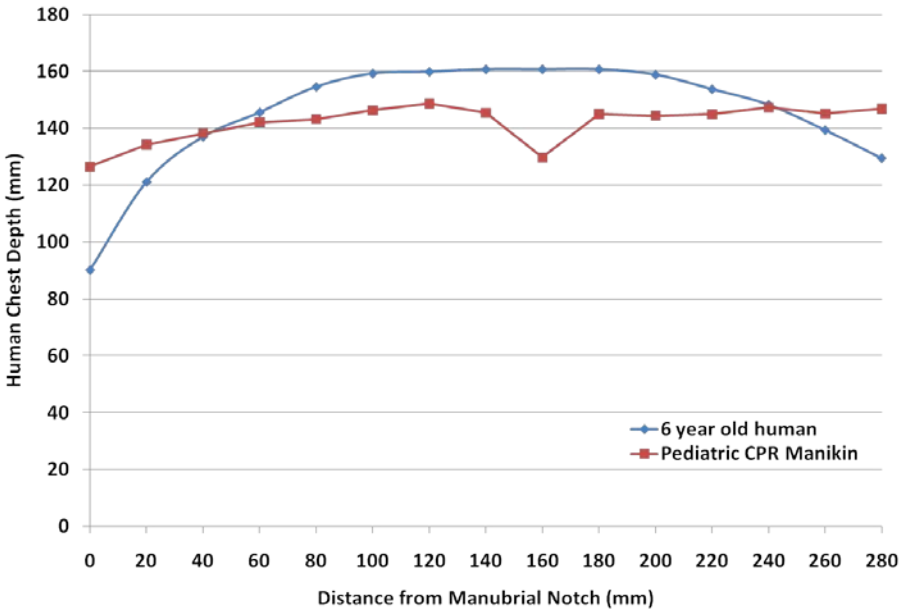

Figure 70: Mid-sagittal chest depth for the human and manikin surfaces.

Table 13: Values for mid-sagittal chest depth for the human and manikin surfaces (with reference to human surface). A positive difference indicates that the manikin surface is higher than the human surface.

Distance from Manubrial Notch (mm)	Human (mm)	Manikin (mm)	Difference
0	90.0	126.5	36.5
20	121.0	134.1	13.1
40	136.9	138.2	1.3
60	145.5	142.0	-3.5
80	154.5	143.3	-11.2
100	159.2	146.3	-12.9
120	159.8	148.7	-11.1
140	160.7	145.4	-15.3
160	160.7	129.7	-31.0
180	160.7	145.0	-15.7
200	158.8	144.4	-14.4
220	153.7	144.9	-8.8
240	148.2	147.2	-1.0
260	139.3	145.2	5.9
280	129.4	146.8	17.4

The difference between corresponding points on the human and manikin surfaces was found not only for the mid-sagittal plane, but for every point placed on each model. These results are shown in Figure 71, and each value for the difference between corresponding points is shown in Table 14.

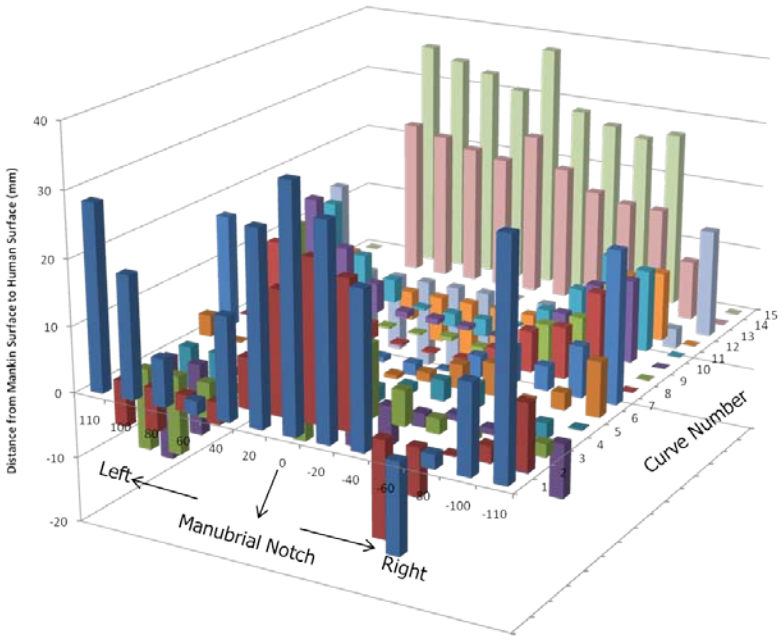

Figure 71: Distance of each point on manikin surface with reference to human surface (shape difference). A positive value indicates that the manikin surface is higher than the human surface.

Table 14: Values for the distance of each point on the manikin surface with reference to human surface.

Distance from Manubrial Notch	Line 1	Line 2	Line 3	Line 4	Line 5	Line 6	Line 7	Line 8	Line 9	Line 10	Line 11	Line 12	Line 13	Line 14	Line 15
110	28.38	-6.99	-12.60	-16.07	-6.70	3.33	17.41	0.00	0.00	0.00	0.00	0.00	13.52	0.00	0.00
100	18.71	-6.73	-12.24	-11.10	-6.43	0.08	5.80	12.64	14.12	16.58	14.37	5.00	-9.33	-16.82	-14.82
80	7.31	-2.56	-5.52	-1.11	-1.44	3.81	3.33	7.88	8.17	9.55	6.77	-2.08	-12.34	23.99	35.65
60	2.10	-3.39	-0.52	-0.78	3.36	3.71	6.62	6.20	4.66	4.67	3.70	-4.62	-14.07	22.80	34.00
40	15.56	7.72	-1.76	1.37	3.09	3.12	3.16	2.46	0.33	1.02	-0.37	-7.25	-13.38	21.49	32.67
20	29.09	18.70	-5.59	-2.09	1.27	0.72	-0.78	0.32	0.21	0.91	-2.15	-8.84	-12.90	20.58	30.65
0	36.50	24.22	0.00	-7.32	-2.33	-0.61	-1.91	-0.24	0.65	0.58	-2.69	-9.15	0.00	25.08	37.76
-20	31.86	22.22	11.07	-5.96	1.29	1.40	-0.16	-0.64	-0.75	-0.01	-0.25	-5.43	-12.49	20.56	28.62
-40	23.34	-14.91	5.32	-2.08	3.13	3.66	3.18	2.57	0.88	1.94	3.50	-0.18	-9.24	17.71	27.09
-60	-13.97	-7.34	2.23	0.88	3.58	4.94	5.62	6.22	5.55	5.63	7.74	4.59	-5.81	16.63	25.80
-80	2.17	-0.19	0.90	-0.93	0.16	0.39	3.70	7.82	7.60	10.94	13.94	9.31	-3.16	16.47	27.09
-100	13.47	2.54	3.13	-5.52	-2.39	2.59	7.71	13.91	13.50	12.51	12.47	10.48	-3.08	9.12	-9.27
-110	34.41	9.72	1.98	-8.09	0.20	8.26	22.82	0.00	0.00	0.00	0.00	0.00	16.38	0.00	0.00

The following table (Table 15) shows results for the sternum angles and lateral chest angles calculated for each model. Because the human is the reference model, a negative sign for the difference in angle indicates that the manikin has a negative angle compared to the human surface.

Table 15: Angle comparisons for human and CPR manikin. A positive value indicates that the manikin surface is more angled than the human surface.

	Human	Manikin	Difference
Sternum angle (at curve 5)	32.9	12.4	-20.5
Sternum angle (at curve 6)	29.4	11.5	-17.8
Right shoulder angle	3.1	-28.1	-31.3
Left shoulder angle	6.3	-28.1	-34.4

2.5 Discussion

Comparison of the human and manikin models indicates substantial differences in the entire shape of the thorax. Differences were seen in the distance between surfaces as well as sternum and lateral chest angles. Results here indicate a need for further research of the differences between the human thorax and the pediatric CPR manikin thorax. At the preliminary stage of this research, only one subject was used to determine the feasibility of this method. However this comparison does not represent the overall child population. More subjects should be evaluated and compared to the CPR manikin. Future work will include a shape comparison of the ribs and outer surface of the thorax between human subjects using Generalized Procrustes Analysis (GPA) or linear regression analysis to develop an average thorax shape for different age groups. This analysis can be used to develop age-specific pediatric CPR manikins for more pediatric age groups. This method of comparison can also be applied to the design of many simulation tools including other CPR manikin ages and crash test dummies.

One immediate improvement for this portion of the study would be to obtain software that would allow a more simple comparison of the two surfaces. Because ProEngineer is a solid-modeling software and the surface models were obtained in STL format, no volume comparison was possible. Investigation of the

conversion of an STL file to a solid model, or a different software that easily compares STL surfaces would greatly increase the ease and scope of measurements to compare the surfaces.

Chapter 3: CONCLUSIONS AND FUTURE DIRECTIONS

In the first part of this study, pediatric age-specific geometric differences were observed in the pediatric thoracic cage structure. This likely influences thoracic response to many types of compression, including CPR compression, seatbelt compression in automotive accidents, and other injury compressions. Data available on the shape of the pediatric thoracic cage also affects the design of medical devices, restraint devices, and medical simulation tools, which impacts the well-being of the child population. This study prevents novel data that can allow improvements in all of these applications. Immediate future work includes an average shape analysis for each age group analyzed using principal component analysis.

In the second part of this study, comparison of the outer thorax surface of a pediatric CPR manikin and one six year old human subject showed considerable differences between the outer thorax shapes. Since thoracic response is related to thoracic shape, there is a need to further investigate the difference between the current pediatric CPR manikin thorax and pediatric subjects. Once more subjects are evaluated and an average shape of the outer thorax surface is determined through principal component analysis, the shape of pediatric CPR manikins can be evaluated and modified.

List of References

1. Alkadhi, H., Wildermuth, S., Marincek, B., Boehm, T. (2004). Accuracy and Time Efficiency for the Detection of Thoracic Cage Fractures: Volume Rendering Compared With Transverse Computed Tomography Images. Journal of Computer Assisted Tomography. 28(3):378-385

2. Blubber Busters.com (2010) eHealth International, Inc. Accessed at http://www.blubberbuster.com/height_weight.html.

3. Brook, C.G.D. (1971) Determination of body composition of children from skinfold measurements. Arch Dis Child. 46:182-184.

4. Campbell, R.J., Adcox, B.M., Smith, M.D., Simmons, J.W., Cofer, B.R., Inscore, S.C., Grohman, C. (2007) The effect of mid-thoracic VEPTR opening wedge thoracostomy on cervical tilt associated with congenital thoracic insufficiency syndrome. Spine. 32(20): 2171-2177.

5. Chang, P.Y., Lai, J.Y., Chen, J.C., Wang, C.J. (2007) Quantitative evaluation of bone and cartilage changes after the Ravitch throacoplasty by multislice computed tomography with 3-dimensional reconstruction. Journal of Thoracic and Cardiovascular Surgery. 134(5): 1279-1283.

6. American Heart Association (2005) Part 3: Overview of CPR. Circulation. http://circ.ahajournals.org/cgi/content/full/112/24_suppl/IV-12

7. Doershuk C.F., Fisher B.J., Matthews L.W (1975). Pulmonary physiology of the young child. Pulmonary physiology of the Fetus, Newborn and Child. Edited by E.M. Scarpelli and P.A.M. Auld. Philadelphia, PA: Lea & Febiger p. 166-182

8. Dean J.M., Koehler R.C., Schleien C.L., Michael J.R., Chantarojanasiri T., Rogers M.C., Traystman R.J. (1987). Age-related changes in chest geometry during cardiopulmonary resuscitation. J Appl Physiol. 62(6):2212-9.

9. Durnin, J.V.G.A., Rahaman, M.M. (1967) The assessment of the amount of fat in the human body from measurements of skinfold thickness. Br J Nutr. 21: 681-689.

10. Fujimoto L.K., Jacobs G., Przybysz J., Collins S., Meaney T., Smith W.A., et al. (1984). Human thoracic anatomy based on computed tomography for development of a totally implantable left ventricular assist system. Artificial Organs. 8: 436–444.

11. Garn, S.M., Haskell, J.A. (1959) Fat and growth during childhood. Science. 130: 1711-1712.

12. Gayzik F.S., Yu M.M., Danelson K.A., Slice D.E., Stitzel J.D. (2008). Quantification of age-related shape change of the human rib cage through geometric morphometrics. J Biomech. 41(7):1545-54.

13. Givens, M.L., Ayotte, K., Manifold, C. (2004) Needle thoracostomy: implications of computed tomography chest wall thickness. Academic Emergency Medicine. 11(2): 211-213.

14. Glasbey, J. A. (1983). A study of vertebral body shape and skeletal shape in healthy and scoliotic children. Thesis, University of Nottingham.

15. Goh, S., Price, R.I., Leedman, P.J., Singer, K.P. (2000) A comparison of three methods for measuring thoracic kyphosis: implications for clinical studies. Rheumatology. 39:310-315.

16. Grivas T.B., Burwell R.G., Purdue M., Webb J.K., Moulton A. (1991). A segmental analysis of thoracic shape in chest radiographs of children. Changes related to spinal level, age, sex, side and significance for lung growth and scoliosis. Journal of Anatomy. 178:21-38.

17. Hamilton M.N., Chen H.H., Guenther D.A (1986). Adult to child scaling and normalizing of lateral thoracic impact data. Society of Automotive Engineers, Warrendale, PA. Paper# 861883. pp 143-156.

18. Kangarloo H. (1988). Chest MRI in children. Radiol Clin North Am. 26(2):263-75.

19. Kent R., Lee S.H., Darvish K., Wang S., Poster C.S., Lange A.W., Brede C., Lange D., Matsuoka F. (2005). Structural and material changes in the aging thorax and their role in crash protection for older occupants. Stapp Car Crash J. 49:231-49.

20. Laerdal Medical Website (2006) Quality CPR: 50 years of evolving needs and solutions. Accessed at http://www.laerdal.com/doc/43568627/50-years-of-evolving.html.

21. Laerdal Medical Website (2006) Laerdal Parts Catalog Updated. Accessed at http://www.laerdal.com/doc/26452017/Laerdal-Parts-Catalog.html.

22. Lagundoye, S.B. (1974) Subcutaneous fat and muscle layers in chest x-rays of children with kwashiorkor. Journal of Tropical Pediatrics. 20(6): 287-290.

23. Mohr M., Abrams E., Engel C., Long W.B., Bottlang M.J (2007). Geometry of human ribs pertinent to orthopedic chest-wall reconstruction. Journal of Biomechanics. 40 (6):1310-7.

24. Nussbaum M.A., Chaffin D.B. (1996). Development and evaluation of a scalable and deformable geometric model of the human torso. Clinical Biomechanics. 11, 25–34.

25. Openshaw P., Edwards S., Helms P. (1984). Changes in rib cage geometry during childhood. Thorax. 39(8): 624-7.

26. Reed M., Ebert, S.M., Sherwood, C.P., Klinich, K.D., Manary, M.A. (2009) Evaluation of the static belt fit provided by belt-positioning booster seats. Accident Analysis and Prevention. 41: 598–607

27. Scheuer L., Black S (2000). Developmental juvenile osteology. San Diego: Academic Press. ISBN: 0-12-624000-0.

28. Schultz A.B., Sorensen S.E., Andersson G.B.J (1984). Measurements of spine morphology in children, ages 10-16. Spine. 9: 70-73.

29. Snyder, R.G., Spencer, M.L., Owings, C.L., Schneider, L.W. (1975) Physical characteristics as related to death and Injury for consumer product safety design. U.S. Consumer Product Safety Comission. Highway Safety Research Institute,The University of Michigan, Ann Arbor.

30. Snyder, R.G., Schneider, L.W., Owings, C.L., Reynolds, H.M., Golomb, D.H., Schork, M.A. (1977) Anthropometry of infants, children and youths to age 18 for product safety design. U.S. Consumer Product Safety Commission. Highway Safety Research Institute, The University of Michigan, Ann Arbor.

31. Smith, M.D,, Campbell, R.M. (2006) Use of a biodegradable patch for reconstruction of large thoracic cage defects in growing children. Journal of Pediatric Surgery. 41: 46-49.

32. Takahashi H., Frost H.M. (1966). Age and sex related changes in the amount of cortex of normal human ribs. Acta Orthopaedica Scandinavica. 37: 122–130.

33. Taylor, R.W., Gold, E., Manning, P., Goulding, A. (1997) Gender differences in body fat content are present well before puberty. Int J. Obes Relat Metab Disord. 21(11): 1082-1084.

34. Tortora, G.L., Nielsen, M.T. (2009) Principles of human anatomy. John Wiley & Sons, Inc. ISBN: 13-978-0-471-78931-4.

35. Tuggle, D.W., Mantor, C., Foley, D.S., Markley, M.M., Puffinbarger, N. (2004) Using a bioabsorbable copolymer plate for chest wall reconstruction. Journal of Pediatric Surgery. 39: 626-628.

36. Wehrli NE., Bural G., Houseni M., Alkhawaldeh K., Alavi A., Torigian D.A. (2007). Determination of age-related changes in structure and function of skin, adipose tissue, and skeletal muscle with computed tomography, magnetic resonance imaging, and positron emission tomography. Semin Nucl Med. 37(3): 195-205.

37. Well D.S., Meier J.M., Mahne A., Houseni M., Hernandez-Pampaloni M., Mong A., Mishra S., Zhuge Y., Souza A., Udupa J.K., Alavi A., Torigian D.A. (2007). Detection of age-related changes in thoracic structure and function by computed tomography, magnetic resonance imaging, and positron emission tomography.Semin Nucl Med. 37(2):103-19.

38. Yoganandan N., Pintar F.A. (1998). Biomechanics of human thoracic ribs. Journal of Biomechanical Engineering. 120(1): 100-4.

Appendix 1: Clinical protocol for CT scans

Guidelines for using Adult v. Child protocols:

Body: If patient weighs less than 55kg, use Child.
If patient weighs over 55kg, use Adult.
If the patient weighs over 85kg, use Adult LARGE.

Neuro: The protocols are listed by age.
If there is no age next to a specific protocol, use an adult protocol if the patient is over 9yr old.

NOTE: Should you choose a CHILD protocol due to the patient weighing less than 55kg, but the child is 'adult' in age or height, and the radiologist has Protocolled at 5mm, please be sure to change your scan thickness to 5mm x 1.2 collimation.
In doing so, all of your recon jobs below will also change.
NOTE: You will have to change the THINS to 1.5 x 0.7 for Chest and 1.5 x 1.0 for Abdomen, if you don't change this everything will reconstruct at 5mm.

CHILD CHEST – NEONATE (0 – 3mths)

Indications: respiratory distress, chronic lung disease, pneumothorax, congenital lobular emphysema, pulmonary interstitial emphysema, sequestration, CCAM (CPAM)

itient Position: Supine, arms above head

anner Default Position: Head first, supine

Contrast: Per Radiologist Protocol

anning Range: Apices thru lung bases

an Direction: Craniocaudal

Scanner Protocol: Neonate_Chest_0_3mths (Child)

Range	kV	Quality Ref. mAs	CARE DOSE (4D)	CARE DOSE TYPE	CTDIVol mGy	Rot. Time	Pitch	Coll.	Slice	API
Topogram	80	50mA	off	CAREDose	0	0.5	1.0	0.6	0.6	
Chest	80	32	on	CAREDose 4D	0.58	0.5	0.9	1.2	3.0	

econstruction Parameters:

Series Description	Slice	Increment	Kernel	Window	Transfer 1
Chest 3.0 ST	3.0	3.0	B31f	Mediastinum	
Chest 1.5 ST Thins	1.5	0.7	B31f	Mediastinum	TeraRecon
Chest 3.0 Lung	3.0	3.0	B60f	Baby Lung	

eformats / 3D:
erform SAG and COR reformats under 3D card on Wizard, using the 1.5 ST Thins
eset: Body Child

ansferring Images:
anually send images to PACS – Topo, ST, LUNG, SAG & COR, & Patient Protocol Page

echnologist Notes:
using IV Contrast, please note in Comments

CHILD CHEST – ENHANCED

Indications: follow up lymphoma, follow up mediastinal mass, adenopathy, empyema, complicated pneumonia, fungus

Patient Position: Supine, arms above head

Scanner Default Position: Head first, supine

IV Contrast: Yes - Max. dose 75ml
Begin scan 45sec after start of contrast injection

Scanning Range: Apices thru lung bases

Scan Direction: Craniocaudal

Scanner Protocol: Chest_Contrast (Child)

Range	kV	Quality Ref. mAs	CARE DOSE (4D)	CARE DOSE TYPE	CTDIVol mGy	Rot. Time	Pitch	Coll.	Slice	API
Topogram	100	40mA	off	CAREDose	0	0.5	1.0	0.6	0.6	
Chest	100	55	on	CAREDose 4D	2.16	0.5	1.0	1.2	3.0	

Reconstruction Parameters:

Series Description	Slice	Increment	Kernel	Window	Transfer 1
Chest 3.0 ST	3.0	3.0	B31f	Mediastinum	
Chest 1.5 ST Thins	1.5	0.7	B31f	Mediastinum	TeraRecon
Chest 3.0 Lung	3.0	3.0	B60f	Baby Lung	

Reformats / 3D:
Perform SAG and COR reformats under 3D card on Wizard, using the 1.5 ST Thins
Preset: Body Child

Transferring Images:
Manually send images to PACS – Topo, ST, LUNG, SAG & COR, & Patient Protocol Page

Technologist Notes:
Be sure to include axilla for lymphoma studies

CHILD CHEST – UNENHANCED

Indications: pulmonary mets, parenchymal/interstitial lung disease, lung transplant, pneumonia, bronchiectasis, pneumothorax

Patient Position: Supine, arms above head

Scanner Default Position: Head first, supine

IV Contrast: None

Scanning Range: Apices thru lung bases

Scan Direction: Craniocaudal

Scanner Protocol: Chest_Unenhanced (Child)

Range	kV	Quality Ref. mAs	CARE DOSE (4D)	CARE DOSE TYPE	CTDIVol mGy	Rot. Time	Pitch	Coll.	Slice	API
Topogram	120	35mA	off	CAREDose	0	0.5	1.0	0.6	0.6	
Chest	120	40	on	CAREDose 4D	2.70	0.5	0.9	1.2	3.0	

Reconstruction Parameters:

Series Description	Slice	Increment	Kernel	Window	Transfer 1
Chest 3.0 ST	3.0	3.0	B31f	Mediastinum	
Chest 1.5 ST Thins	1.5	0.7	B31f	Mediastinum	TeraRecon
Chest 3.0 Lung	3.0	3.0	B60f	Baby Lung	

Reformats / 3D:
Perform SAG and COR reformats under 3D card on Wizard using the 1.5 ST Thins
Preset: Body Child

Transferring Images:
Manually send images to PACS – Topo, ST, LUNG, SAG & COR, & Patient Protocol Page

Technologist Notes:

ADULT CHEST - ENHANCED

Indications: follow up lymphoma; follow up mediastinal mass; adenopathy, empyema, complicated pneumonia, fungus

Patient Position: Supine, arms above head

Scanner Default Position: Head first, supine

IV Contrast: Yes - Max. dose 75ml
Begin scan 45sec after start of contrast injection

Scanning Range: Apices thru lung bases

Scan Direction: Craniocaudal

Scanner Protocol: Chest (Adult)

Range	kV	Quality Ref. mAs	CARE DOSE (4D)	CARE DOSE TYPE	CTDIVol mGy	Rot. Time	Pitch	Coll.	Slice	API
Topogram	120	35mA	off	CAREDose	0	0.5	1.0	0.6	0.6	Inspiration CHOP
Chest	120	100	on	CAREDose 4D	6.74	0.5	1.0	1.2	5.0	Inspiration CHOP

Reconstruction Parameters:

Series Description	Slice	Increment	Kernel	Window	Transfer 1
Chest 5.0 ST	5.0	5.0	B31f	Mediastinum	
Chest 1.5 ST Thins	1.5	0.7	B31f	Mediastinum	TeraRecon
Chest 5.0 Lung	5.0	5.0	B70f	Lung	

Reformats / 3D:
Perform SAG and COR reformats under 3D card on Wizard, using the 1.5 ST Thins
Preset: Adult Body

Transferring Images:
Manually send images to PACS – Topo, ST, LUNG, SAG & COR, & Patient Protocol Page

Technologist Notes:
Be sure to include the axilla for lymphoma studies

ADULT CHEST - UNENHANCED

Indications: pulmonary mets, parenchymal/interstitial disease, lung transplant, pneumonia, pneumothorax

Patient Position: Supine, arms above head

Scanner Default Position: Head first, supine

IV Contrast: None

Scanning Range: Apices thru lung bases

Scan Direction: Craniocaudal

Scanner Protocol: Chest (Adult)

Range	kV	Quality Ref. mAs	CARE DOSE (4D)	CARE DOSE TYPE	CTDIVol mGy	Rot. Time	Pitch	Coll.	Slice	API
Topogram	120	35mA	off	CAREDose	0	0.5	1.0	0.6	0.6	Inspiration CHOP
Chest	120	100	on	CAREDose 4D	6.74	0.5	1.0	1.2	5.0	Inspiration CHOP

Reconstruction Parameters:

Series Description	Slice	Increment	Kernel	Window	Transfer 1
Chest 5.0 ST	5.0	5.0	B31f	Mediastinum	
Chest 1.5 ST Thins	1.5	0.7	B31f	Mediastinum	TeraRecon
Chest 5.0 Lung	5.0	5.0	B70f	Lung	

Reformats / 3D:
Perform SAG and COR reformats under 3D card on Wizard, using the 1.5 ST Thins
Preset: Adult Body

Transferring Images:
Manually send images to PACS – Topo, ST, LUNG, SAG & COR, & Patient Protocol Page

Technologist Notes:
Be sure to include the axilla for lymphoma studies
Please remove the IV Contrast from the Comment box

Appendix 2: CT image reconstruction in Analyze

1. In the Analyze workspace, go to Display, then Volume Render.
2. Open the preview window and thresholds window found in the Generate menu.
3. Change the minimum threshold until the rib cage is clearly visible, leaving no soft tissue outside of the rib cage. There may still be soft tissue visible inside of the rib cage.
4. Click the render button in the threshold window and close it.
5. In the volume render window, go to Tools, Manipulate then Trace. This command allows you to clip the scapulas and any other object that is interfering with the surface of the rib shafts.
6. Use the draw and flood fill tools to trace around unwanted bone and delete them by clicking on Change Memory.
7. Save the changed memory in the Analyze workspace.

Appendix 3: Point placement on the ribcage surface in Analyze

After the reconstructed image of the ribcage was obtained, a Microsoft Excel document was created for each subject to record the Cartesian coordinates of each digitized point. The Excel documents contained one tab for general information (such as age, height, weight, and threshold), one tab for each rib (1-12), one tab for spine measurements, one tab for sternum measurements and one tab for screenshots. Points were placed in Analyze using the Point command in the Volume Render window. This command is found in the Tools menu under Measure. The Point tool opens a reconstructed view of the rib cage, and the Rotation tool can be used to show either named views (front, back, left, right, top and bottom) or volume absolute views in which the X, Y and Z coordinates can be adjusted between 0 and 180 degrees. The left and right named views were used to place points along the left and right side of the ribs respectively. The back named view was used to place points along the back of each rib. The Left named view was used to place points along the sagittal plane of the spine and sternum. Slight adjustments were made using the volume absolute adjustments as necessary. Once the appropriate view was found, points were placed on the surface of the bone and the X, Y and Z coordinate points were automatically logged in Analyze. These coordinate points were then copied and pasted into the Excel document.

Points placed on the spine included nine points on each vertebral body in the sagittal and coronal views. Points were placed using the same procedure as the rib points, however the Clip tool found under the Generate menu in the Volume Render window was used to find the midline of the vertebral bodies in each view. The midline was found in the sagittal direction by using the curvature of the spinous processes. The midline in the coronal direction was found by estimating based on the most anterior and posterior point of the vertebral body. In the sagittal plane, three points were placed on the anterior edge of the vertebral body (top, middle and bottom). Three points were placed on the posterior edge and center of the vertebral body in the same manner. In the coronal plane, three points were placed along the left, right and center of the vertebral body. Points placed on the spine and sternum in the sagittal view is shown in the figure below.

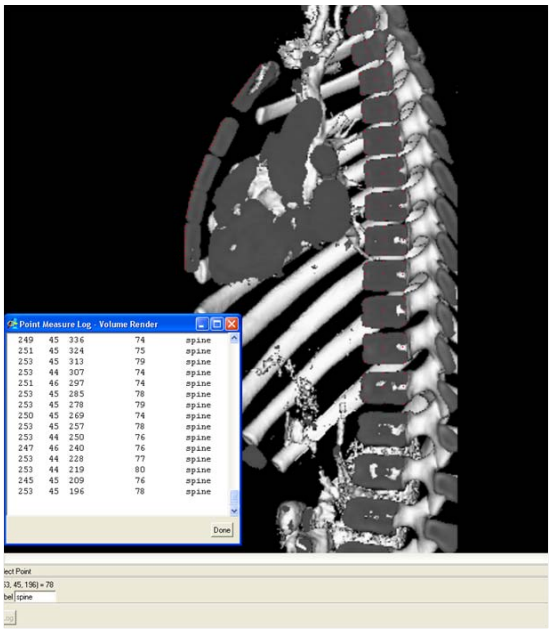

Figure: Points placed on the spine and sternum in the sagittal plane.

Points placed on the sternum were taken from the sagittal plane. The midline of the sternum in the sagittal plane was found the same way as the spine midline, so the measurements were taken for the sagittal spine and the sternum at the same time. Points were placed along the anterior edge of the sternum from the bottom of the xyphoid process to the top of the manubrium. The xyphoid, sternum body and manubrium points were labeled respectively. The Line tool was used to take width measurements of the sternum. The Line tool is found in the Tools menu under Measure. Using the front named view, a horizontal line was placed at the widest location of the sternum and manubrium. A vertical line was placed from the horizontal line to the bottom point of the sternum or manubrium. Analyze logged the x, y and z coordinates of all points as well as the length of each line.

Appendix 4: Custom MATLAB code used to process rib cage parameters

```
1
2 %Preparing Workspace
3 close all
4 clear all
5 clc
6
7 for sub=1
8 [filename,pathname]=uigetfile({'*.xls','excel files';'*.*','all files'},'Select Excel File','Excel File');
9
10 sub=xlsread([pathname,filename],'Subject Info','B2');
11 age=xlsread([pathname,filename],'Subject Info','B3');
12 scalefactor=xlsread([pathname,filename],'Subject Info','B7');
13 height=xlsread([pathname,filename],'Subject Info','B8');
14 weight=xlsread([pathname,filename],'Subject Info','B9');
15
16 %=========================================================================
17 % Setting up figures
18 fignewton1=figure('Name','Rib Structure','Visible','off');
19 hold on
20 raspberryfilling=get(fignewton1,'Children');
21
22 fignewton2=figure('Name','Thoracic Index','Visible','off');
23 hold on
24 applefilling=get(fignewton2,'Children');
25
26 %=========================================================================
27 %=========================SCALING=========================================
28
29 scaling_matrix=xlsread('scalinginfo.xlsx','D2:K25');
30
31 %=========================================================================
32
33 for allribs=1:12
34
35 ribstring=['rib ' num2str(allribs)];
36
37 %LEFT RIBS
38
39 Ltop=xlsread([pathname,filename],ribstring,'A3:C150');
40 Lmiddle=xlsread([pathname,filename],ribstring,'F3:H150');
41 Lbottom=xlsread([pathname,filename],ribstring,'K3:M150');
42
43 spineT1=[(xlsread([pathname,filename],'spine','A3:C3'))];
44 LY=flipud((Lmiddle(:,1)-spineT1(:,1))*scalefactor);
45 LX=flipud((Lmiddle(:,2)-spineT1(:,2))*scalefactor);
46 LZ=flipud((Lmiddle(:,3)-spineT1(:,3))*scalefactor);
47 LY1=flipud((Ltop(:,1)-spineT1(:,1))*scalefactor);
48 LX1=flipud((Ltop(:,2)-spineT1(:,2))*scalefactor);
49 LZ1=flipud((Ltop(:,3)-spineT1(:,3))*scalefactor);
50 LY2=flipud((Lbottom(:,1)-spineT1(:,1))*scalefactor);
51 LX2=flipud((Lbottom(:,2)-spineT1(:,2))*scalefactor);
52 LZ2=flipud((Lbottom(:,3)-spineT1(:,3))*scalefactor);
53 %=========================================================================
54 %interpolation - Left rib
55
56 [Lnewmid,Lmidlength]=ribpercent([LX,LY,LZ],allribs);
57 [Lnewtop,Ltoplength]=ribpercent([LX1,LY1,LZ1],allribs);
58 [Lnewbottom,Lbottomlength]=ribpercent([LX2,LY2,LZ2],allribs);
59
60 %=========================================================================
61 %Left Rib Length Normalized by Height
62 Lnormriblength=Lmidlength/(height*10);
63
64 %Left Radius of Curvature
```

```
65 j=1;
66 for j=2:2:length(Lnewmid)-1
67 Lp1=[Lnewmid(j-1,:); Lnewmid(j,:)];
68 Lp2=[Lnewmid(j,:); Lnewmid(j+1,:)];
69 Lp3=[Lnewmid(j-1,:); Lnewmid(j+1,:)];
70 La(j)=pdist(Lp1);
71 Lb(j)=pdist(Lp2);
72 Lc(j)=pdist(Lp3);
73 Ls(j)=(La(j)+Lb(j)+Lc(j))/2;
74 LK(j)=sqrt(Ls(j)*(Ls(j)-La(j))*(Ls(j)-Lb(j))*(Ls(j)-Lc(j)));
75 Lr(j)=(La(j)*Lb(j)*Lc(j))/(4*LK(j));
76 LAC(j)=1/Lr(j);
77 j=j+1;
78 end
79
80
81 %==========================================================================
82
83 %Left Longitudinal Twist
84 for i=2:2:length(Lnewmid)-1
85 % i=2:2:18
86 L_LONGTW_1=Lnewtop(i,2:3)-Lnewbottom(i,2:3);
87 Ltheta(i)=((atan2(L_LONGTW_1(:,2),L_LONGTW_1(:,1)))*(180/pi))-90;
88 end
89
90 %==========================================================================
91
92 %Left Rib angle
93 LRAP=abs(Lnewmid(2,[1,3])-Lnewmid(end-1,[1,3]));
94 LRA=90-(atan2((LRAP(1,2)),(LRAP(1,1)))*(180/pi));
95
96 %==========================================================================
97
98 %Left Coefficients
99
100 Clx(:,allribs)=polyfit(0.05:0.05:0.95,Lnewmid(:,1)',2);
101 Cly(:,allribs)=polyfit(0.05:0.05:0.95,Lnewmid(:,2)',2);
102 Clz(:,allribs)=polyfit(0.05:0.05:0.95,Lnewmid(:,3)',2);
103
104 Clx3(:,allribs)=polyfit(0.05:0.05:0.95,Lnewmid(:,1)',3);
105 Cly3(:,allribs)=polyfit(0.05:0.05:0.95,Lnewmid(:,2)',3);
106 Clz3(:,allribs)=polyfit(0.05:0.05:0.95,Lnewmid(:,3)',3);
107
108 % xlswrite(['C:\Documents and Settings\Amanda\My Documents\MATLAB\Pediatric Thorax\' num2str(age) '_' num2str(sub)
'_polyfit.xlsx'],Clx','Left','B3:
D14');
109 % xlswrite(['C:\Documents and Settings\Amanda\My Documents\MATLAB\Pediatric Thorax\' num2str(age) '_' num2str(sub)
'_polyfit.xlsx'],Cly','Left','E3:
G14');
110 % xlswrite(['C:\Documents and Settings\Amanda\My Documents\MATLAB\Pediatric Thorax\' num2str(age) '_' num2str(sub)
'_polyfit.xlsx'],Clz','Left','H3:
J14');
111 %
112 % xlswrite(['C:\Documents and Settings\Amanda\My Documents\MATLAB\Pediatric Thorax\' num2str(age) '_' num2str(sub)
'_polyfit.xlsx'],Clx3','Left','P3:
S14');
113 % xlswrite(['C:\Documents and Settings\Amanda\My Documents\MATLAB\Pediatric Thorax\' num2str(age) '_' num2str(sub)
'_polyfit.xlsx'],Cly3','Left','T3:
W14');
114 % xlswrite(['C:\Documents and Settings\Amanda\My Documents\MATLAB\Pediatric Thorax\' num2str(age) '_' num2str(sub)
'_polyfit.xlsx'],Clz3','Left','X3:
AA14');
115
116 %==========================================================================
117 %==========================================================================
118 %==========================================================================
119 %==========================================================================
120
121 %RIGHT RIBS
122
```

```
Rtop=xlsread([pathname,filename],ribstring,'Q3:S150');
Rmiddle=xlsread([pathname,filename],ribstring,'V3:X150');
Rbottom=xlsread([pathname,filename],ribstring,'AA3:AC150');

RY=flipud((Rmiddle(:,1)-spineT1(:,1))*scalefactor);
RX=flipud((Rmiddle(:,2)-spineT1(:,2))*scalefactor);
RZ=flipud((Rmiddle(:,3)-spineT1(:,3))*scalefactor);
RY1=flipud((Rtop(:,1)-spineT1(:,1))*scalefactor);
RX1=flipud((Rtop(:,2)-spineT1(:,2))*scalefactor);
RZ1=flipud((Rtop(:,3)-spineT1(:,3))*scalefactor);
RY2=flipud((Rbottom(:,1)-spineT1(:,1))*scalefactor);
RX2=flipud((Rbottom(:,2)-spineT1(:,2))*scalefactor);
RZ2=flipud((Rbottom(:,3)-spineT1(:,3))*scalefactor);

%=========================================================================
%interpolation - Right rib

[Rnewmid,Rmidlength]=ribpercent([RX,RY,RZ],allribs);
[Rnewtop,Rtoplength]=ribpercent([RX1,RY1,RZ1],allribs);
[Rnewbottom,Rbottomlength]=ribpercent([RX2,RY2,RZ2],allribs);

%=========================================================================
%Right rib length normalized by Height
Rnormriblength=Rmidlength/(height*10);

%Right Radius of Curvature
j=1;
for j=2:2:length(Rnewmid)-1
Rp1=[Rnewmid(j-1,:); Rnewmid(j,:)];
Rp2=[Rnewmid(j,:); Rnewmid(j+1,:)];
Rp3=[Rnewmid(j-1,:); Rnewmid(j+1,:)];
Ra(j)=pdist(Rp1);
Rb(j)=pdist(Rp2);
Rc(j)=pdist(Rp3);
Rs(j)=(Ra(j)+Rb(j)+Rc(j))/2;
RK(j)=sqrt(Rs(j)*(Rs(j)-Ra(j))*(Rs(j)-Rb(j))*(Rs(j)-Rc(j)));
Rr(j)=(Ra(j)*Rb(j)*Rc(j))/(4*RK(j));
RAC(j)=1/Rr(j);
j=j+1;
end

%=========================================================================

%Right Longitudinal Twist
for i=2:2:length(Rnewmid)-1
R_LONGTW_1=Rnewtop(i,2:3)-Rnewbottom(i,2:3);
Rtheta(i)=-(((atan2(R_LONGTW_1(:,2),R_LONGTW_1(:,1)))*(180/pi))-90);
end

%=========================================================================

%Right Rib Angle
RRAP=abs(Rnewmid(2,[1,3])-Rnewmid(end-1,[1,3]));
RRA=90-(atan2((RRAP(1,2)),(RRAP(1,1)))*(180/pi));

%=========================================================================

%Right Coefficients

Crx(:,allribs)=polyfit(0.05:0.05:0.95,Rnewmid(:,1)',2);
Cry(:,allribs)=polyfit(0.05:0.05:0.95,Rnewmid(:,2)',2);
Crz(:,allribs)=polyfit(0.05:0.05:0.95,Rnewmid(:,3)',2);

Crx3(:,allribs)=polyfit(0.05:0.05:0.95,Rnewmid(:,1)',3);
Cry3(:,allribs)=polyfit(0.05:0.05:0.95,Rnewmid(:,2)',3);
Crz3(:,allribs)=polyfit(0.05:0.05:0.95,Rnewmid(:,3)',3);

% xlswrite(['C:\Documents and Settings\Amanda\My Documents\MATLAB\Pediatric Thorax\' num2str(age) '_' num2str(sub)
'_polyfit.xlsx'],Crx','Right','B3:
D14');
```

```
% xlswrite(['C:\Documents and Settings\Amanda\My Documents\MATLAB\Pediatric Thorax\' num2str(age) '_' num2str(sub) '_polyfit.xlsx'],Cry','Right','E3:G14');
% xlswrite(['C:\Documents and Settings\Amanda\My Documents\MATLAB\Pediatric Thorax\' num2str(age) '_' num2str(sub) '_polyfit.xlsx'],Crz','Right','H3:J14');
%
% xlswrite(['C:\Documents and Settings\Amanda\My Documents\MATLAB\Pediatric Thorax\' num2str(age) '_' num2str(sub) '_polyfit.xlsx'],
Crx3','Right','P3:S14');
% xlswrite(['C:\Documents and Settings\Amanda\My Documents\MATLAB\Pediatric Thorax\' num2str(age) '_' num2str(sub) '_polyfit.xlsx'],
Cry3','Right','T3:W14');
% xlswrite(['C:\Documents and Settings\Amanda\My Documents\MATLAB\Pediatric Thorax\' num2str(age) '_' num2str(sub) '_polyfit.xlsx'],
Crz3','Right','X3:AA14');

%==========================================================================
%Plots

plot3(raspberryfilling,LX,LY,LZ,'-b')
plot3(raspberryfilling,LX1,LY1,LZ1,'-r')
plot3(raspberryfilling,LX2,LY2,LZ2,'-g')
plot3(raspberryfilling,Lnewmid(2:2:length(Lnewmid)-1,1),Lnewmid(2:2:length(Lnewmid)-1,2),Lnewmid(2:2:length(Lnewmid)-1,3),'*k')
plot3(raspberryfilling,RX,RY,RZ,'-k')
plot3(raspberryfilling,RX1,RY1,RZ1,'-y')
plot3(raspberryfilling,RX2,RY2,RZ2,'-m')
plot3(raspberryfilling,Rnewmid(2:2:length(Rnewmid)-1,1),Rnewmid(2:2:length(Rnewmid)-1,2),Rnewmid(2:2:length(Rnewmid)-1,3),'*k')
% plot3(spineT1(:,1),spineT1(:,2),spineT1(:,3),'ok','MarkerSize',5)
axis square

% Thoracic index
A=max(LY);
B=min(RY);
C=max(LX);
D=min(LX);
distLAT=A-B;
distAP=C-D;
TI=distAP/distLAT;

% Structure
subjects(sub).Lrib(allribs).Ltop=Ltop;
subjects(sub).Lrib(allribs).Lmiddle=Lmiddle;
subjects(sub).Lrib(allribs).Lbottom=Lbottom;
subjects(sub).Lrib(allribs).Ltheta=Ltheta;
subjects(sub).Lrib(allribs).Lriblengthtop=Ltoplength;
subjects(sub).Lrib(allribs).Lriblengthmiddle=Lmidlength;
subjects(sub).Lrib(allribs).Lriblengthbottom=Lbottomlength;
subjects(sub).Lrib(allribs).Lnormriblength=Lnormriblength;
subjects(sub).Lrib(allribs).Lradiusofcurvature=Lr;
subjects(sub).Lrib(allribs).Lapparentcurvature=LAC;
subjects(sub).Lrib(allribs).Ldatainterp=Lnewmid;
subjects(sub).Rrib(allribs).Rdatainterp=Rnewmid;
subjects(sub).Lrib(allribs).LRA=LRA;

subjects(sub).Rrib(allribs).Rtop=Rtop;
subjects(sub).Rrib(allribs).Rmiddle=Rmiddle;
subjects(sub).Rrib(allribs).Rbottom=Rbottom;
subjects(sub).Rrib(allribs).Rtheta=Rtheta;
subjects(sub).Rrib(allribs).Rriblengthtop=Rtoplength;
subjects(sub).Rrib(allribs).Rriblengthmiddle=Rmidlength;
subjects(sub).Rrib(allribs).Rriblengthbottom=Rbottomlength;
subjects(sub).Rrib(allribs).Rnormriblength=Rnormriblength;
subjects(sub).Rrib(allribs).Rradiusofcurvature=Rr;
subjects(sub).Rrib(allribs).Rapparentcurvature=RAC;
subjects(sub).Rrib(allribs).RRA=RRA;
subjects(sub).Rrib(allribs).Rnewmid=Rnewmid;

```

```
subjects(sub).ribcage(allribs).TI=TI;
subjects(sub).ribcage(allribs).distAP=distAP;
subjects(sub).ribcage(allribs).distLAT=distLAT;
subjects(sub).ribcage(allribs).A=A;
subjects(sub).ribcage(allribs).B=B;
subjects(sub).ribcage(allribs).C=C;
subjects(sub).ribcage(allribs).D=D;

if allribs<=10
tiplot(allribs)=[subjects(sub).ribcage(allribs).TI];
end

% Longitudinal Twist - 90% site - 10% site

Ltheta90_10(allribs)=subjects(sub).Lrib(allribs).Ltheta(18)-subjects(sub).Lrib(allribs).Ltheta(2);
subjects(sub).Lrib(allribs).Ltheta90_10=Ltheta90_10;

Rtheta90_10(allribs)=subjects(sub).Rrib(allribs).Rtheta(18)-subjects(sub).Rrib(allribs).Rtheta(2);
subjects(sub).Rrib(allribs).Rtheta90_10=Rtheta90_10;

save([num2str(age) '_' num2str(sub)],'subjects')
end %ENDING ENTIRE RIB LOOP

plot(applefilling,1:10,tiplot,'-ob','LineWidth',4,'MarkerSize',6)
xlabel('Rib Number','FontSize',20)
ylabel('Thoracic Index','FontSize',20)
set(gca,'XTick',1:10,'FontSize',18);
saveas(gcf,'C:\Documents and Settings\Amanda\Desktop\Amanda Thesis\Thorax Project Matlab Data\Thoracic Index
10_5','png');

%=========================================================================
% SPINE
%=========================================================================

pointshift1=[spineT1];
pointshift=repmat(pointshift1,36,1);
SpA=(xlsread([pathname,filename],'spine','E3:G38')-pointshift)*scalefactor; %Anterior line of spine (sagittal view), 3 points for
each vb, starting from the
top
SpM=(xlsread([pathname,filename],'spine','I3:K38')-pointshift)*scalefactor; %Middle line of spine (sagittal view), 3 points for
each vb, starting from the top
SpP=(xlsread([pathname,filename],'spine','M3:O38')-pointshift)*scalefactor; %Posterior line of spine (sagittal view), 3 points for
each vb, starting from the
top
SpR=(xlsread([pathname,filename],'spine','Q3:S38')-pointshift)*scalefactor; %Right line of spine(coronal view), 3 points for each
vb, starting from the top
SpCM=(xlsread([pathname,filename],'spine','U3:W38')-pointshift)*scalefactor; %Middle line of spine (coronal view), 3 points for
each vb, starting from the
top
SpL=(xlsread([pathname,filename],'spine','Y3:AA38')-pointshift)*scalefactor; %Left line of spine (coronal view), 3 points for
each vb, starting from the top

%Depth (x,z direction)
for i=1:12
int=3*i;
depth(i)=sqrt(((SpA(int,2)-SpP(int,2))^2)+((SpA(int,3)-SpP(int,3))^2));
end
subjects(sub).spine.VBdepth=depth;

%Height (x,z direction)
for i=1:12
int1=(3*i)-2;
int2=3*i;
height(i)=sqrt(((SpM(int1,2)-SpM(int2,2))^2)+((SpM(int1,3)-SpM(int2,3))^2));
end
subjects(sub).spine.VBheight=height;

%Width
%top (y,z direction)
for i=1:12
```

```
int3=(3*i)-2;
topwidth(i)=sqrt(((SpR(int3,1)-SpL(int3,1))^2)+((SpR(int3,3)-SpL(int3,3))^2));
end
subjects(sub).spine.VBwidthtop=topwidth;
%middle (y,z direction)
for i=1:12
int4=(3*i)-1;
midwidth(i)=sqrt(((SpR(int4,1)-SpL(int4,1))^2)+((SpR(int4,3)-SpL(int4,3))^2));
end
subjects(sub).spine.VBwidthmid=midwidth;
%bottom (y,z direction)
for i=1:12
int5=(3*i);
bottomwidth(i)=sqrt(((SpR(int5,1)-SpL(int5,1))^2)+((SpR(int5,3)-SpL(int5,3))^2));
end
subjects(sub).spine.VBwidthbottom=bottomwidth;

%Radius of Curvature (x,z direction)VB 1-12
spinepoints=(xlsread([pathname,filename],'spine','I3:k38')-pointshift)*scalefactor;
spinea=sqrt(((spinepoints(1,2)-spinepoints(17,2))^2)+((spinepoints(1,3)-spinepoints(17,3))^2));
spineb=sqrt(((spinepoints(17,2)-spinepoints(36,2))^2)+((spinepoints(17,3)-spinepoints(36,3))^2));
spinec=sqrt(((spinepoints(36,2)-spinepoints(1,2))^2)+((spinepoints(36,3)-spinepoints(1,3))^2));
spines=.5*(spinea+spineb+spinec);
spineK=sqrt(spines*(spines-spinea)*(spines-spineb)*(spines-spinec));
spineR=(spinea*spineb*spinec)/(4*spineK);
subjects(sub).spine.Radiusofcurvature=spineR;

%Radius of Curvature VB 3-9
spinea=sqrt(((spinepoints(7,2)-spinepoints(18,2))^2)+((spinepoints(7,3)-spinepoints(18,3))^2));
spineb=sqrt(((spinepoints(18,2)-spinepoints(30,2))^2)+((spinepoints(18,3)-spinepoints(30,3))^2));
spinec=sqrt(((spinepoints(30,2)-spinepoints(7,2))^2)+((spinepoints(30,3)-spinepoints(7,3))^2));
spines=.5*(spinea+spineb+spinec);
spineK=sqrt(spines*(spines-spinea)*(spines-spineb)*(spines-spinec));
spineR39=(spinea*spineb*spinec)/(4*spineK);
subjects(sub).spine.Radiusofcurvature39=spineR39;

%Radius of Curvature top 1/3 of spine (T1-T4) (x,z direction)
spinea1=sqrt(((spinepoints(1,2)-spinepoints(6,2))^2)+((spinepoints(1,3)-spinepoints(6,3))^2));
spineb1=sqrt(((spinepoints(6,2)-spinepoints(12,2))^2)+((spinepoints(6,3)-spinepoints(12,3))^2));
spinec1=sqrt(((spinepoints(12,2)-spinepoints(1,2))^2)+((spinepoints(12,3)-spinepoints(1,3))^2));
spines1=.5*(spinea1+spineb1+spinec1);
spineK1=sqrt(spines1*(spines1-spinea1)*(spines1-spineb1)*(spines1-spinec1));
spineR1=(spinea1*spineb1*spinec1)/(4*spineK1);
subjects(sub).spine.Radiusofcurvature1=spineR1;

%Radius of Curvature middle 1/3 of spine (T5-T8) (x,z direction)
spinea2=sqrt(((spinepoints(13,2)-spinepoints(18,2))^2)+((spinepoints(13,3)-spinepoints(18,3))^2));
spineb2=sqrt(((spinepoints(18,2)-spinepoints(24,2))^2)+((spinepoints(18,3)-spinepoints(24,3))^2));
spinec2=sqrt(((spinepoints(24,2)-spinepoints(13,2))^2)+((spinepoints(24,3)-spinepoints(13,3))^2));
spines2=.5*(spinea2+spineb2+spinec2);
spineK2=sqrt(spines2*(spines2-spinea2)*(spines2-spineb2)*(spines2-spinec2));
spineR2=(spinea2*spineb2*spinec2)/(4*spineK2);
subjects(sub).spine.Radiusofcurvature2=spineR2;

%Radius of Curvature bottom 1/3 of spine (T9-T12)(x,z direction)
spinea3=sqrt(((spinepoints(25,2)-spinepoints(30,2))^2)+((spinepoints(25,3)-spinepoints(30,3))^2));
spineb3=sqrt(((spinepoints(30,2)-spinepoints(36,2))^2)+((spinepoints(30,3)-spinepoints(36,3))^2));
spinec3=sqrt(((spinepoints(36,2)-spinepoints(25,2))^2)+((spinepoints(36,3)-spinepoints(25,3))^2));
spines3=.5*(spinea3+spineb3+spinec3);
spineK3=sqrt(spines3*(spines3-spinea3)*(spines3-spineb3)*(spines3-spinec3));
spineR3=(spinea3*spineb3*spinec3)/(4*spineK3);
subjects(sub).spine.Radiusofcurvature3=spineR3;

%spline
x=SpM(:,2);
z=SpM(:,3);
fit=polyfit(z,x,2);
f=polyval(fit,z);

figure
```

```
379 plot(z,x,'ob','LineWidth',2,'MarkerSize',4)
380 axis square
381 axis([-300,50,-150,200]);
382 xlabel('distance(mm)','FontSize',20)
383 ylabel('distance(mm)','FontSize',20)
384 set(gca,'FontSize',18)
385 saveas(gcf,'C:\Documents and Settings\Amanda\Desktop\Amanda Thesis\Thorax Project Matlab Data\Spine Spline Points
10_5','png');
386
387 figure
388 plot(z,f,'-b','LineWidth',5)
389 axis square
390 axis([-300,50,-150,200]);
391 xlabel('distance(mm)','FontSize',20)
392 ylabel('distance(mm)','FontSize',20)
393 set(gca,'FontSize',18)
394 saveas(gcf,'C:\Documents and Settings\Amanda\Desktop\Amanda Thesis\Thorax Project Matlab Data\Spine Spline 10_5','png');
395
396 %Cobb Angle
397 cobb1=abs([SpA(1,2),SpA(1,3)]-[SpP(1,2),SpP(1,3)]);
398 cobbanglet1=atan2((cobb1(1,2)),(cobb1(1,1)))*(180/pi);
399
400 cobb3=abs([SpA(9,2),SpA(9,3)]-[SpP(9,2),SpP(9,3)]);
401 cobbanglet3=atan2((cobb3(1,2)),(cobb3(1,1)))*(180/pi);
402
403 cobb9=abs([SpA(27,2),SpA(27,3)]-[SpP(27,2),SpP(27,3)]);
404 cobbanglet9=atan2((cobb9(1,2)),(cobb9(1,1)))*(180/pi);
405
406 cobb12=abs([SpA(36,2),SpA(36,3)]-[SpP(36,2),SpP(36,3)]);
407 cobbanglet12=atan2((cobb12(1,2)),(cobb12(1,1)))*(180/pi);
408
409 cobbangle39=cobbanglet3+cobbanglet9;
410 cobbangle112=cobbanglet1+cobbanglet12;
411 subjects(sub).spine.cobbangle39=cobbangle39;
412 subjects(sub).spine.cobbangle112=cobbangle112;
413
414 %Cobb Angle Normalized by Weight (T3-T9)
415 normcobbangle=cobbangle39/weight;
416 subjects(sub).spine.normcobbangle=normcobbangle;
417
418 %Spine Length
419 spinelength112=sum(sqrt(sum(diff(SpM).^2,2)));
420 subjects(sub).spine.spinelength112=spinelength112;
421
422 spinelength39=sum(sqrt(sum(diff(SpM(7:30,:)).^2,2)));
423 subjects(sub).spine.spinelength112=spinelength39;
424
425 spineangle112=(360*spinelength112)/(2*pi*spineR);
426 subjects(sub).spine.spineangle112=spineangle112;
427
428 spineangle39=(360*spinelength39)/(2*pi*spineR39);
429 subjects(sub).spine.spineangle39=spineangle39;
430
431 %=========================================================================
432 % STERNUM
433 %=========================================================================
434
435 %Width of Xyphoid, height of measurement from lowest point
436 Xwidth=(xlsread([pathname,filename],'sternum','Y4'))*scalefactor;
437 Xd2w=(xlsread([pathname,filename],'sternum','Y7'))*scalefactor;
438 subjects(sub).sternum.Xyphoidwidth=Xwidth;
439 subjects(sub).sternum.Xyphoidd2w=Xd2w; %d2w=distance to width measured from the lowest point
440
441 %Width of Sternum, height of measurement from lowest point
442 Swidth=(xlsread([pathname,filename],'sternum','G4'))*scalefactor;
443 Sd2w=(xlsread([pathname,filename],'sternum','G7'))*scalefactor;
444 subjects(sub).sternum.Sternumwidth=Swidth;
445 subjects(sub).sternum.Sternumd2w=Sd2w;
446
447 %Width of Manubrium, height of measurement from lowest point
```

```
448 Mwidth=(xlsread([pathname,filename],'sternum','P4'))*scalefactor;
449 Md2w=(xlsread([pathname,filename],'sternum','P7'))*scalefactor;
450 subjects(sub).sternum.Manubriumwidth=Mwidth;
451 subjects(sub).sternum.Manubriumd2w=Md2w;
452
453 %Radius of Curvature
454 sternumpoints11=(xlsread([pathname,filename],'sternum','G13:I100'))*scalefactor;
455 pointshift2=repmat(pointshift1,length(sternumpoints11),1);
456 sternumpoints=(sternumpoints11-pointshift2);
457 sternum1=sternumpoints(1,:);
458 if rem(length(sternumpoints),2)==0
459 sternum2=sternumpoints((length(sternumpoints)/2),:);
460 else
461 sternum2=sternumpoints((length(sternumpoints)+1)/2,:);
462 end
463 sternum3=sternumpoints(end,:);
464
465 sternuma=sqrt(((sternum1(:,2)-sternum2(:,2))^2)+((sternum1(:,3)-sternum2(:,3))^2));
466 sternumb=sqrt(((sternum2(:,2)-sternum3(:,2))^2)+((sternum2(:,3)-sternum3(:,3))^2));
467 sternumc=sqrt(((sternum3(:,2)-sternum1(:,2))^2)+((sternum3(:,3)-sternum1(:,3))^2));
468 sternums=.5*(sternuma+sternumb+sternumc);
469 sternumK=sqrt(sternums*(sternums-sternuma)*(sternums-sternumb)*(sternums-sternumc));
470 sternumR=(sternuma*sternumb*sternumc)/(4*sternumK);
471 subjects(sub).sternum.Sternumradiusofcurvature=sternumR;
472
473 %Sternum Length
474 sternumlength=sum(sqrt(sum(diff(sternumpoints11).^2,2)));
475 subjects(sub).sternum.sternumlength=sternumlength;
476
477 %Modified Cobb Angle for sternum (equation for arc of a circle,
478 %L=(theta/360)*2r(pi)
479
480 sternumcobb=(360*sternumlength)/(2*pi*sternumlength);
481 subjects(sub).sternum.sternumcobb=sternumcobb;
482
483 %=========================================================================
484 %=========================================================================
485
486 %%%%Making figures visible
487 set(fignewton1,'Visible','on')
488 view(raspberryfilling,50,10)
489 saveas(gcf,'C:\Documents and Settings\Amanda\Desktop\Amanda Thesis\Thorax Project Matlab Data\Rib Structure ISO
10_5','png');
490 set(fignewton2,'Visible','on')
491
492 %=========================================================================
493 %=========================================================================
494
495 %Writing Data to Excel Files
496
497 loc=sub+2;
498
499 %Right Rib Length
500 riblengthrx=[subjects(sub).Rrib(1:12).Rriblengthmiddle];
501 xlswrite(['C:\Documents and Settings\Amanda\Desktop\Amanda Thesis\Thorax Project Matlab Data\' num2str(age) ' year old
thorax.xlsx'],riblengthrx,'Rib
Length',['B' num2str(loc) ':M' num2str(loc)]);
502
503 %Left Rib Length
504 riblengthlx=[subjects(sub).Lrib(1:12).Lriblengthmiddle];
505 xlswrite(['C:\Documents and Settings\Amanda\Desktop\Amanda Thesis\Thorax Project Matlab Data\' num2str(age) ' year old
thorax.xlsx'],riblengthlx,'Rib
Length',['B' num2str(loc+9) ':M' num2str(loc+9)]);
506
507 %Right Rib Length Normalized
508 normriblengthrx=[subjects(sub).Rrib(1:12).Rnormriblength];
509 xlswrite(['C:\Documents and Settings\Amanda\Desktop\Amanda Thesis\Thorax Project Matlab Data\' num2str(age) ' year old
thorax.xlsx'],
normriblengthrx,'Normalized Rib Length',['B' num2str(loc) ':M' num2str(loc)]);
510
```

```
%Left Rib Length Normalized
normriblengthlx=[subjects(sub).Lrib(1:12).Lnormriblength];
xlswrite(['C:\Documents and Settings\Amanda\Desktop\Amanda Thesis\Thorax Project Matlab Data\' num2str(age) ' year old thorax.xlsx'],
normriblengthlx,'Normalized Rib Length',['B' num2str(loc+9) ':M' num2str(loc+9)]);

%Right Rib Angle
ribangleRx=[subjects(sub).Lrib(1:12).LRA];
xlswrite(['C:\Documents and Settings\Amanda\Desktop\Amanda Thesis\Thorax Project Matlab Data\' num2str(age) ' year old thorax.xlsx'],ribangleRx,'Rib
Angle',['B' num2str(loc) ':M' num2str(loc)]);

%Left Rib Angle
ribangleLx=[subjects(sub).Rrib(1:12).RRA];
xlswrite(['C:\Documents and Settings\Amanda\Desktop\Amanda Thesis\Thorax Project Matlab Data\' num2str(age) ' year old thorax.xlsx'],ribangleLx,'Rib
Angle',['B' num2str(loc+9) ':M' num2str(loc+9)]);

%Right Longitudinal Twist : DIFFERENCE, 90%-10% site
Ltwist_90_10_R=[subjects(sub).Rrib(allribs).Rtheta90_10];
xlswrite(['C:\Documents and Settings\Amanda\Desktop\Amanda Thesis\Thorax Project Matlab Data\' num2str(age) ' year old thorax.xlsx'],
Ltwist_90_10_R,'Right Longitudinal Twist',['B' num2str(loc+11) ':M' num2str(loc+11)]);

%Left Longitudinal Twist : DIFFERENCE, 90%-10% site
Ltwist_90_10_L=[subjects(sub).Lrib(allribs).Ltheta90_10];
xlswrite(['C:\Documents and Settings\Amanda\Desktop\Amanda Thesis\Thorax Project Matlab Data\' num2str(age) ' year old thorax.xlsx'],
Ltwist_90_10_L,'Left Longitudinal Twist',['B' num2str(loc+11) ':M' num2str(loc+11)]);

radiusofcurvatureLx1=NaN(12,9);
radiusofcurvatureRx1=NaN(12,9);
apparentcurvatureLx1=NaN(12,9);
apparentcurvatureRx1=NaN(12,9);
thetaLx1=NaN(12,9);
thetaRx1=NaN(12,9);

for i=1:12
radiusofcurvatureLx1(i,1:9)=subjects(sub).Lrib(i).Lradiusofcurvature(2:2:18);
radiusofcurvatureRx1(i,1:9)=subjects(sub).Rrib(i).Rradiusofcurvature(2:2:18);
apparentcurvatureLx1(i,1:9)=subjects(sub).Lrib(i).Lapparentcurvature(2:2:18);
apparentcurvatureRx1(i,1:9)=subjects(sub).Rrib(i).Rapparentcurvature(2:2:18);
thetaLx1(i,1:9)=subjects(sub).Lrib(i).Ltheta(2:2:18);
thetaRx1(i,1:9)=subjects(sub).Rrib(i).Rtheta(2:2:18);
end

radiusofcurvatureLx=reshape(radiusofcurvatureLx1',108,1)';
radiusofcurvatureRx=reshape(radiusofcurvatureRx1',108,1)';
apparentcurvatureLx=reshape(apparentcurvatureLx1',108,1)';
apparentcurvatureRx=reshape(apparentcurvatureRx1',108,1)';
thetaLx=reshape(thetaLx1',108,1)';
thetaRx=reshape(thetaRx1',108,1)';

xlswrite(['C:\Documents and Settings\Amanda\Desktop\Amanda Thesis\Thorax Project Matlab Data\' num2str(age) ' year old thorax.xlsx'],reshape
(radiusofcurvatureLx',1,108),'Left Radius of Curvature',['B' num2str(loc+1) ':DE' num2str(loc+1)]);
xlswrite(['C:\Documents and Settings\Amanda\Desktop\Amanda Thesis\Thorax Project Matlab Data\' num2str(age) ' year old thorax.xlsx'],reshape
(radiusofcurvatureRx',1,108),'Right Radius of Curvature',['B' num2str(loc+1) ':DE' num2str(loc+1)]);
xlswrite(['C:\Documents and Settings\Amanda\Desktop\Amanda Thesis\Thorax Project Matlab Data\' num2str(age) ' year old thorax.xlsx'],reshape
(apparentcurvatureLx',1,108),'Left Apparent Curvature',['B' num2str(loc+1) ':DE' num2str(loc+1)]);
xlswrite(['C:\Documents and Settings\Amanda\Desktop\Amanda Thesis\Thorax Project Matlab Data\' num2str(age) ' year old thorax.xlsx'],reshape
(apparentcurvatureRx',1,108),'Right Apparent Curvature',['B' num2str(loc+1) ':DE' num2str(loc+1)]);
xlswrite(['C:\Documents and Settings\Amanda\Desktop\Amanda Thesis\Thorax Project Matlab Data\' num2str(age) ' year old thorax.xlsx'],reshape
(thetaLx',1,108),'Left Longitudinal Twist',['B' num2str(loc+1) ':DE' num2str(loc+1)]);
xlswrite(['C:\Documents and Settings\Amanda\Desktop\Amanda Thesis\Thorax Project Matlab Data\' num2str(age) ' year old thorax.xlsx'],reshape
```

```
(thetaRx',1,108),'Right Longitudinal Twist',['B' num2str(loc+1) ':DE' num2str(loc+1)]);
560
561 %Thoracic Index
562 distAPx=NaN(1,12);
563 distLATx=NaN(1,12);
564 tix=NaN(1,12);
565 for i=1:12
566 distAPx(i)=subjects(sub).ribcage(i).distAP;
567 distLATx(i)=subjects(sub).ribcage(i).distLAT;
568 tix(i)=subjects(sub).ribcage(i).TI;
569 end
570 xlswrite(['C:\Documents and Settings\Amanda\Desktop\Amanda Thesis\Thorax Project Matlab Data\' num2str(age) ' year old
thorax.xlsx'],
distAPx,'Thoracic Index',['B' num2str(loc) ':M' num2str(loc)]);
571 xlswrite(['C:\Documents and Settings\Amanda\Desktop\Amanda Thesis\Thorax Project Matlab Data\' num2str(age) ' year old
thorax.xlsx'],
distLATx,'Thoracic Index',['B' num2str(loc+7) ':M' num2str(loc+7)]);
572 xlswrite(['C:\Documents and Settings\Amanda\Desktop\Amanda Thesis\Thorax Project Matlab Data\' num2str(age) ' year old
thorax.xlsx'],tix,'Thoracic
Index',['B' num2str(loc+14) ':M' num2str(loc+14)]);
573
574
575 %Spine/Sternum
576 SS=[subjects(sub).spine.cobbangle39,subjects(sub).spine.Radiusofcurvature,...
577 subjects(sub).spine.Radiusofcurvature1,...
578 subjects(sub).spine.Radiusofcurvature2,...
579 subjects(sub).spine.Radiusofcurvature3,...
580 fit(:,1),fit(:,2),fit(:,3),...
581 subjects(sub).sternum.Sternumwidth,...
582 subjects(sub).sternum.Manubriumwidth,...
583 subjects(sub).sternum.Sternumradiusofcurvature,...
584 subjects(sub).sternum.sternumlength,...
585 subjects(sub).spine.cobbangle112,...
586 subjects(sub).sternum.sternumcobb,...
587 subjects(sub).spine.normcobbangle,...
588 subjects(sub).spine.spineangle112,...
589 subjects(sub).spine.spineangle39];
590 xlswrite(['C:\Documents and Settings\Amanda\Desktop\Amanda Thesis\Thorax Project Matlab Data\' num2str(age) ' year old
thorax.xlsx'],SS,'Spine-
Sternum',['B' num2str(loc) ':R' num2str(loc)]);
591
592 %VB Height, depth, width
593 vbheightx=[subjects(sub).spine.VBheight];
594 vbwidthx=[subjects(sub).spine.VBwidthmid];
595 vbdepthx=[subjects(sub).spine.VBdepth];
596 xlswrite(['C:\Documents and Settings\Amanda\Desktop\Amanda Thesis\Thorax Project Matlab Data\' num2str(age) ' year old
thorax.xlsx'],vbheightx,'VB',
['B' num2str(loc) ':M' num2str(loc)]);
597 xlswrite(['C:\Documents and Settings\Amanda\Desktop\Amanda Thesis\Thorax Project Matlab Data\' num2str(age) ' year old
thorax.xlsx'],vbwidthx,'VB',
['B' num2str(loc+16) ':M' num2str(loc+16)]);
598 xlswrite(['C:\Documents and Settings\Amanda\Desktop\Amanda Thesis\Thorax Project Matlab Data\' num2str(age) ' year old
thorax.xlsx'],vbdepthx,'VB',
['B' num2str(loc+8) ':M' num2str(loc+8)]);
599
600 end
```

```
1 function [Lnew,Lriblength]=ribpercent(L,num)
2 %Checking for duplicate values
3 if ~isempty(find(sum(abs(diff(L)),2)==0, 1))
4 errordlg(['Duplicate Values in rib ' num2str(num) '!!!!!'],'Duplicate Values')
5 return
6 end
7 %calculating riblength
8 Ldistance=[0; sqrt(sum(diff(L).^2,2))];
9 Lriblength=sum(Ldistance);
10 %finding % points of raw data
11 a=cumsum(Ldistance)./Lriblength;
12 c=[.05:.05:.95]';
13 Lnew(:,1)=interp1(a,L(:,1),c);
```

```
14 Lnew(:,2)=interp1(a,L(:,2),c);
15 Lnew(:,3)=interp1(a,L(:,3),c);
16 end
```

Appendix 5: 6 year old human surface characterization in Analyze

1. From the main Analyze workspace, select Segment then Image Edit.
2. From the File menu select Create Object Map, then Add Object. Change the name in the appropriate field to identify the object map, then click done.
3. From the Generate menu select Orientation then Transverse.
4. Start at slice 1 and auto trace the outer surface of the skin as well as the inner surface of the fat and muscle.
5. Select Delayed Floodfill from the picture menu on the left side of the screen. Click inside of the space made between the two auto trace lines.
6. Set the 'Change Option' on the bottom left of the screen to 'Object Map', then select the object map named in step 2.
7. From the Tools menu select Edit Review then Previous to view each Floodfill.
8. Click the Apply & Advance button for each slice of the CT scan, adjusting the auto trace lines as necessary.
9. Export the surface as an STL file.